ON THE
INLET VORTEX SYSTEM

Final Report

of

NASA Research Grant NGL 43-001-086
Flow Visualization and Analytical Research
for the Development of
Mathematical Models in Incompressible Flow

by

Norbert C. Bissinger

and

Gerhard W. Braun

September, 1974

University of Tennessee
Space Institute
Tullahoma, Tennessee

CONTENTS

ABSTRACT

The flow field of a jet engine with an inlet vortex, which is able to pick up heavy debris from the ground and to damage the engine, was simulated in a small water tunnel by means of the hydrogen bubble technique.

It was found that the known engine inlet vortex, here called ground based inlet vortex, is accompanied by a vortex system, which consists of two inlet vortices, the ground based and the trailing one, secondary vortices, and ground vortices. Simulation of the ground effect by an inlet image proved that the inlet vortex feeds on free stream vorticity and can exist without the presence of a ground boundary layer.

The structural form of the inlet vortex system was explained by a simple potential flow model, which showed the importance, the number and the location of the stagnation points. A retractable horizontal screen or an up-tilt of the engine is suggested as countermeasure against debris ingestion.

NOMENCLATURE

A, B, C.	Stagnation points
C_1, C_2	Integration constants
D	Inner diameter of inlet
F	Function given in Equation 3
F_1	Function given in Equation 39
G	Function given in Equation 5
G_1	Function given in Equation 40
h	Height of inlet center line above ground
$\bar{h}$	Half the horizontal distance between double inlets over ground
k	Wave number
m*	Sink strength, volume per sec
m	Dimensionless sink strength
mA	Milliamperes
r*	Radius defined by $r^* = \sqrt{x^{*2} + y^{*2}}$
r	$= \frac{r^*}{h}$ Dimensionless radius
$\bar{r}$	Radius vector measured from stagnation point S, see Figure 35
Re	Reynold's number defined in Equation 15
U_∞	Uniform flow velocity
U_i	Inlet velocity
u	Dimensionless velocity in x-direction
v	Dimensionless velocity in y-direction
$\bar{v}_o$	Basic undisturbed velocity vector
V_r, V_γ, V_z	Dimensionless velocity components of basic, undisturbed velocity vector in cylindrical coordinates

v_x, v_y	Dimensionless velocity components in x and y direction of $\bar{w}_i$
w	Dimensionless velocity in z-direction
$\bar{w}_i$	Dimensionless induced velocity vector
x^*, y^*, z^*	Coordinates in three-dimensional coordinate system
α	Angle between vortex and inlet axis
Γ^*	Circulation of vortex
Γ	Dimensionless circulation of vortex $= \Gamma^* \cdot \frac{1}{U_\infty \cdot h}$
ξ, η, ζ	Coordinates defined in Figure 36
ν	Viscosity
ξ_o	ξ -coordinate of stagnation point S
ψ	Angle in cylindrical coordinates
ψ^*	Angle defined in Figure 35
ψ_1^*	Maximum value of ψ^* defined in Figure 35
Φ^*	Velocity potential of sink and image sink in free stream flow
Φ	Dimensionless velocity potential of Φ^*
ω	Dimensionless vorticity vector
ω_r, ω_ψ, ω_z	Dimensionless components of vorticity vector in cylindrical coordinates

I. INTRODUCTION.

The ground based engine inlet vortex has aroused the interest of the engine designer because of the severe damage caused by solid particles which the vortex sucks up into the engine. "Roughly half of all jet engines removed from aircraft for repairs are removed due to foreign material damaging the engines" states H. Klein in Ref. [1] *).

The inlet vortex has been investigated for more than twenty years, but a study of the available literature gives the impression that no practical solution for preventing particle ingestion has been found.

Therefore the inlet vortex was considered a worthwhile object for a systematic investigation. Observations of the simulated inlet flow in the water tunnel of the UT Space Institute revealed very soon, that the inlet vortex is not stationary and that it is only one individual of an inlet vortex system.

The peculiar structure of this vortex system captivated the first author of this reprt so strongly that he selected the inlet vortex system as thesis subject. The present report is a revision of this thesis.

The reported research work was funded by the NASA Grant NGL-43-001-086. The grant was administered by Mr. Harry H. Heyson of the NASA Langley Research Center. This report offers a welcome occasion for thanking Mr. Heyson for many suggestions and for his unobtrusive guidance, which left the authors the widest possible freedom in this research and stimulated their efforts.

*) Numbers in brackets refer to the bibliography at the end of the report.

II. LITERATURE SURVEY.

The earliest available report dates back to 1953 [3]. In it Klein describes tests with an inlet of one inch in diameter which was connected to a vacuum cleaner. The tests were made at zero wind speed. The picking up of particles was recorded as a function of the ratio of inlet height above the ground to inlet diameter and the ratio of particle terminal speed to inlet air speed. The result was the threshold of particle inhalation as function of the two ratios.

In 1955 Rodert and Garrett [2] made pictures and movies of the inlet vortex during tests with a full scale jet engine mounted underneath the wing of a cargo plane. They showed that the vortex was able to pick up particles large enough to damage a jet engine if sucked into it. Engine speed, engine height from ground and surface wind were found to play a role in the vortex formation. Vortices were observed between inlet and ground (Maximum distance 8 feet) and even between inlet and fueselage (distance 15 feet).

Two years later Klein [1] reported on tests with a 20-percent scale model jet engine. Adding circulation to the crosswind with the help of a fan resulted in a strong consistent vortex. An increase of the circulation or of the updraft caused by the inlet intensified the vortex. Tests with two inlets, simulating a jet in ground effect, showed that the boundary layer of the ground surface played no significant role in the creation of the vortex. All measures, tried to prevent swallowing of pebbles, failed. A jet was then tried in a 40-percent scale model set-up. A second small jet was directed downward so that it removed the stagnation point underneath the inlet. The stagnation point is necessary for the formation of the inlet vortex. It was concluded that, "The Blowaway Jet represents a simple, safe, economical scheme for effecting a very large reduction in the amount of engine damage to be expected due to material pick-up from the runways."

E. E. Glenny [4] arrived at about the same scaling laws as Klein by making a dimensional analysis for the force acting on a particle when the inlet vortex sweeps over it. The use of a seven horsepower fan allowed variation of the crosswind velocity, on which a horizontal velocity gradient was superimposed, i.e., the crosswind carried vertical vorticity. The systematic experiments showed that the scaling laws were valid and could be used to determine the ingestion thresholds and the sizes of particles that can be lifted by the vortex. The report stated that, "For a given inlet velocity the strength of the vortex, and thus the maximum size of particles that can be lifted, is very much a function of the ambient vorticity, and of the strength of the wind blowing onto the intake." Because no method to prevent particle ingestion worked satisfactorily during his experiments, D. E. Glenny proposed to keep the ratio of inlet velocity to crosswind velocity small as long as a jet aircraft is on the ground.

The report by A. Ya. Miroshnichenko [5] shows that the Russians were also working on the inlet vortex problem, but states nothing new.

J. L. Colehour and B. W. Farquhar [6] constructed a flow model with the help of the observations of other researchers and some small scale tests of their own. They calculated the inviscid, potential flow into two cylindrical inlets with and without headwind by using the method of Rubbert, et al. [7] . An increase in headwind moved the stagnation point in the ambient flow direction [6] until the stagnation point was removed from the symmetry plane, i.e., ground plane, between the two inlets. The method allowed to add an irrotational vortex to the flow-field [6] . A comparison of the ground plane velocities of the flows with and without vortex with the measured velocities is found in [8] . A paper by Kendall [9] on a vortex in a vortex tube was used to explain the velocity distribtuions in the boundary layer near the stagnation point. The conducted experimental program provided one new point: "Stability of the vortex decreases as inlet height increases [6] ." Vortex suppression methods for jet engines and other inlet flows were given.

Nearly all of the papers mentioned here stress the following points:

1. A ground based inlet vortex can exist only if there is:
    a. vorticity in the ambient flow,
    b. a stagnation point on the ground underneath the inlet with a streamline connecting it with the inlet.
2. The inlet vortex is unsteady. It is not only moving--sometimes very fast--along an irregular path on the ground plane, it also appears and disappears irregularly.

III. WATER TUNNEL TESTS.

In order to gain insight into the mechanism of the inlet vortex it was considered necessary to visualize the whole flow field around an inlet. It was thought especially important to observe the formation of the inlet vortex while the flow conditions changed from a flow without inlet vortex to a flow with inlet vortex. In addition the threshold of first inlet vortex appearance was to be determined by a separate test series.

For these tests The University of Tennessee Space Institute water tunnel was used. It has a rectangular, open test section of 12 x 18 inches and the flow velocities are variable from 0 to 1 ft/sec. (See References [10] and [11] .) For the visualization the hydrogen bubble method [12] was applied. Streaklines were formed with both bubble surface generators and bubble line producers. A bubble surface generator consists of a kinked banjo wire spanning the width or depth of the test section and shedding a bubble line at each of its downstream bends. A bubble line producer was made of an insulated wire with a bare end of a bout half an inch width. It produces one single streakline. The bubble lines were illuminated by a light plane about one inch thick produced by four 500 watt bulbs. The flow pictures were recorded on 400 ASA TRI-X PAN film or on Ektachrome Super 8 Colorfilm. The inlets consisted of copper tubes with an inner diameter of 9/16 inch. The copper tube extended downstream and was connected with a suction pump. This means the engine outlet was not simulated by the described tests. For most of the tests a piece of translucent plastic tube about one inch long with an inner diameter of 5/8 inch was slipped over the copper tubing in order to improve the lighting conditions directly underneath the inlets. (See Figure 1) The diameter of the inlets are considered small enough to neglect the influences of the tunnel side walls.

Before the test program was started, the flow field was systematically surveyed by bubble generators. The survey

revealed that an inlet vortex never comes alone but rather is an individual of a vortex system. The fact that only the ground based inlet vortex and its horizontal equivalent between two side by side inlets is mentioned in the literature is understandable, because the other members of the system represent no danger to the engine.

After many trial tests, systematic tests were made with

1. One inlet above a false bottom 30 inches downstream of the false bottom's leading edge.
2. Two inlets side by side above a false bottom at the 30 inch station.
3. A vertical inlet above a false bottom at the 30 inch station.
4. An inlet and an image inlet far from any tunnel wall.

In all tests with a horizontal inlet, the inlet center line was aligned with the free stream direction. Crosswind was not included as test parameter because trial tests showed that the influence of the tunnel side walls became too large when the inlet was substantially inclined to the tunnel free stream.

The test conditions consisted of the test-set-up geometry, inlet velocity and tunnel velocity. The test results were obtained in the form of notes on visual observations during the tests plus still photographs and a few movies. The inlet velocity was calibrated against the back-pressure, p, of the pump used, the tunnel velocity was calibrated against a galvanometer (indicating milliamps) which is part of the tunnel driving motor circuit.

The variables changed in these tests were:

1. Height of center line of inlet above ground.
2. Tunnel velocity.
3. Inlet velocity.

During a test series the inlet velocity was increased in steps from nearly zero to maximum inlet velocity, whereas the inlet height and the tunnel velocity were kept constant.

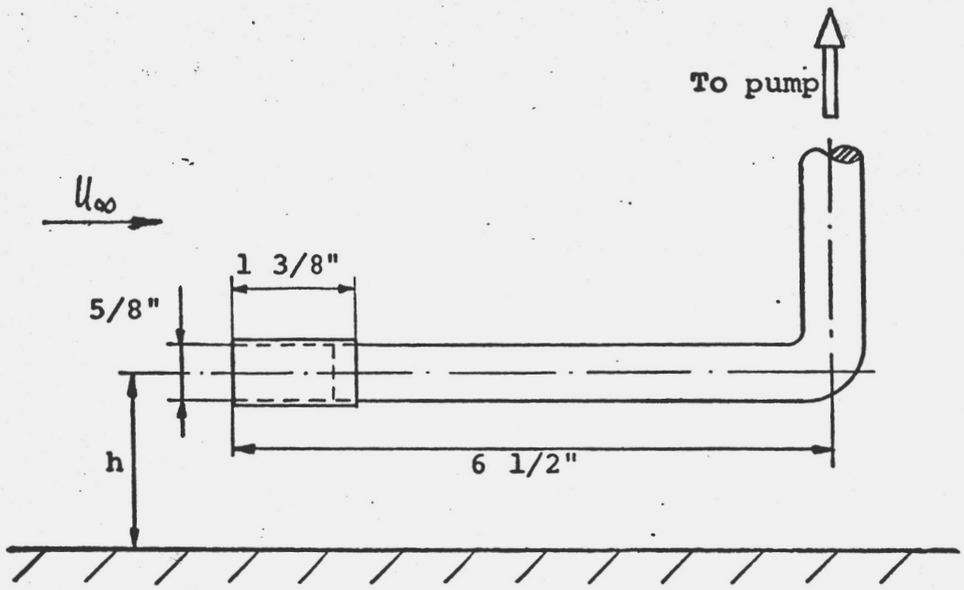

(a) Single inlet over ground, side view

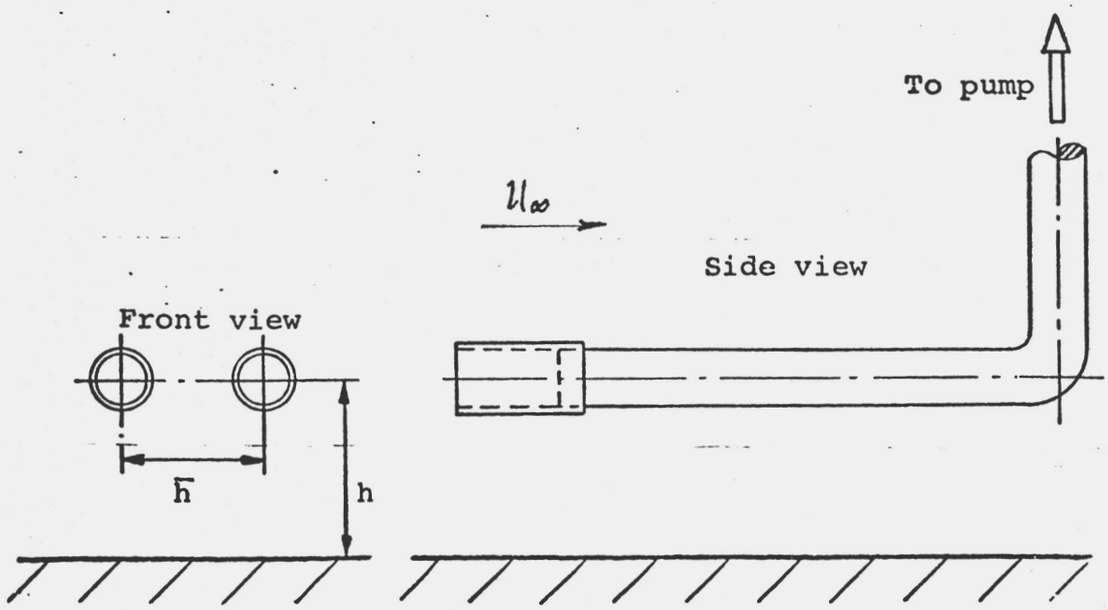

(b) Double inlet over ground, side view

Figure 1. Geometry of inlets used.

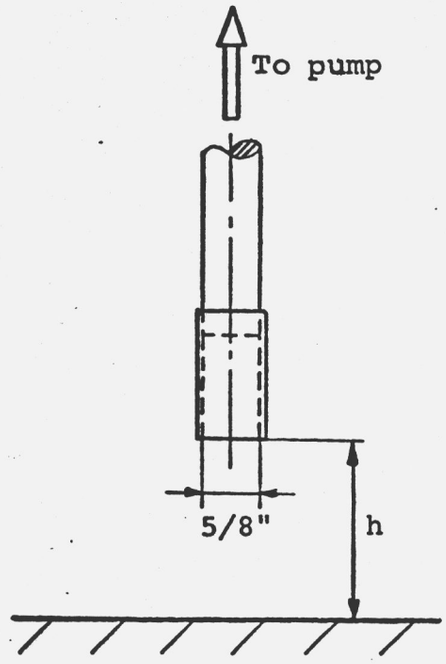

(c) Vertical inlet over ground, side view

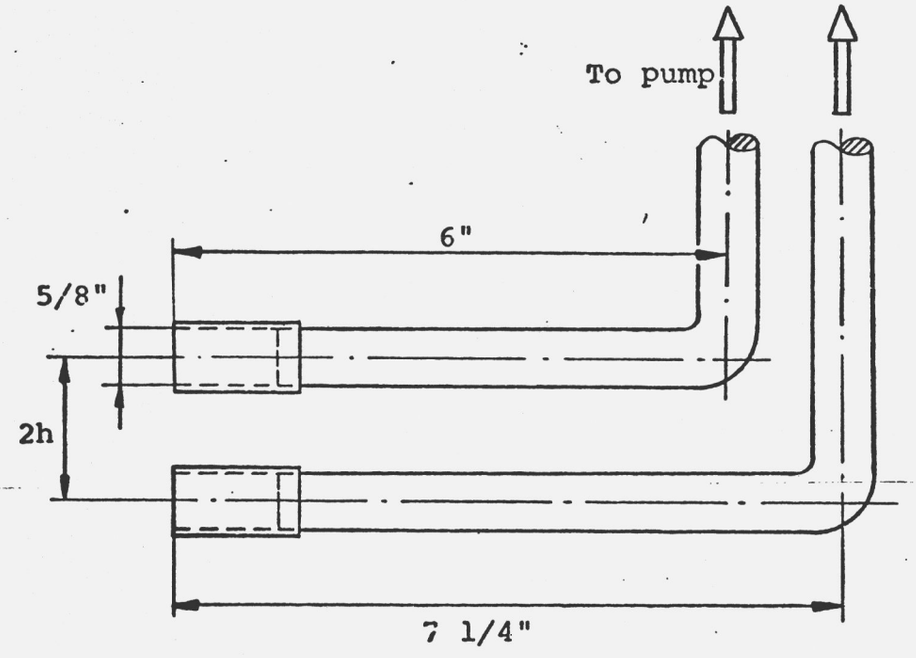

(d) Image inlets, side view

Figure 1. (continued).

The stepwise increase of the inlet velocity was repeated with different inlet heights and tunnel velocities. This test procedure was least time consuming because it was easier to change the back-pressure behind the pump by opening or closing a valve than to change the other parameters. In addition, the person conducting the tests could stay in his place and observe the flow during the change of the inlet velocity. The constant tunnel velocity during a test series made sure that the initial conditions far upstream were kept constant, so that vorticity and turbulence in the freestream remained the same.

The tests and their results are described on the following pages.

1. SINGLE HORIZONTAL INLET OVER GROUND.

The data of the tests with a simple horizontal inlet over ground are compiled in Table I.

TABLE I

TEST DATA

h/D	I (mA)	p (psig)
1.5	0.0; 2.0; 4.0; 6.0; 8.0	22 to 5 in steps of 1 psig
2.0	0.0; 2.0; 4.0; 6.0; 8.0	22 to 5 in steps of 1 psig
2.5	0.0; 2.0; 4.0; 6.0; 8.0	22 to 5 in steps of 1 psig
3.0	0.0; 2.0; 4.0; 6.0; 8.0	22 to 5 in steps of 1 psig

It was already mentioned that the inlet vortex in the water tunnel was always accompanied by a vortex system. It never appeared alone. The formation of this vortex system during a tests series is sketched in Figure 2. In a tests series the inlet height above the ground and the free stream velocity U_∞ were kept constant. A kinked bubble generator wire spanned the test section horizontally about one to two inches in front of the inlet and close to the ground. Without inlet flow it produced streaklines parallel to the free stream flow without any visible influences from the inoperative inlet.

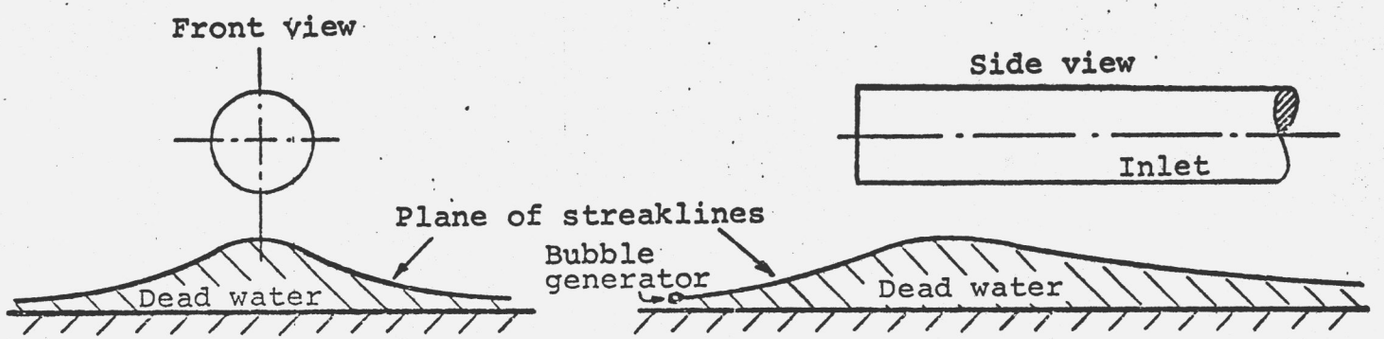

(a) U_{ia}

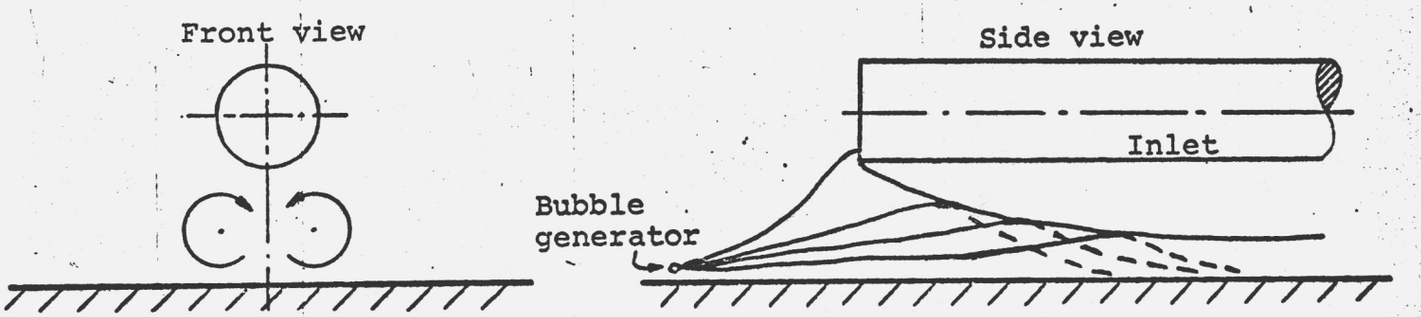

(b) U_{ib}

$$U_{ia} < U_{ib} < U_{ic} < U_{id};\ U_{\infty} = \text{constant}$$

Figure 2. Formation of inlet vortex system.

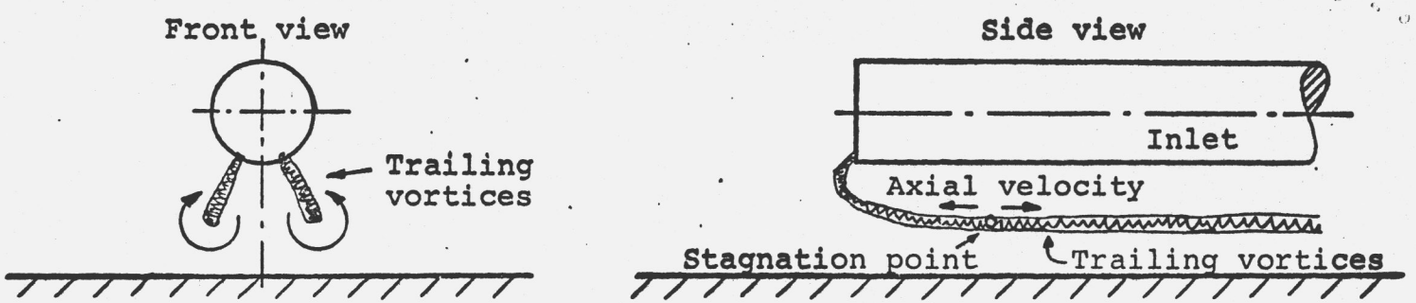

(c) U_{ic}

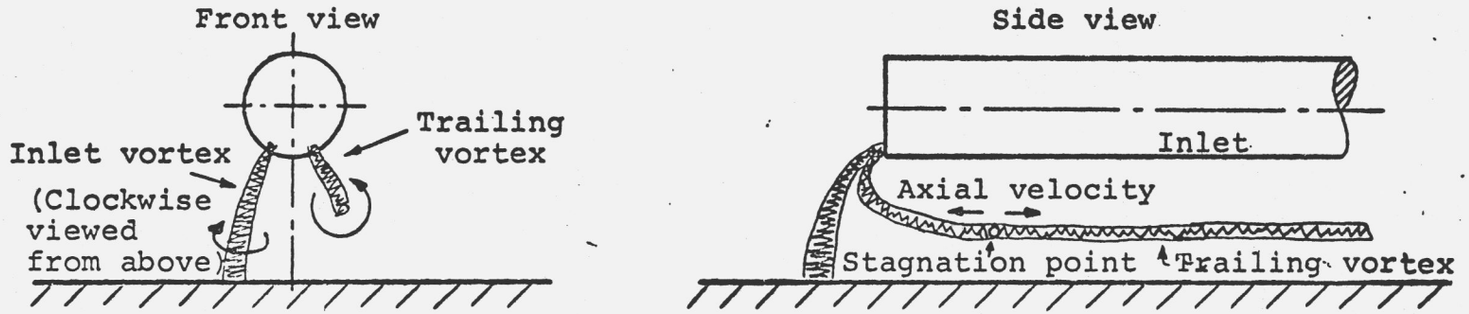

(d) U_{id}

Figure 2. (continued).

At a small inlet velocity, U_{ia}, the streaklines underneath the inlet were lifted over a dead water region (Figure 2a). The highest point was at about one inlet diameter downstream from the inlet plane. Bubbles created in that region by a bubble line producer rose straight up, which is a good indication that the local flow velocity is there very small.

An increase in the inlet velocity lifted the streaklines up further until the first streakline was sucked into the inlet and the streaklines on both sides of the inlet started curling in slowly. This is shown in Figure 2b.

Increasing the inlet velocity further increased the rotation on both sides of the inlet until two "trailing inlet vortices" formed as can be seen in Figure 2c. These were vortices reaching from the inlet into the free stream and extending sometimes several feet downstream. They were located between the inlet and the ground approaching the ground for higher inlet velocities. Their axial velocity changed its direction at a stagnation point several inlet diameters downstream of the inlet, upstream of the stagnation point leading into the inlet, downstream of the stagnation point moving in the free stream direction. The stagnation point was the point where the trailing vortex penetrated the catching surface which separates the fluid caught by the inlet from the fluid not caught by the inlet (Fig. 33a).

The next increase in inlet velocity produced the ground based inlet vortex which reached from the ground into the inlet. At that moment one of the trailing inlet vortices disappeared (Figure 2d) and the boundary layer on the ground on both sides of the inlet became unstable and formed vortices called ground vortices in the following (Figure 3). These ground vortices were linked with one end to the inlet vortex foot like a piece of string which was attached there and the rest of which moved along the ground towards the center plane of the inlet. They appeared at an angle of about 45 to 60 degrees relative to the free stream and usually started immediately moving towards the center plane. Because part of them was sucked into the inlet, they were stretched and their rotational speed was increased on their way. The ground vortices on the side of

the inlet vortex were swept underneath the inlet, sometimes even to the other side, where they were destroyed by the action of viscosity and too much stretching. The ground vortices on the side of the trailing vortex moved only to a position parallel to the trailing vortex and disappeared there. The formation and movement of the ground vortices on the two sides of the inlet seemed to be independent from each other.

The whole inlet vortex system consisting of ground based inlet vortex, trailing inlet vortex and ground vortices is sketched in Figure 3.

The formation of the inlet vortex system followed the described steps for all combinations of test parameters. There have been, however, differences in the flow picture. For example, the inlet vortex sometimes could be seen only because of the streaklines spiraling around its invisible core whereas sometimes the core was visible by total reflection as a thin (about 1/32 to 1/16 inch diameter) tube of gas with single bubbles, not streaklines, spiraling around it. The rotational speed in the second case was much higher than in the first. The trailing inlet vortex sometimes occurred as a tube with a continuous distribtuion of bubbles, the ground vortices, however, always contained these bubbles.

All vortices were nonstationary. A vortex would be formed and would break down without any change in the test parameters, its pieces floating downstream. Seconds later it would start forming again. This reforming always began as a very slow rotation which picked up speed until a nearly constant rotation was reached. During this acceleration process the vortex also changed its position. For example, the two trailing vortices always started underneath the inlet tube very close to the symmetry plane and each other. With increasing strength they moved outward from underneath the inlet and away from each other. The ground based inlet vortex usually started underneath the inlet tubing moving upstream and to one side with increasing strength; its trailing vortex behaved like one of the two trailing vortices described before. The breakdown of either the inlet vortex or the trailing vortex was followed by the breakdown of the trailing vortex

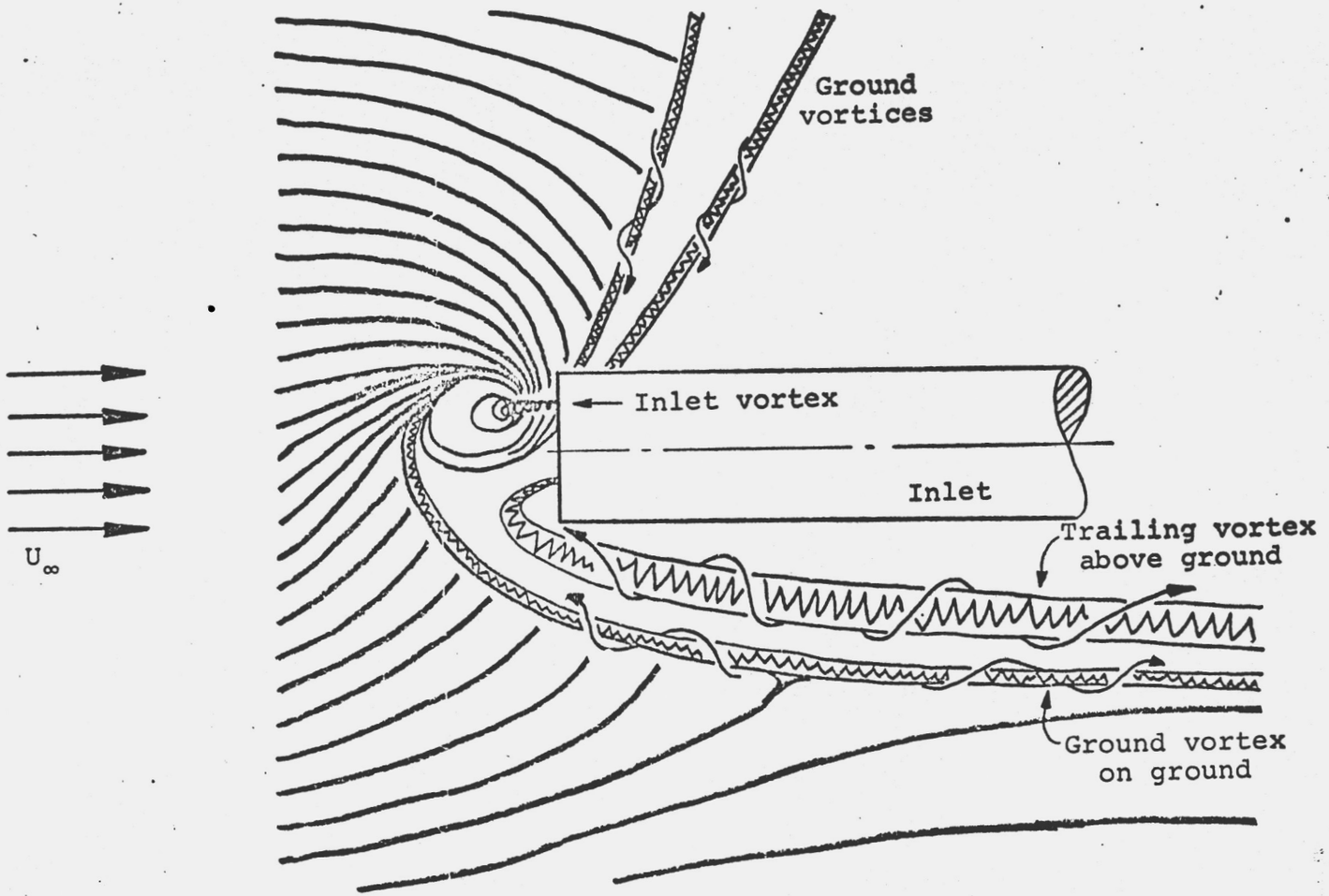

Figure 3. Inlet vortex system and streaklines close to the ground, top view.

or the inlet vortex, respectively. The disappearance of the ground vortices seemed to have no effect on the ground based inlet vortex and the trailing inlet vortex for small values of h/D. In tests with larger values of h/D the ground vortex on the side of the trailing inlet vortex showed the tendency to grow in strength and size while test conditions were kept constant. At the same time it advanced against the flow in front of the inlet vortex. At a certain size it collapsed and started forming again. Photographs of this process are shown in Figures 4, 5, 6, 7, 8, and 9.

These figures show top views of the flow pattern for different free stream velocities U_∞, inlet velocities U_i and inlet height over inlet diameter ratios. For each combination of these test parameters three photographs are presented in order to show that the flow was not stationary. The inlet tubing reaches into the picture from the right side. The translucent plastic tubing appears as a bright white rectangle in about the center of each photograph. The free stream flow (tunnel flow) goes from the left to the right. To visualize the flow one kinked bubble surface generator and two bubble line producers were used. The kinked wire is lying on the ground upstream of the inlet and one can see white hydrogen bubble lines starting from it. The bubble line producers are positioned on opposite sides of the inlet tubing.

Great difficulties can be expected if one tries the suggested method for suppressing the inlet vortex by blowing air into its foot on the ground because the vortex foot wanders randomly in front of the inlet over an area with a diameter about twice the inlet diameter. The movement of the ground based inlet vortex was accompanied by movement of the trailing inlet vortex. The core of both vortices was deformed during these unsteady position changes. In some tests the axis of the trailing inlet vortex looked ragged resembling the tail of a kite in very gusty winds with sharp bends and fast, irregular fluttering. However, the axis of the ground based inlet vortex seemed to be smooth even when the vortex was jumping around very fast.

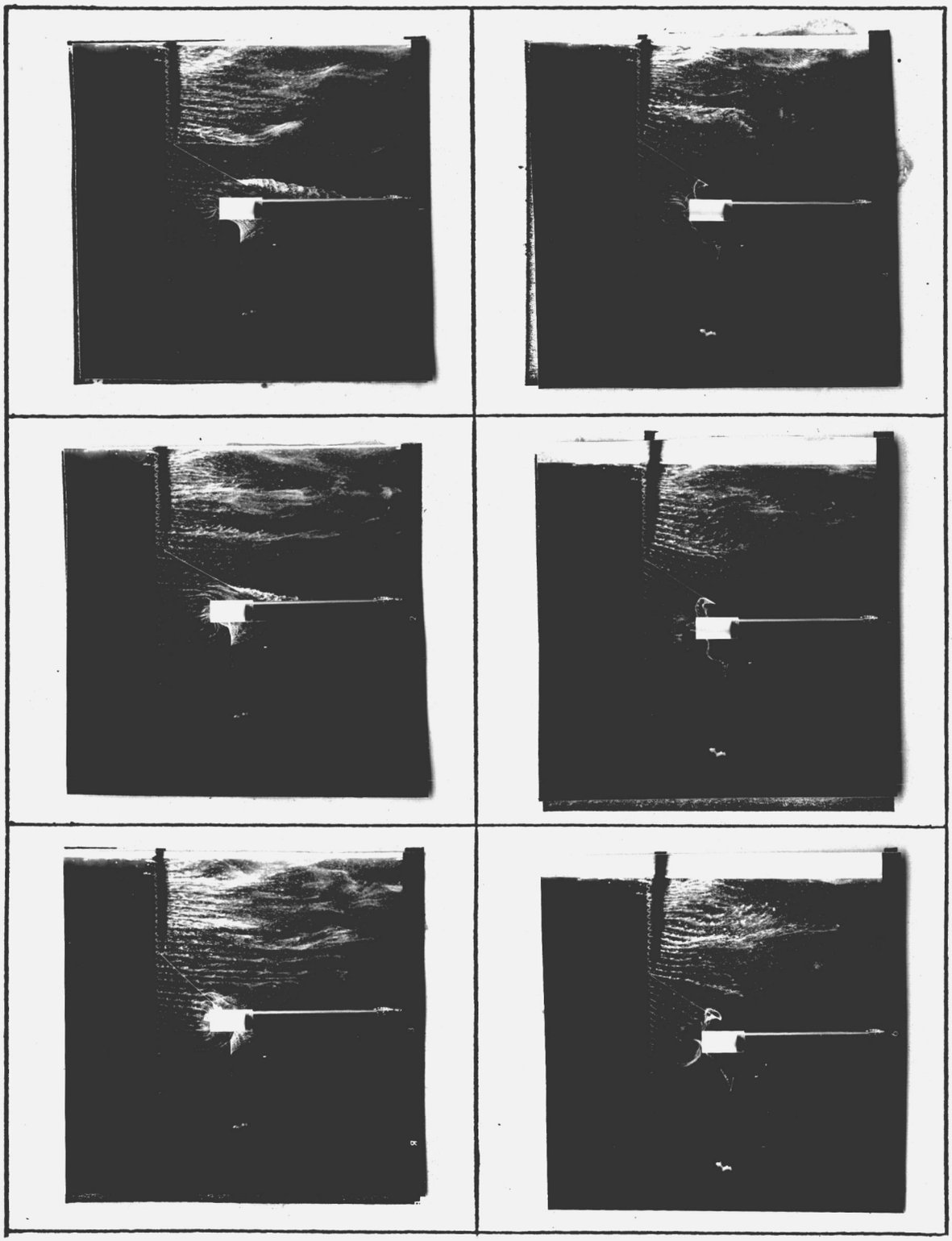

U_i = 130 cm/sec U_i = 285 cm/sec

Figure 4. Single inlet, top view, h/D = 2.5, U_∞ = 25 cm/sec.

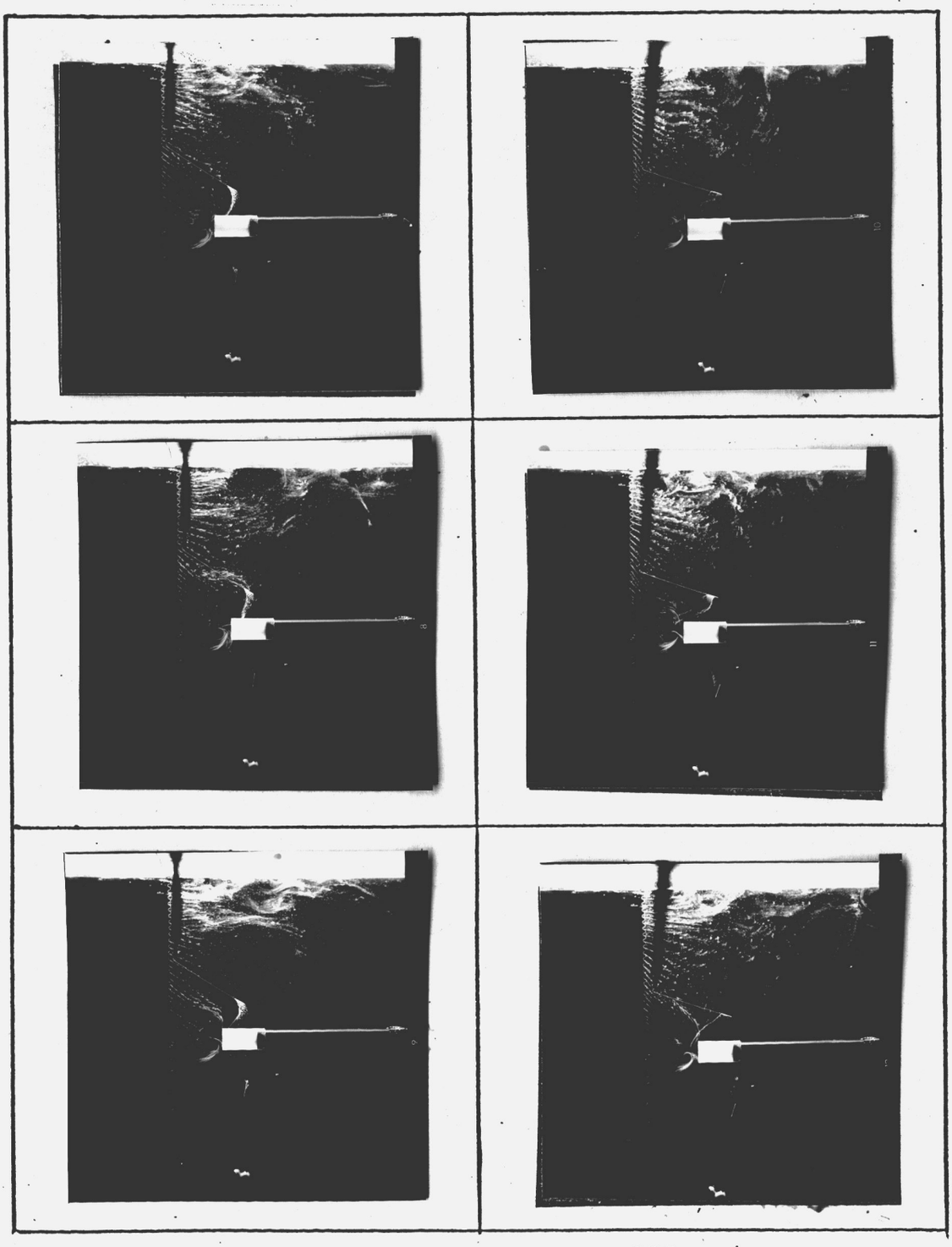

U_i = 410 cm/sec U_i = 525 cm/sec

Figure 4. (continued).

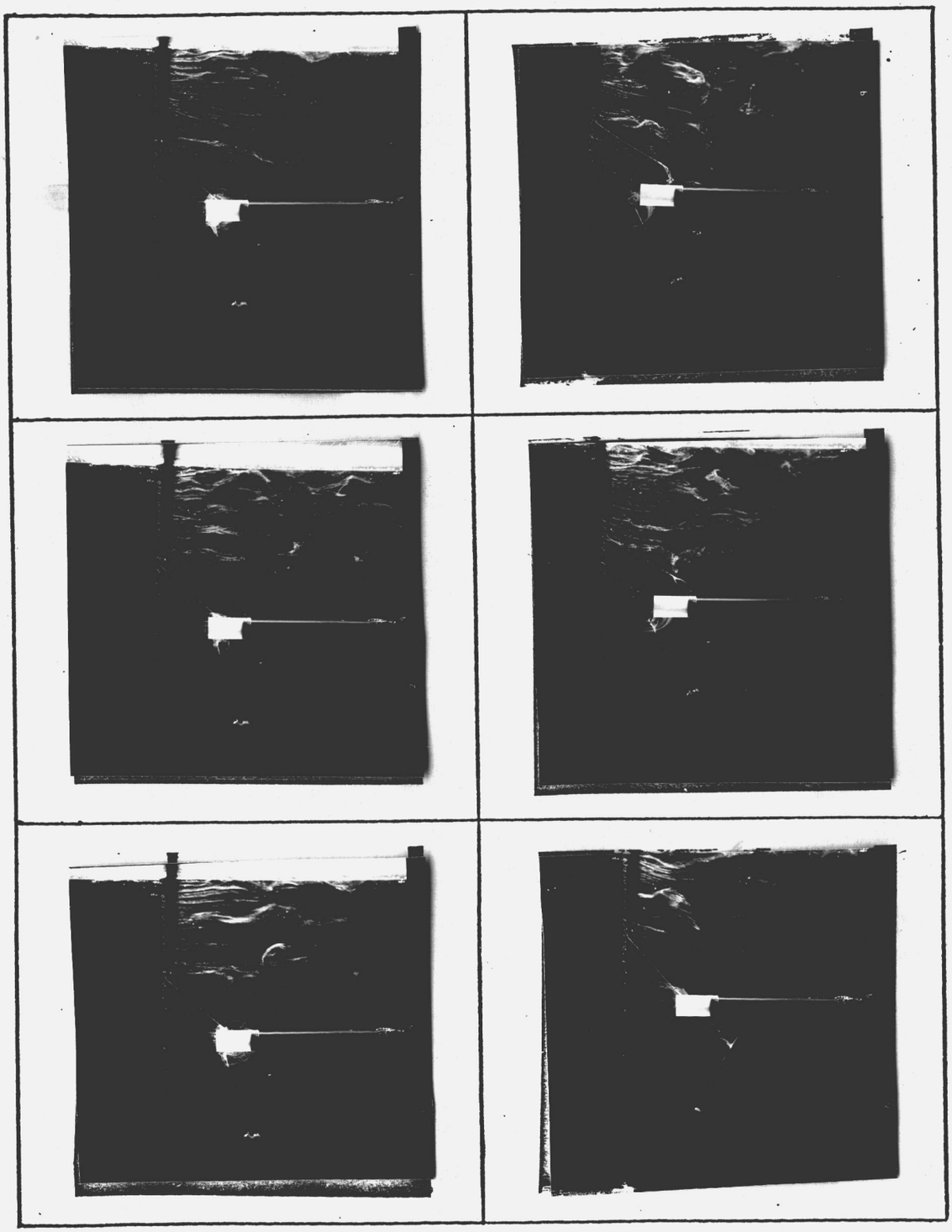

U_i = 165 cm/sec U_i = 285 cm/sec

Figure 5. Single inlet, top view, h/D = 2.5, U_∞ = 65 cm/sec.

U_i = 410 cm/sec U_i =525 cm/sec

Figure 5. (continued).

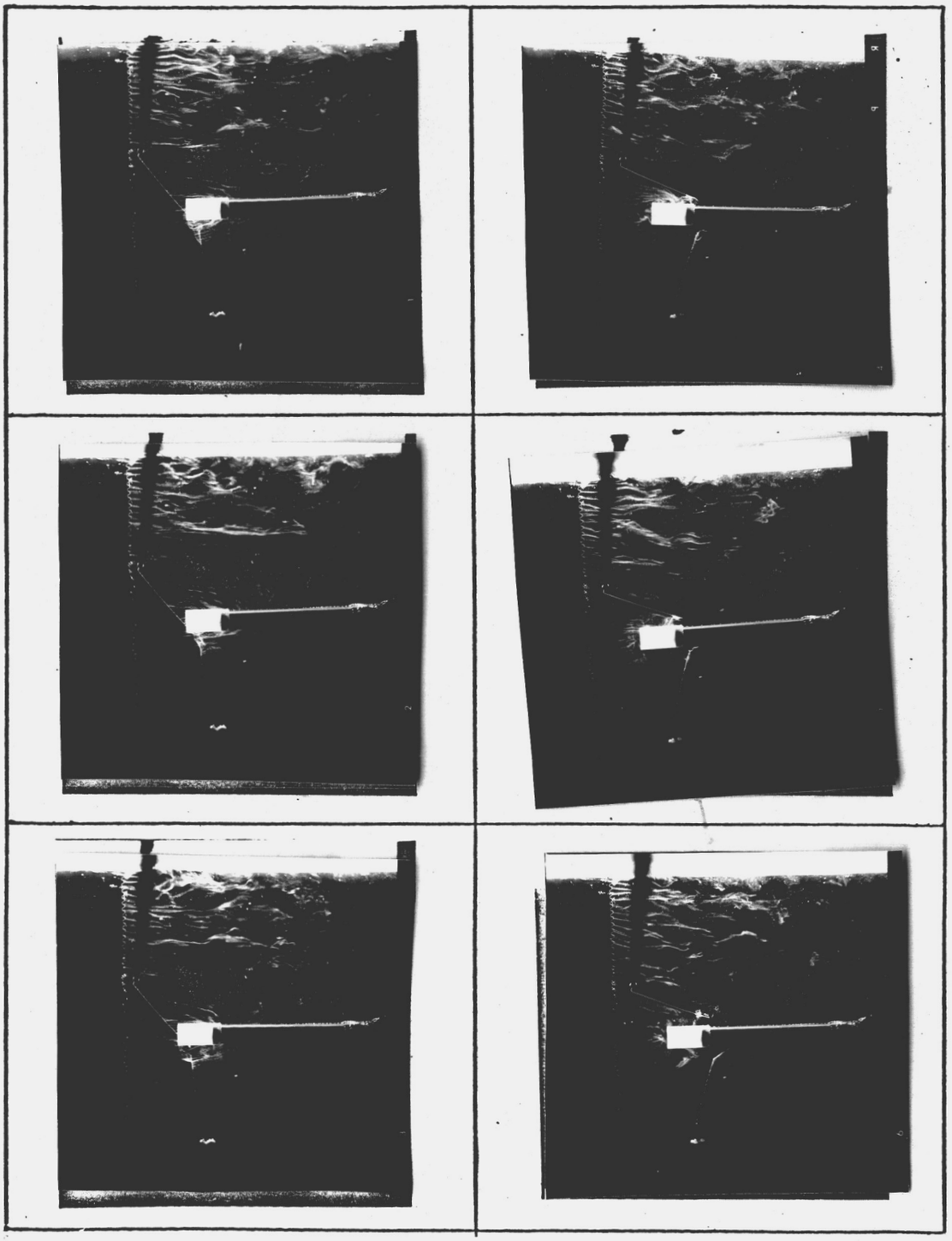

U_i = 195 cm/sec U_i = 310 cm/sec

Figure 6. Single inlet, top view, h/D = 2.5, U_∞ = 10 cm/sec.

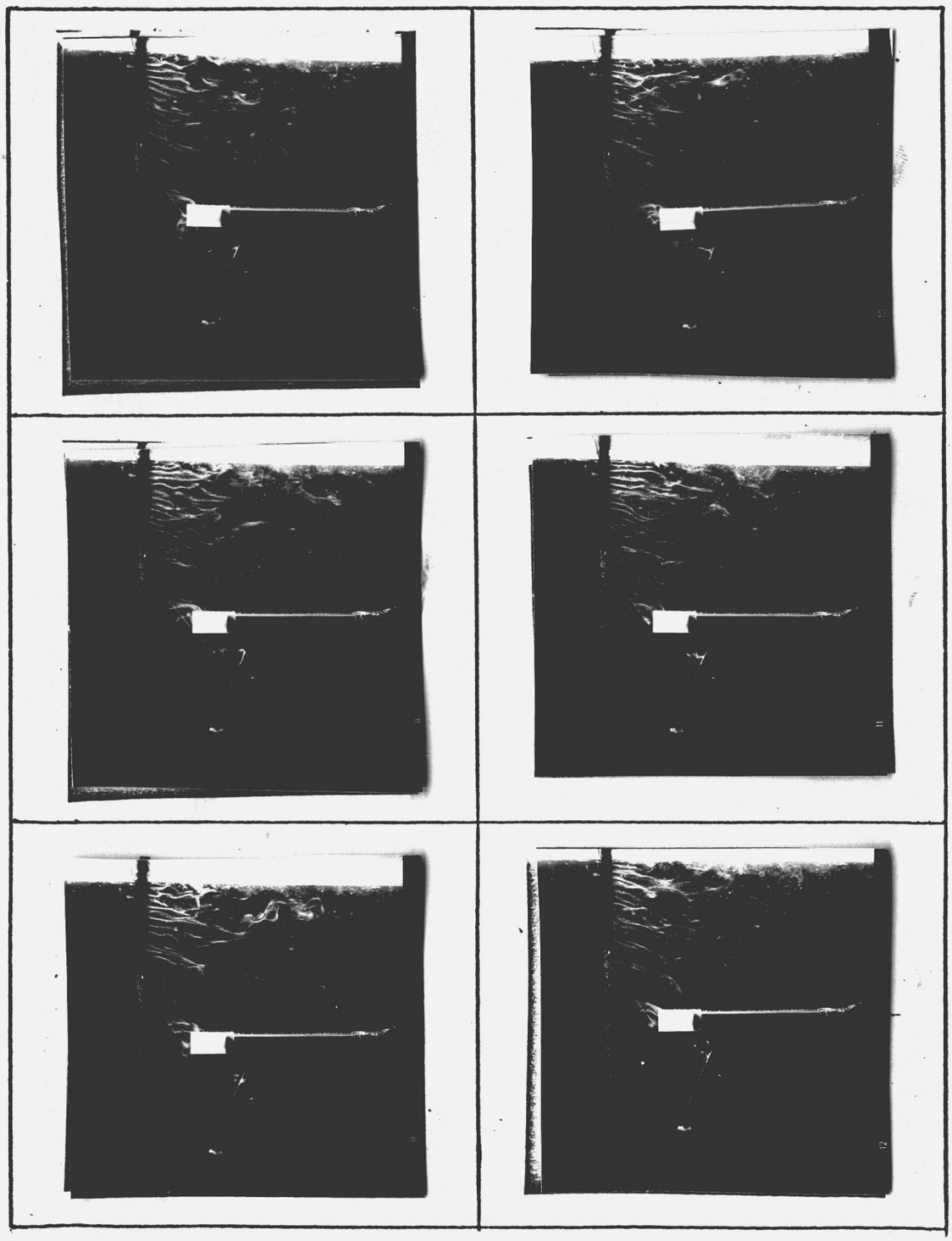

U_i = 435 cm/sec U_i = 525 cm/sec

Figure 6. (continued).

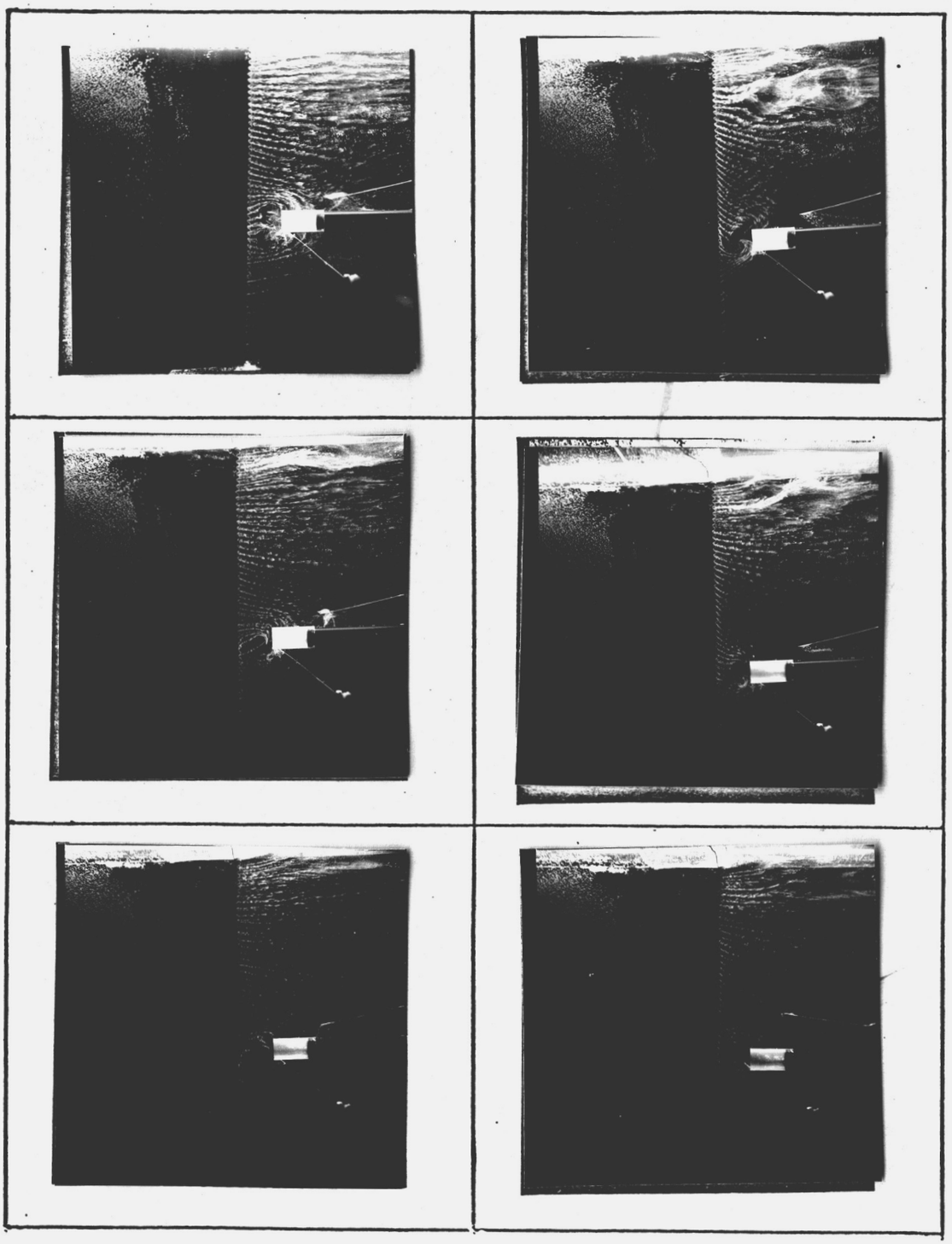

U_i = 165 cm/sec U_i = 360 cm/sec

Figure 7. Single inlet, top view, h/D = 3.0, U_∞ = 25 cm/sec.

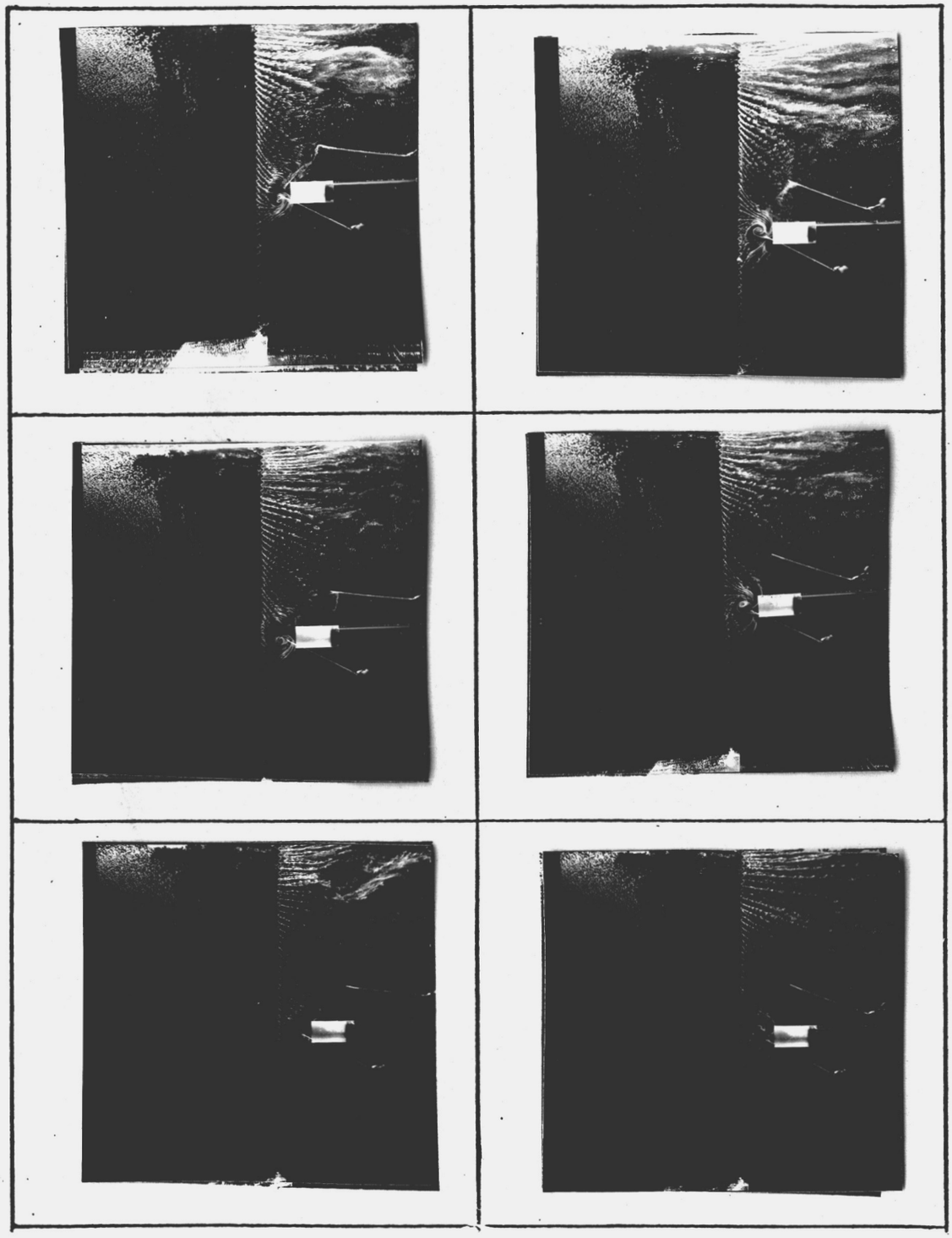

U_i = 460 cm/sec U_i = 525 cm/sec

Figure 7. (continued).

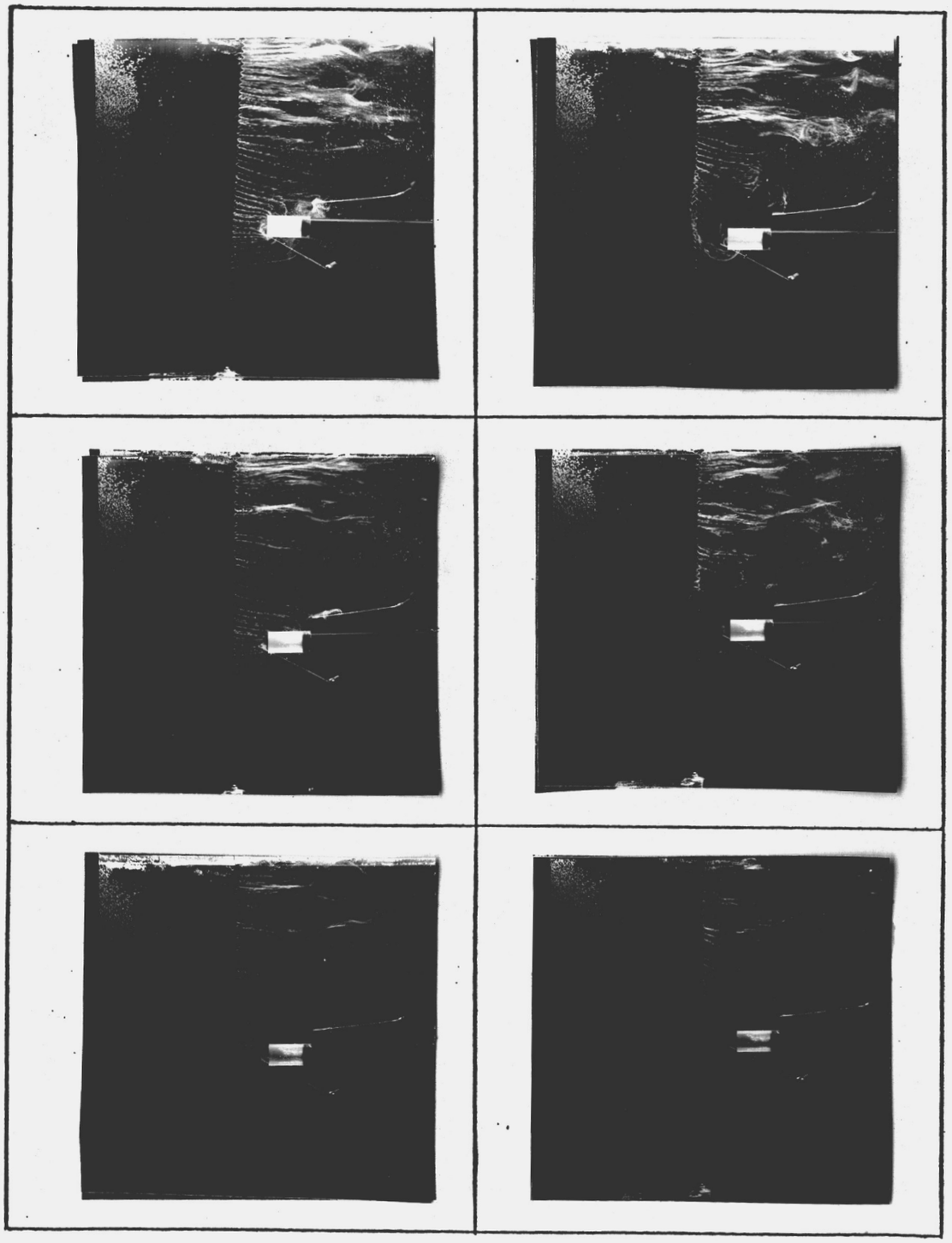

U_i = 255 cm/sec U_i = 435 cm/sec

Figure 8. Single inlet, top view, h/D = 3.0, U_∞ = 6.6 cm/sec.

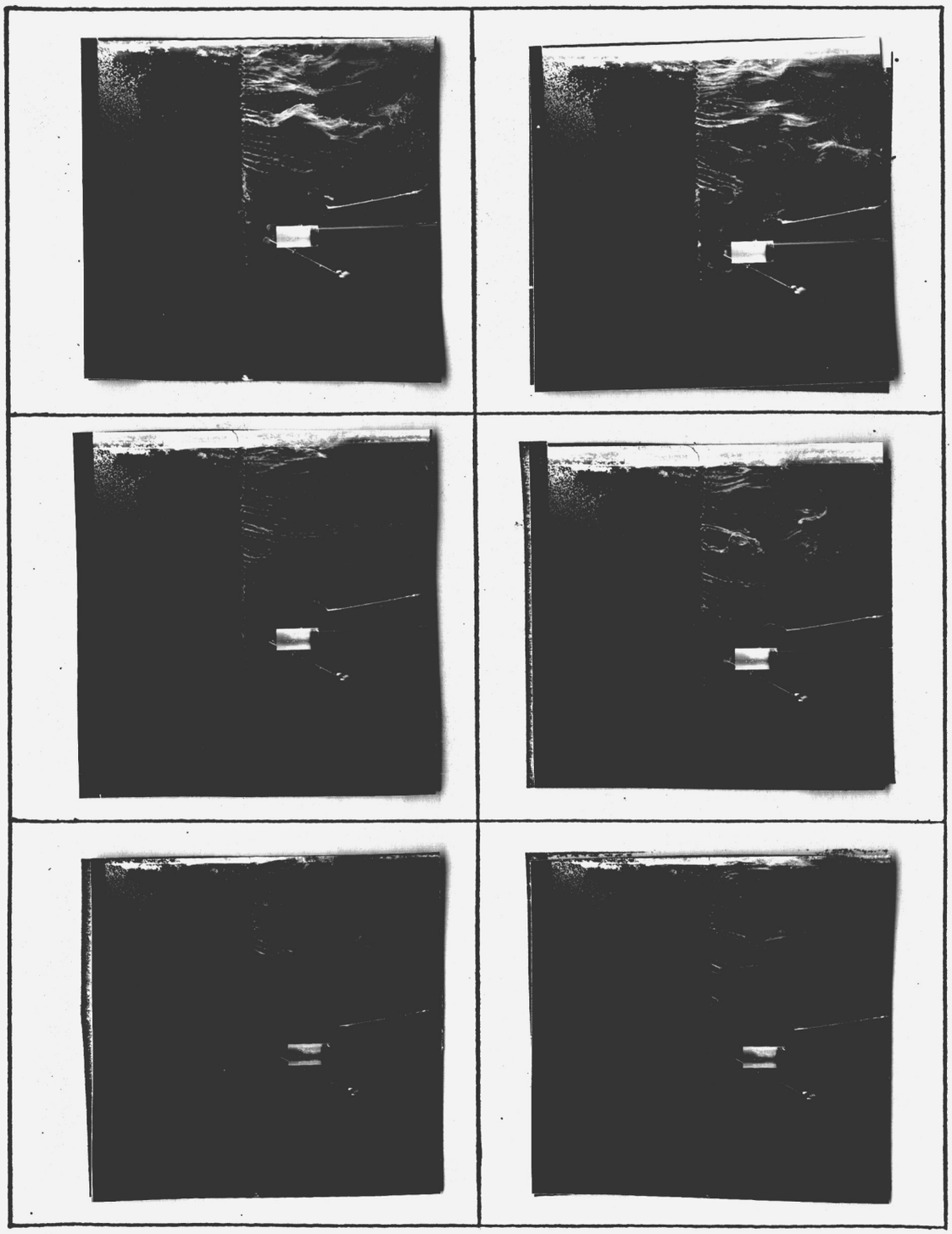

U_i = 480 cm/sec U_i = 525 cm/sec

Figure 8. (continued).

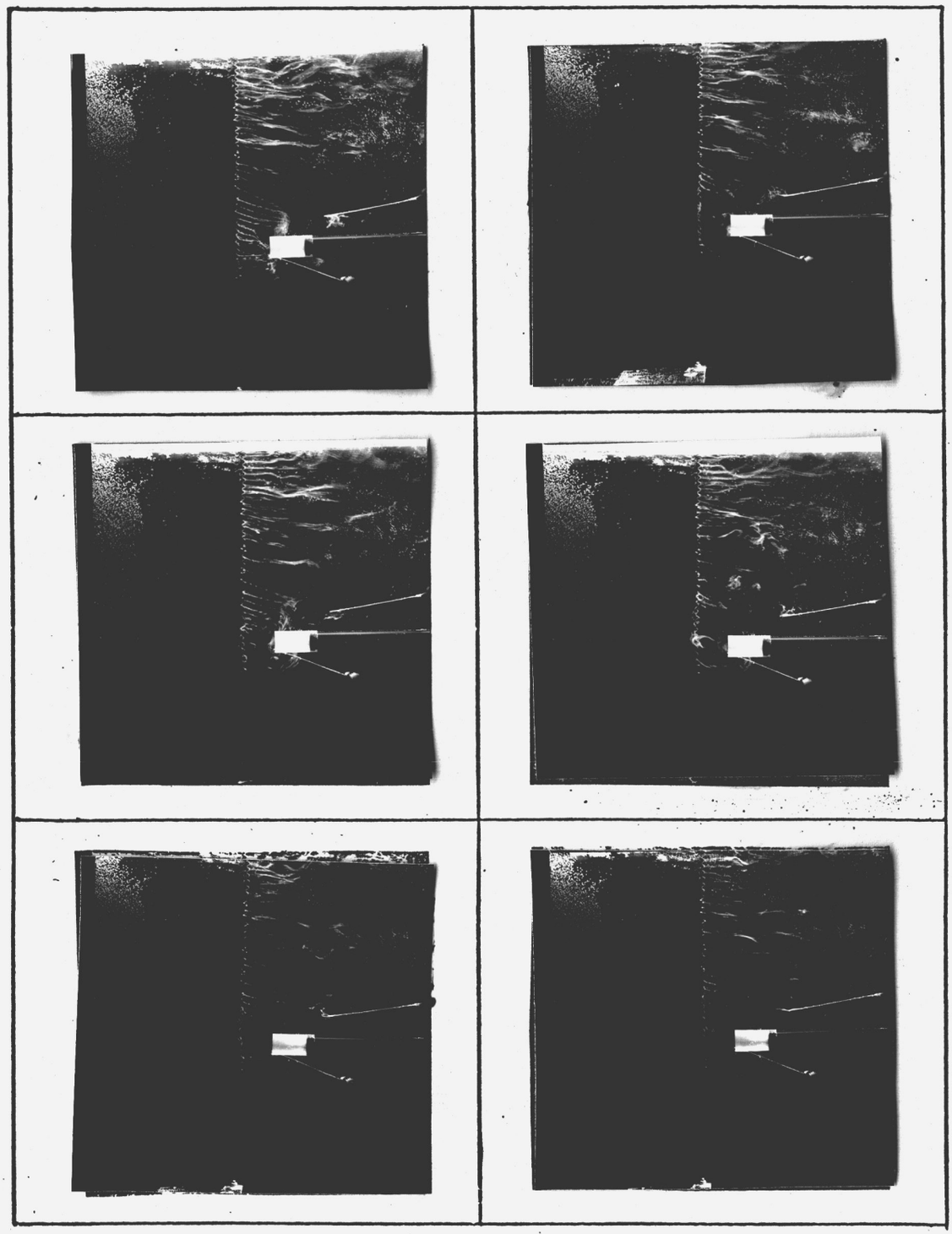

U_i = 435 cm/sec U_i = 480 cm/sec

Figure 9. Single inlet, top view, h/D = 3.0, U_∞ = 10 cm/sec.

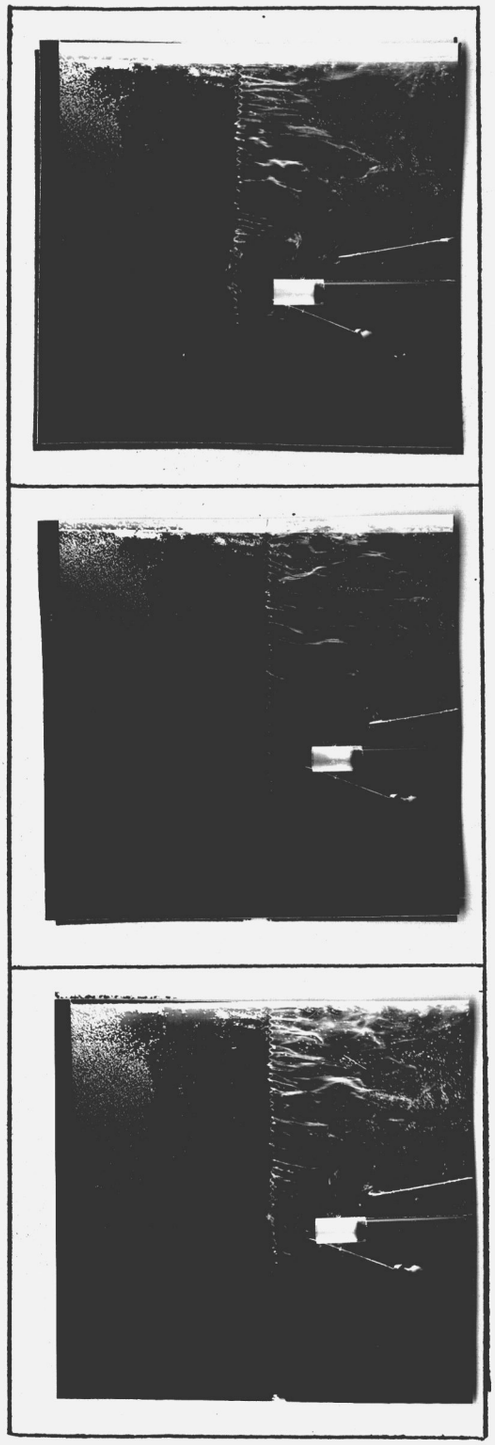

U_i = 525 cm/sec

Figure 9. (continued).

The sense of rotation of the ground based inlet vortex was unpredictable. In some tests, the rotation of the vortices would suddenly slow down, come to a halt and the whole vortex system would form again with the sense of rotation changed. This means the ground based inlet vortex and the trailing inlet vortex exchanged their position and role. Sometimes this happened several times, the rotation switching back and forth without test parameter change, sometimes this was initiated by the change of a test parameter. The ground based inlet vortex and the trailing inlet vortex always stayed on opposite sides of the inlet. A switch in the sense of rotation always meant a switch in position of the vortices from one side of the inlet to the other. (See Figure 10).

In some of the tests with h/D = 2.5 and h/D = 3.0 the pump used for the inlet was not strong enough to form the complete inlet vortex system. For h/D = 3.0 the inlet vortex still did occur at the highest possible inlet velocity of 525 cm/sec (5 psig) and at a free stream velocity of 10 cm/sec (4 mA), but it was very unstable. At the same inlet velocity but with a higher free stream velocity of U_∞ = 14 cm/sec (6 mA) the ground based inlet vortex no longer appeared. Instead, there were two trailing inlet vortices, and in front of them a very turbulent region could be seen in which fast rotating bubbles indicated irregular vorticity concentrations. From this region vortex pieces were shed irregularly into the free stream. A further increase in free stream velocity to U_∞ = 17 cm/sec (8 mA) made the turbulent region disappear.

For h/D = 2.5 the inlet vortex did occur for U_∞ = 14 cm/sec (6 mA) and U_i = 525 cm/sec (5 psig) but was not formed for U_∞ = 17 cm/sec (8 mA) and U_i = 525 cm/sec (5 psig).

Table II gives the values for free stream velocity U_∞ and inlet velocity U_i for different values of ground distance of h/D for which the inlet vortex occurred the first time during the tests with increasing inlet velocity holding everything else constant. At this transition point the flow field switched sometimes back and forth between one with one

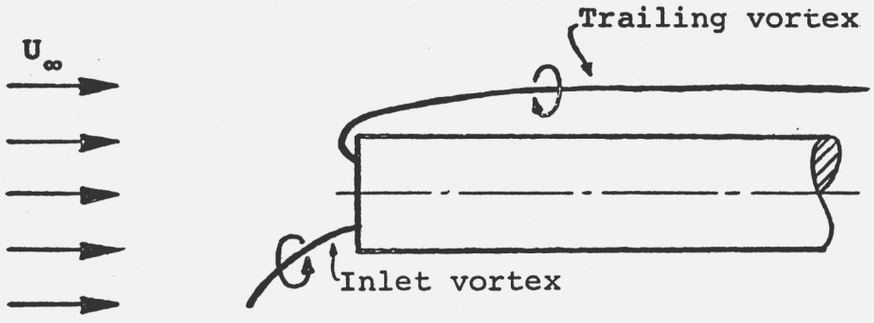

(a) Inlet vortex turning counter-clockwise

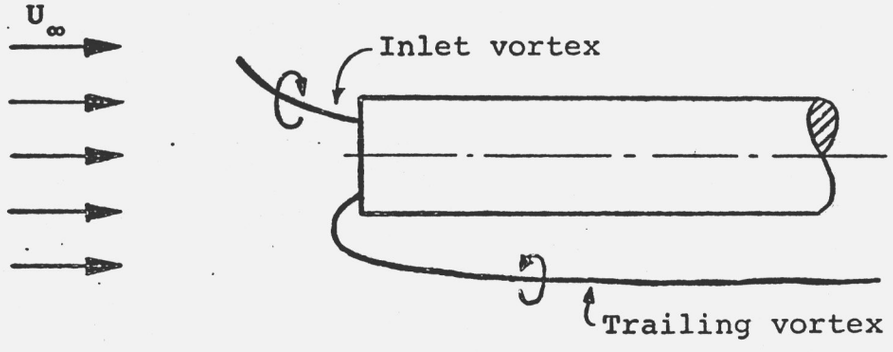

(b) Inlet vortex turning clockwise

Figure 10. Top views of inlet vortex system with different sense of rotation.

ground based and one trailing inlet vortex and one with two trailing inlet vortices.

Figure 11 shows the three-dimensionality of the boundary layer underneath the inlet. The streaklines in flow direction are produced by a kinked bubble surface generator wire 30 cm upstream of the inlet close to the ground. The bubble line producer reaching into the picture from the left side marks in the upper set of photographs a streakline close to the ground and in the lower set a streakline going through a point 6 mm above the ground. One can see that the flow in the boundary layer close to the ground goes nearly straight towards the foot of the inlet vortex which is visible at the tip of the second bubble line producer. However in the lower pictures, the bubbles are swept far downstream before they

TABLE II

FIRST APPEARANCE OF GROUND-BASED INLET VORTEX, SINGLE INLET OVER GROUND

h/D	U_∞ (cm/sec)	U_i / U_∞
1.5	2.5	35.0
1.5	6.6	19.6
1.5	10.0	16.2
1.5	14.0	14.3
1.5	17.0	11.5
2.0	2.5	51.0
2.0	6.6	25.0
2.0	10.0	19.2
2.0	14.0	16.5
2.0	17.0	13.3
2.5	2.5	35.0
2.5	6.6	34.2
2.5	10.0	30.7
2.5	14.0	31.7
2.5	17.0	-
3.0	2.5	77.0
3.0	6.6	38.8
3.0	10.0	45.0
3.0	14.0	-
3.0	17.0	-

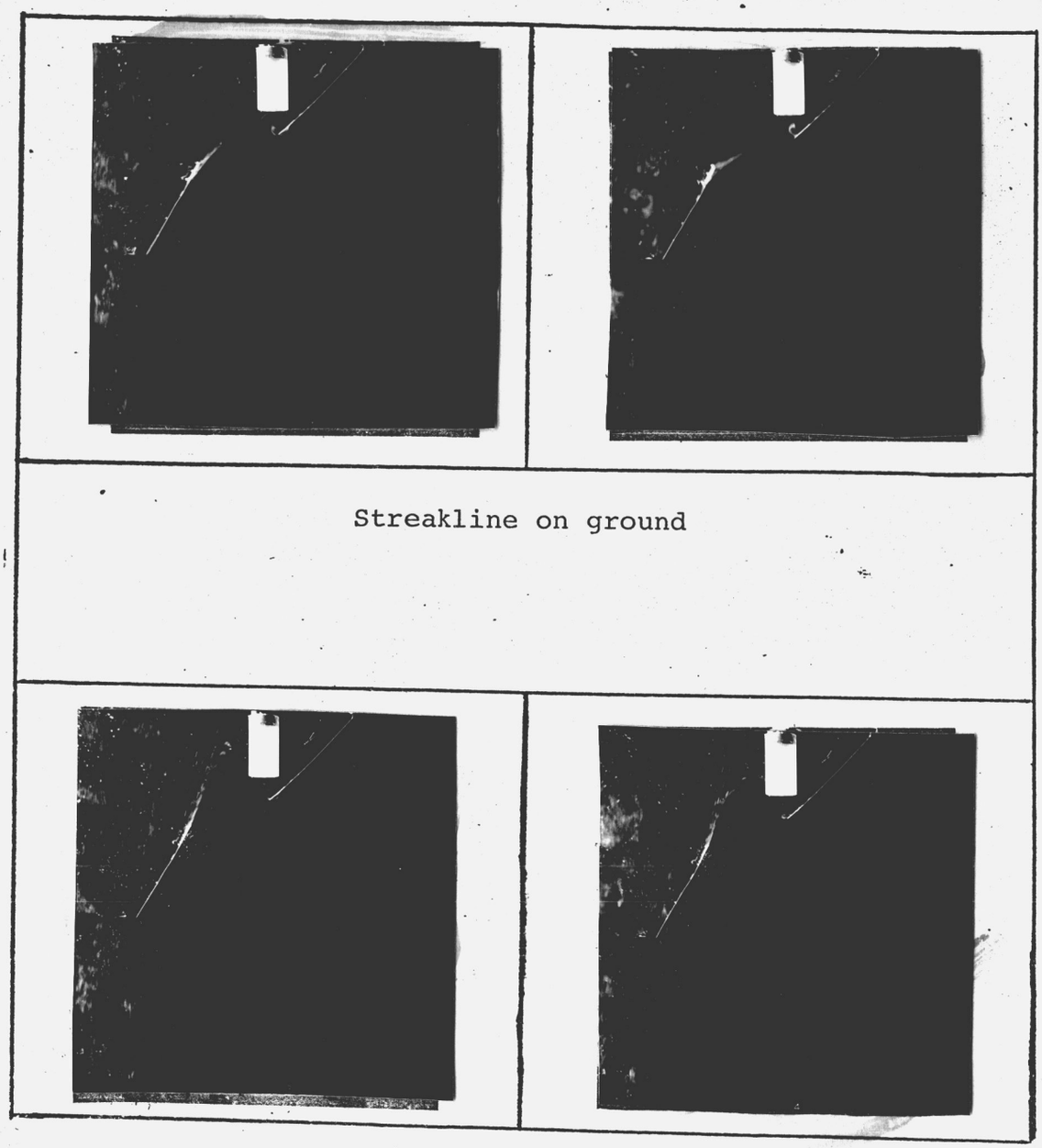

(a) U_{∞} = 17 cm/sec

Figure 11. Streaklines showing three-dimensional boundary layer, top view, h/D = 1.5, U_i 525 cm/sec.

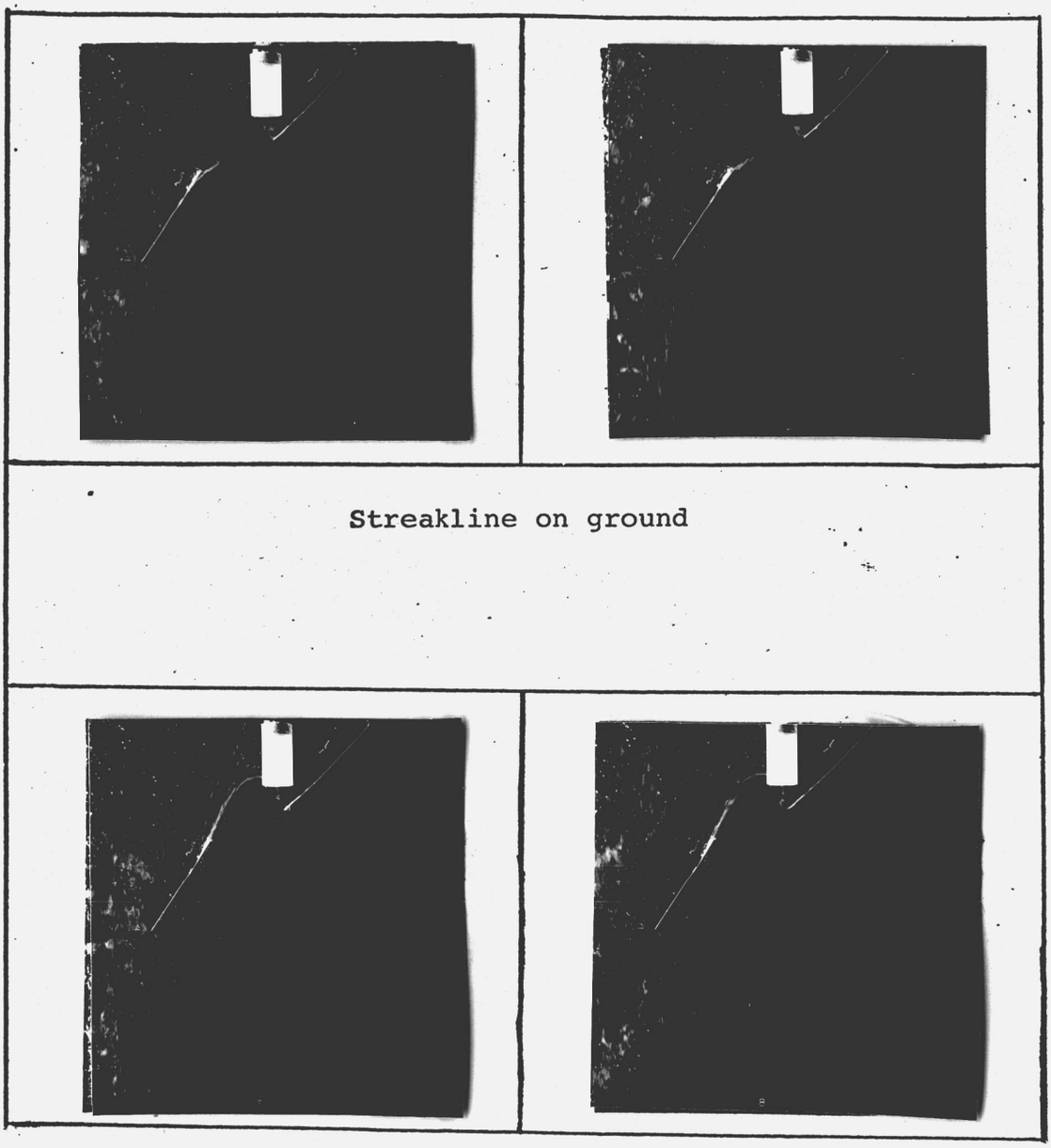

Streakline on ground

Streakline about 6 mm above ground

(b) $U_{\infty} = 14$ cm/sec

Figure 11. (continued).

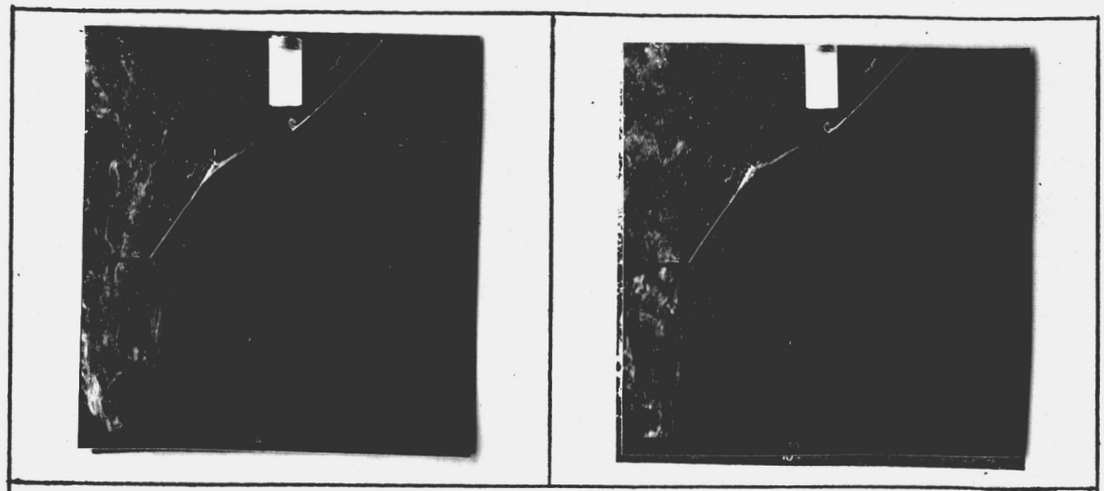

Streakline on ground

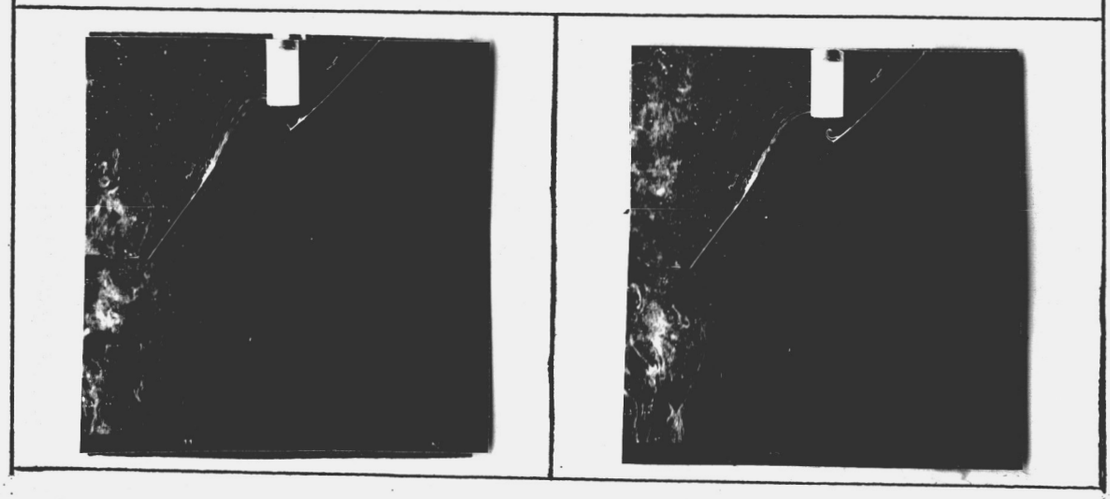

Streakline about 6 mm above ground

(c) U_{∞} = 10 cm/sec

Figure 11. (continued).

are sucked back and swallowed by the inlet. These photographs also show the difficulties involved in the visualization of the inlet vortex system. The trailing vortex and the ground vortices are not visible, because the hydrogen bubbles are released at an unfavorable place.

The trailing inlet vortex can be seen in Figure 12. The streaklines and the vortex enter the inlet in its lower half.

A top view of the trailing inlet vortex and two ground vortices is shown on Figure 13. Notice the curvature of one ground vortex.

The changes in the flow pattern for increasing inlet velocity during different tests are recorded in Figures 4 through 9, pages 16 through 27. The ground based and the trailing inlet vortex can be seen.

Obviously, the disturbances of the flow field by the growing ground vortices mentioned above become larger for increased h/D and increasing U_∞.

2. DOUBLE HORIZONTAL INLET OVER GROUND.

Many jet-engine aricrafts in use today are powered by four jet-engines, two side by side on each wing. Therefore, it was considered interesting to investigate the flow field around two inlets in the vicinity of the ground. To simplify the testing procedure the two inlets were tested side by side at a distance $\bar{h}$, abreast of each other and not in a staggered configuration as on swept wing aircrafts. The narrowness of the water tunnel made a small distance between the centerlines of the two inlets necessary. Trial tests showed that a test-set-up with $\bar{h}/D = 3.2$ and $h/D = 2.5$ (see Figure 1b, page 7) was suitable for tests at different flow conditions. The two inlets were close enough to influence their inlet flow and sufficiently apart not to have the characteristics of one big inlet. The two inlets were connected to the same pump used for the single inlet. So the

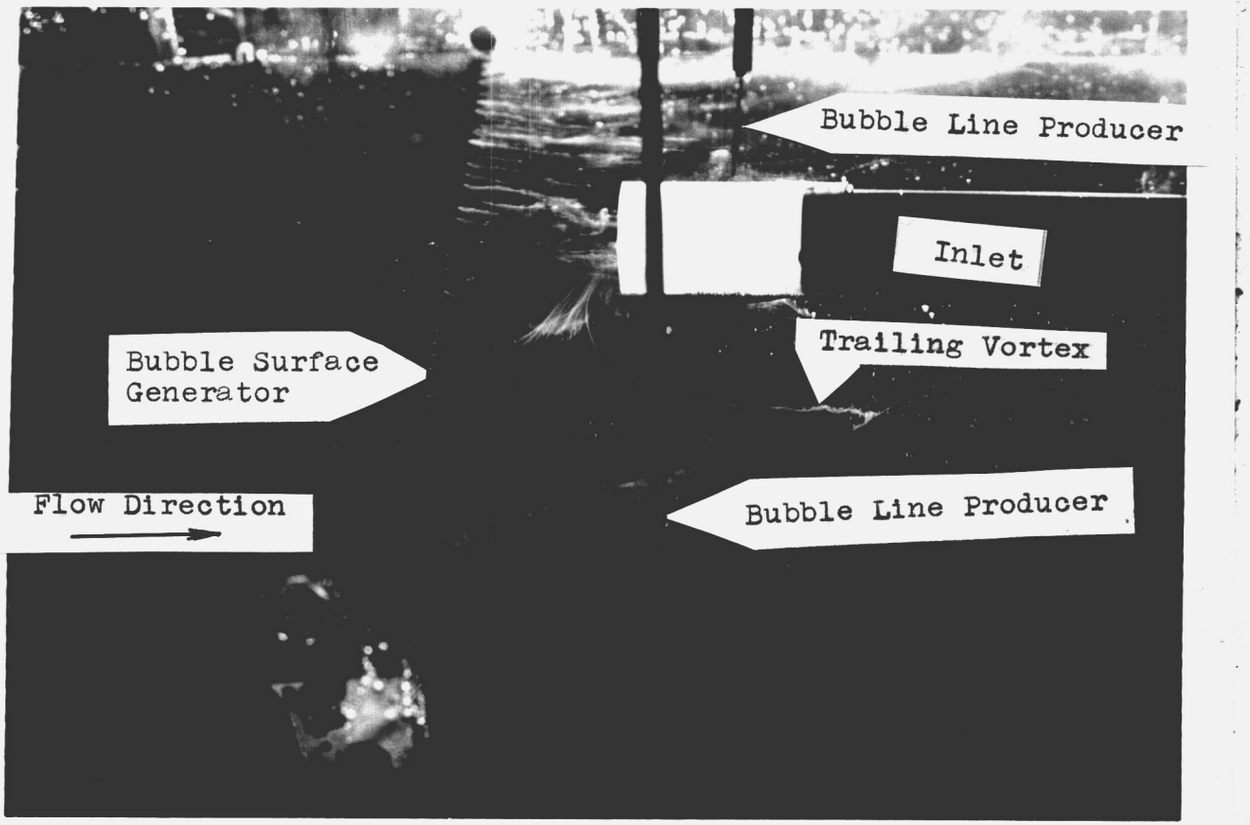

Figure 12. Side view of trailing inlet vortex.

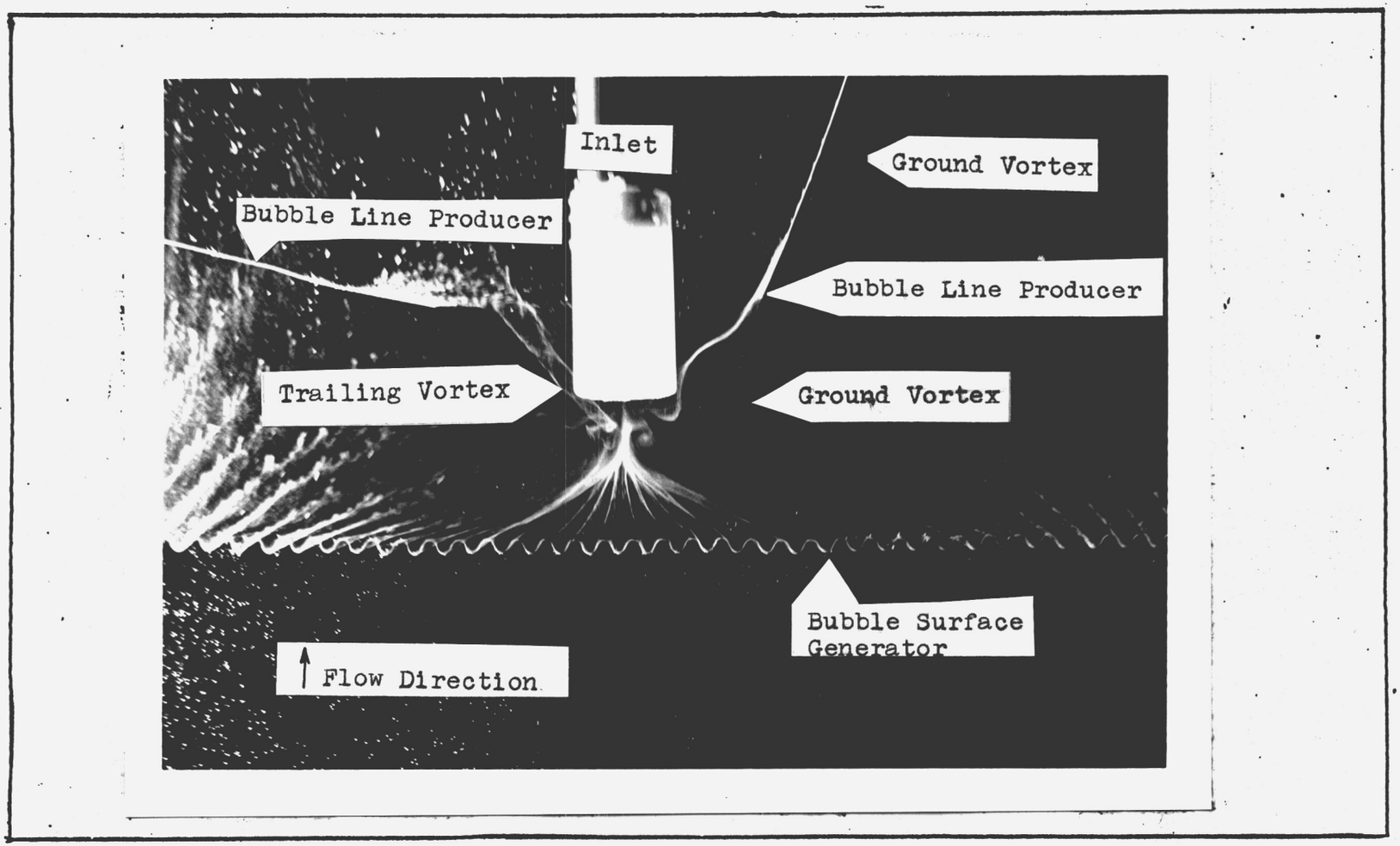

Figure 13. Top view of trailing inlet vortex and ground vortices.

total mass flow per second stayed about the same and the inlet velocity of one inlet dropped considerably compared to the single inlet. The inlet velocities again were calibrated against the pump back-pressure, assuming that half of the total flux went through each inlet. The testing procedure was the same as with the single inlet: geometry and free stream velocity were fixed and the back-pressure of the inlet pump was lowered in steps of one psig so that the inlet velocity increased from step to step.

At low inlet velocities the streaklines from the bubble generator on the ground bent upwards over two dead water regions, one beneath each inlet. When the first streaklines reached the inlets, two trailing vortices at each inlet started rotating. Obviously, the two inlets influenced each other very little. Their flow field at this point of the test resembled therefore that of two single inlets.

The trailing vortices on the outside of the two inlets increased their rotation with increasing inlet velocity. The two trailing vortices between the two inlets moved closer and closer together until they combined and formed one vortex spanning from one inlet to the other. (See Fig. 14a.)

At one of the next steps, a ground based inlet vortex was formed at one inlet only. Also one ground vortex occurred growing and collapsing as before (Figure 14b). The ground based inlet vortex could form at either inlet. Sometimes it disappeared and formed again at the other inlet with an opposite turning direction. Its sense of rotation was always from the outside towards the symmetry plane between the inlets.

At a higher inlet velocity the inlet vortex system consisted of a ground based inlet vortex at each inlet, a vortex between the two inlets and ground vortices in front and on the sides of the inlets (Figure 14c). The system was unstable, sometimes disappearing partially or totally. The ground vortex in front of the inlet vortices formed, grew and collapsed at irregular intervals, the disturbances of the flow field becoming stronger for increasing free stream velocity.

Figures 15 through 17 show some photographs taken during the tests. There are three photographs for each test point to show the unsteadiness of the flow. The ground based inlet vortices, the ground vortex in front of the inlets and the vortex spanning from inlet to inlet can be seen on Figure 15. At U_i = 100 cm/sec (18 psig) the core of the vortex from inlet to inlet is visible whereas on the other pictures only the spiraling path of the bubbles from the bubble line producer around this vortex core can be seen. The bubbles fed into the ground vortex form a bubble tube around its core. The series of photographs show various stages of the growing and collapsing cycle.

Figure 16 shows the stronger disturbances at U_∞ = 6.5 cm/sec. Here is a higher inlet velocity necessary for the formation of the inlet vortex system.

For a free stream velocity of U_∞ = 10.3 cm/sec the inlet vortex occurs sporadically only, bursts immediately and disappears. The inlet velocity is close to the value which is no more sufficient to form the inlet vortex system.

3. VERTICAL INLET OVER GROUND

Up to here only inlets with a horizontal axis pointing into the free stream were tested. The influence of the suction of these inlets was much larger on the flow upstream than on the flow downstream of the inlet plane. However, the analytical flow model which will be developed in Chapter IV replaces the inlet by a potential sink and does not have this upstream pointing suction of the horizontal inlets. An inlet with a flow field which comes closer to that of a sink is the vertical inlet shown in Figure 1c, page 8 . Therefore it was tested at the same flow conditions and in the same way as the single, horizontal inlet. (See Section 1.) The inlet velocities for which the ground based inlet vortex appeared are given in Table III.

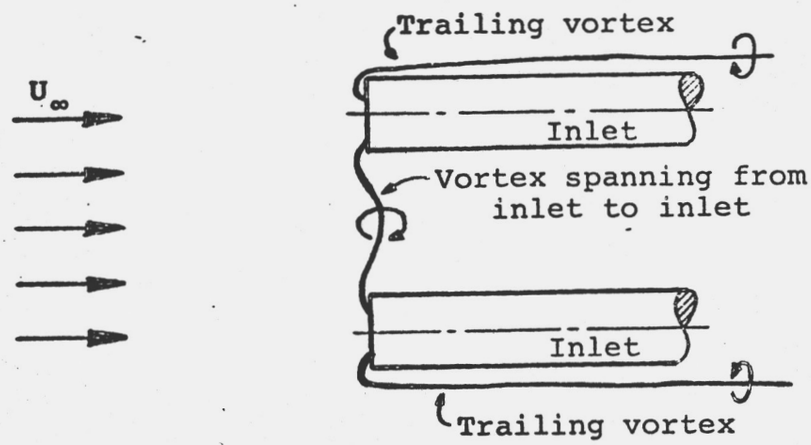

(a) U_{ia}

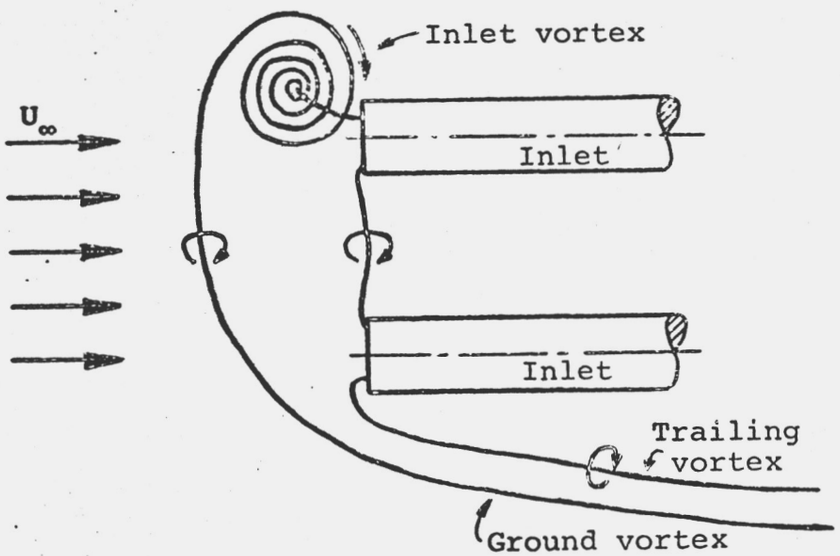

(b) U_{ib}

$U_{ia} < U_{ib} < U_{ic}$; U_∞ = constant

Figure 14. Vortex system of double inlets over ground, top views.

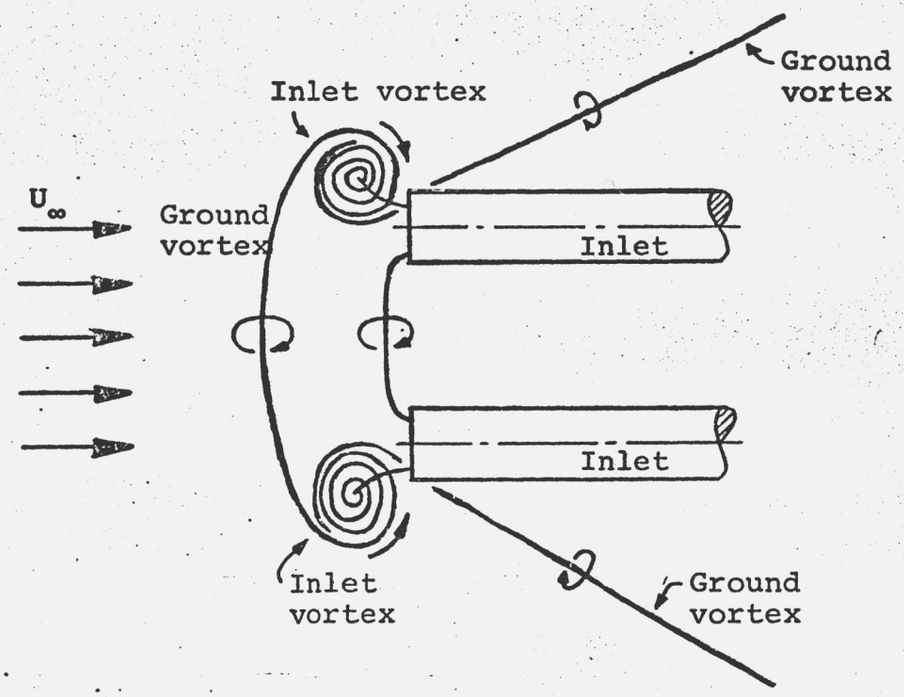

(c) U_{ic}

Figure 14. (continued)

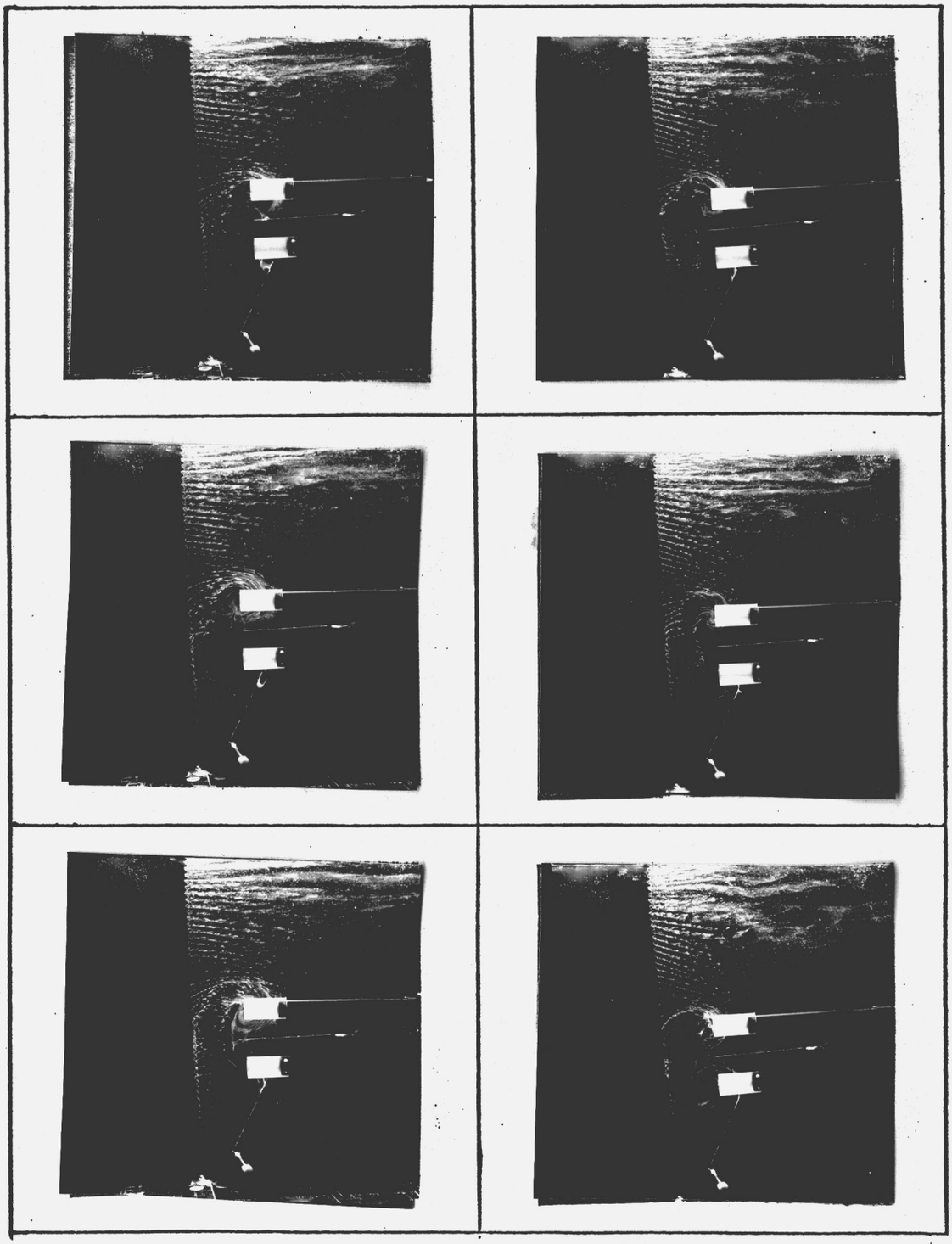

U_i = 100 cm/sec U_i = 165 cm/sec

Figure 15. Double inlet, top view, h/D = 2.5, $\bar{h}$/D = 3.2, U_∞ = 2.5 cm/sec.

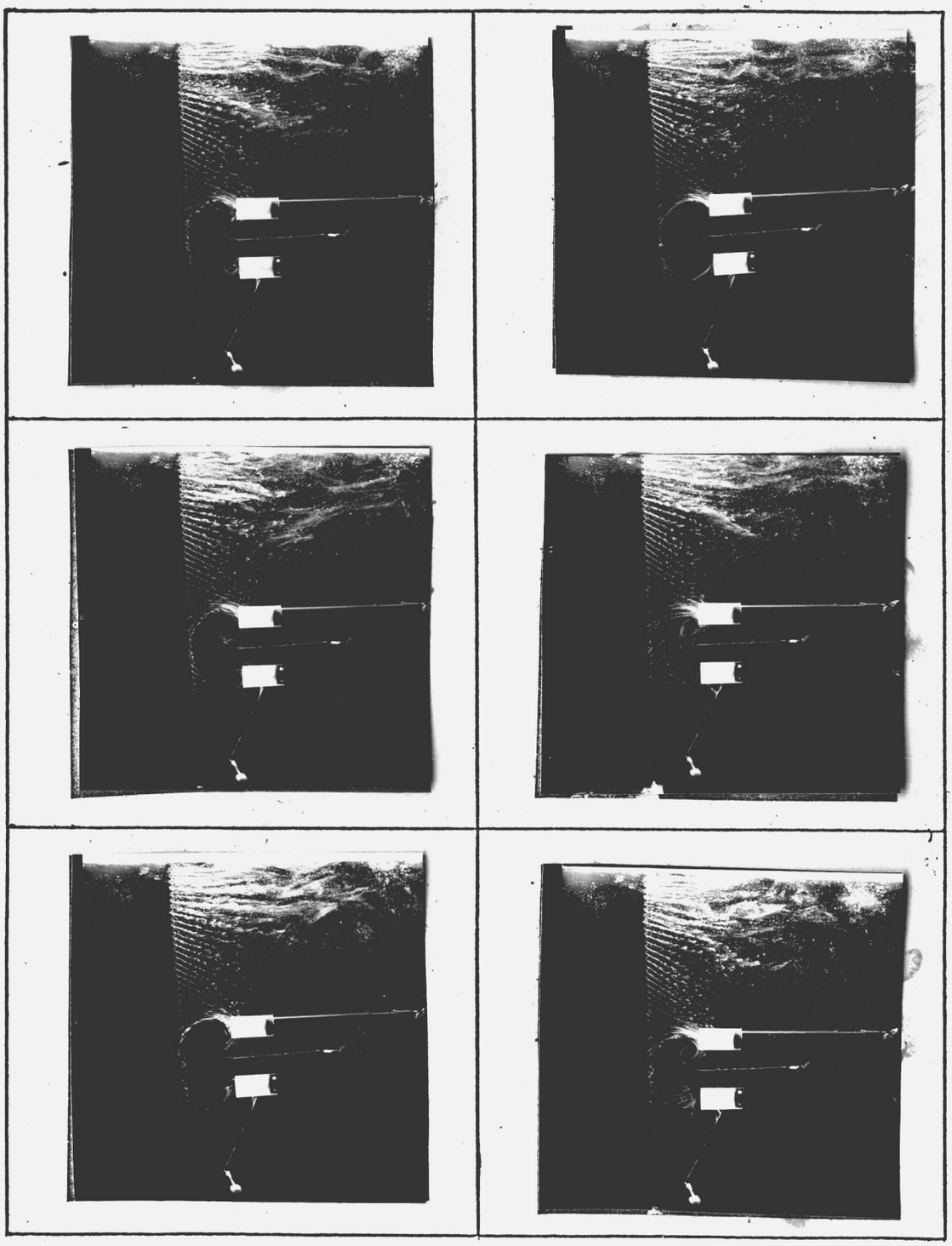

U_i = 230 cm/sec U_i = 270 cm/sec

Figure 15. (continued).

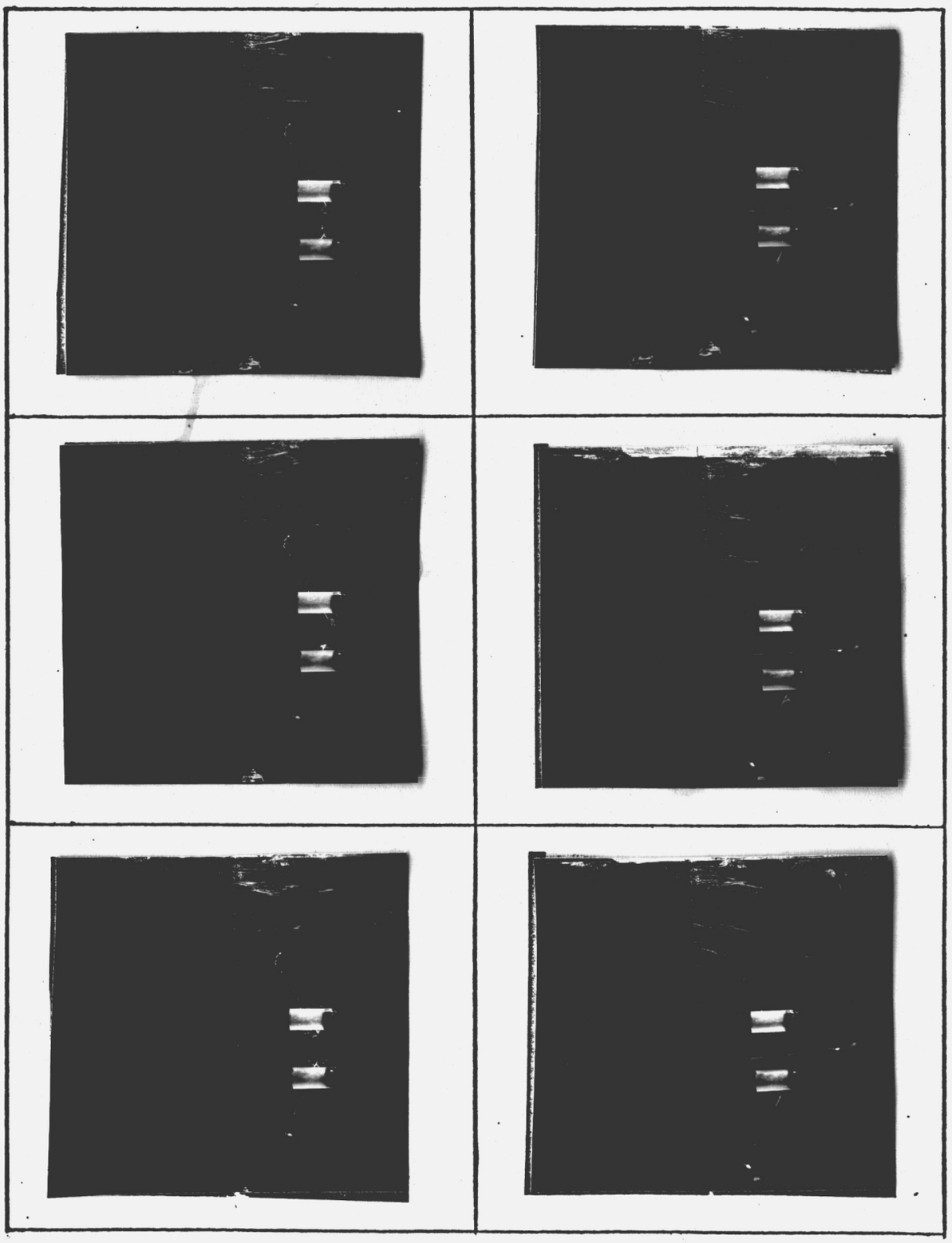

U_i = 150 cm/sec U_i = 203 cm/sec

Figure 16. Double inlet, top view, h/D = 2.5, $\bar{h}$/D = 3.2, U_∞ = 6.5 cm/sec.

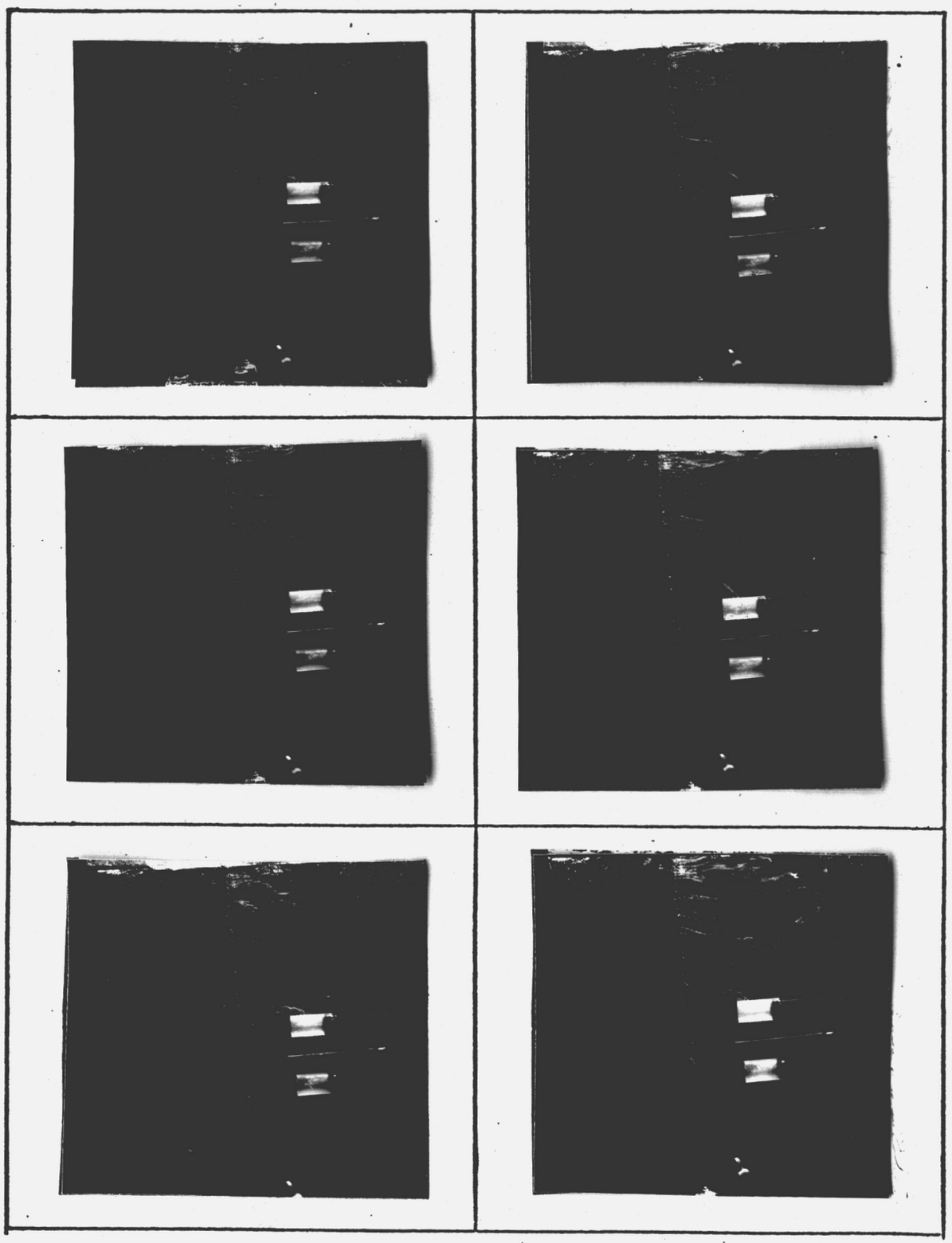

U_i = 240 cm/sec U_i = 272 cm/sec

Figure 16. (continued).

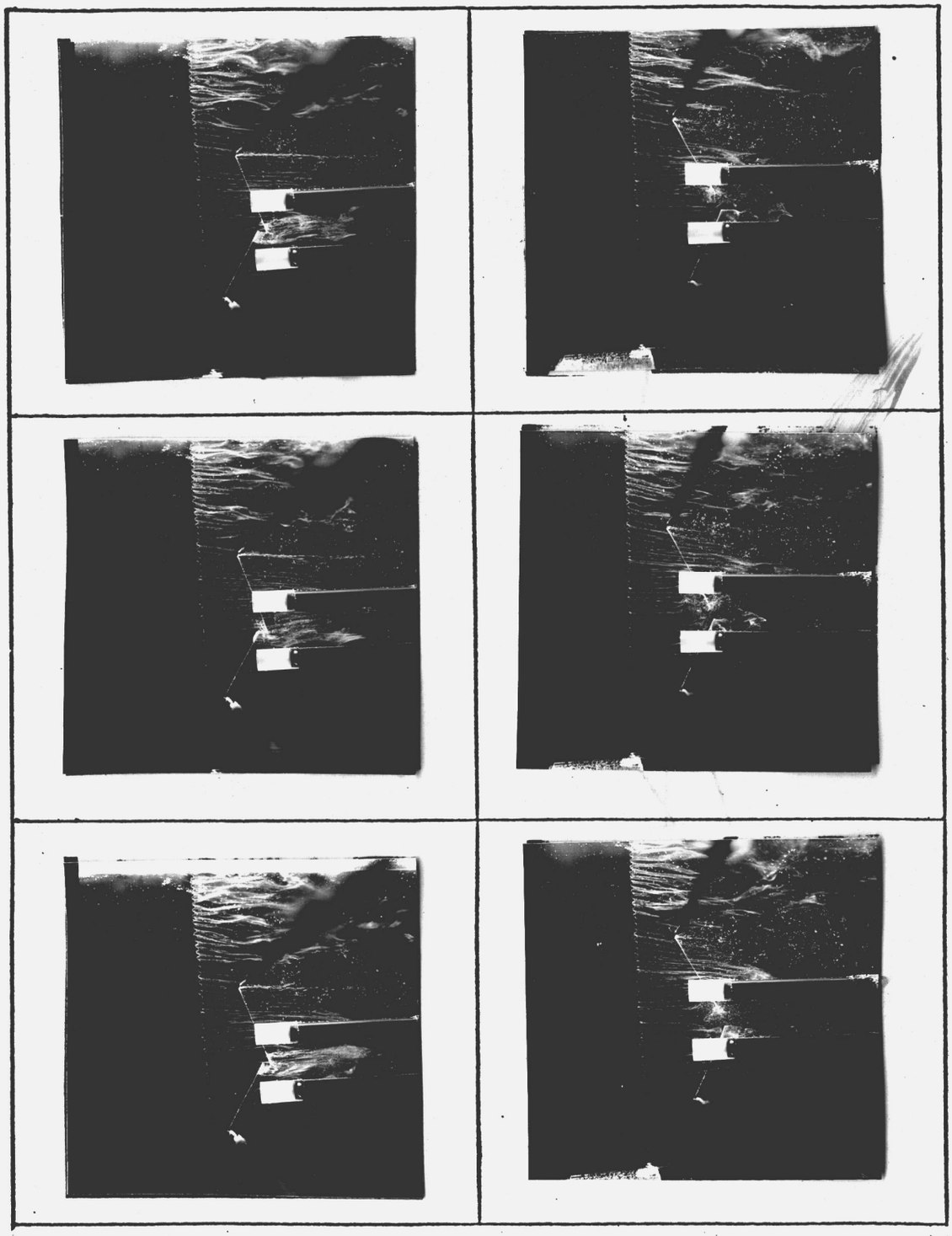

U_i = 165 cm/sec U_i = 203 cm/sec

Figure 17. Double inlet, top view, h/D = 2.5, $\bar{h}$/D = 3.2, U_∞ = 10.3 cm/sec.

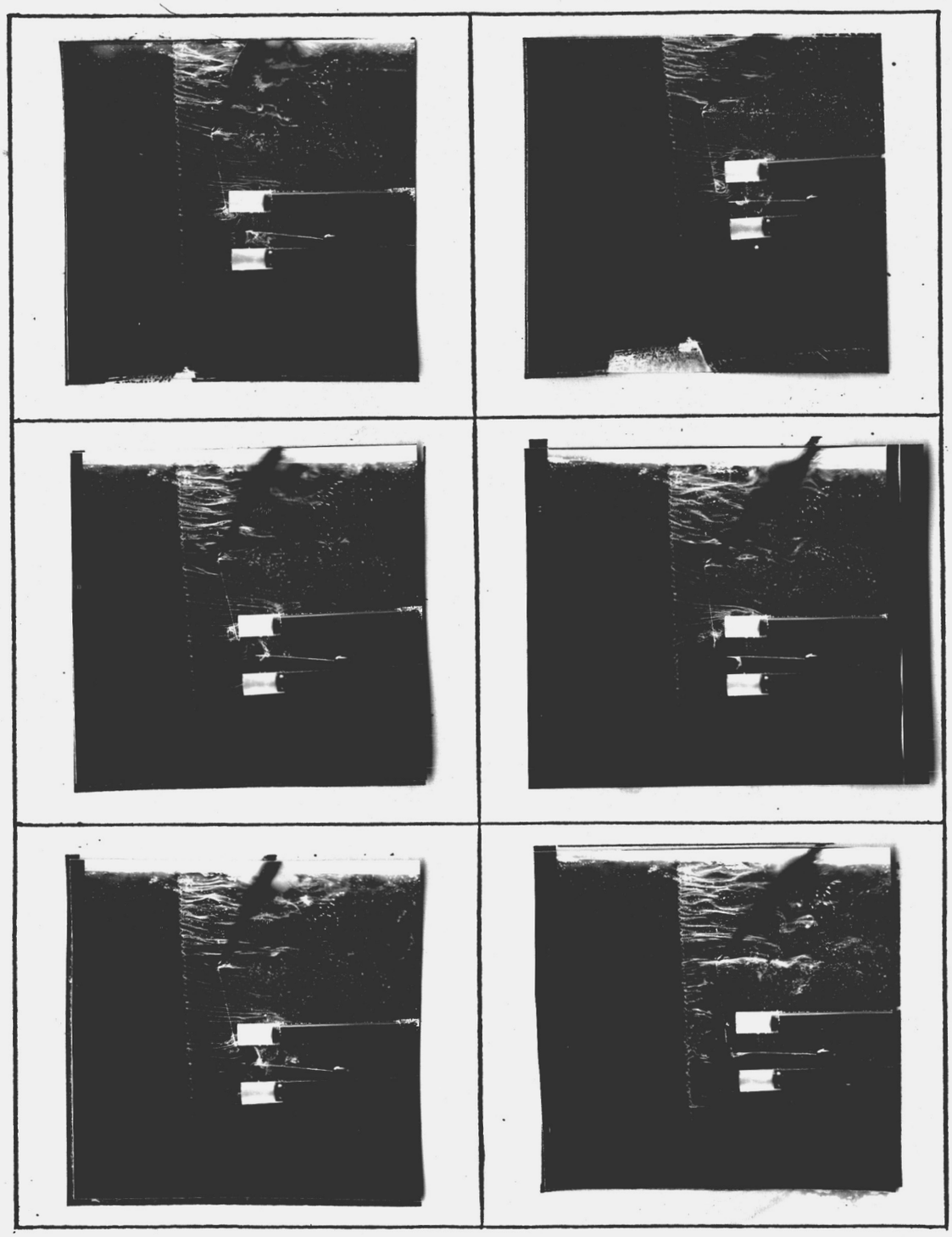

U_i = 240 cm/sec U_i = 270 cm/sec

Figure 17. (continued).

TABLE III

FIRST APPEARANCE OF GROUND BASED INLET VORTEX, VERTICAL INLET

h/D	U_∞ (cm/sec)	U_i (cm/sec)	U_i/U_∞
1.5	2.5	43	17.0
1.5	6.6	43	6.5
1.5	10.0	76	7.5
1.5	14.0	94	6.8
1.5	17.0	112	6.6
2.0	2.5	76	30.0
2.0	6.6	76	11.5
2.0	10.0	112	11.0
2.0	14.0	266	19.4
2.0	17.0	300	17.6
2.5	2.5	112	44.0
2.5	6.6	150	22.7
2.5	10.0	191	18.7
2.5	14.0	266	19.4
2.5	17.0	315	18.5
3.0	2.5	191	75.0
3.0	6.6	231	35.0
3.0	10.0	330	32.5
3.0	14.0	386	28.1
3.0	17.0	483	28.4

Except for slight differences the formation of the inlet vortex system was the same as with the inlets before. For low inlet velocities a dead water was formed behind the inlet. However, when the streaklines reached the inlet the turning in the dead water was irregular. This was due to the influences of the vortices shed behind the inlet tubing. The ends of these vortices were sucked into the inlet and the flow bent and stretched them such that they ended up in a horizontal position close to the inlet. Some of them even reached the ground. At a higher inlet velocity the ground based inlet vortex, a trailing inlet vortex and the ground vortices appeared. During the tests with h/D = 3.0 the foot of the inlet vortex was sometimes moving to a point which was up to four inlet diameters downstream from the inlet center line. This was the furthest the vortex foot

moved during all tests and with all inlets. The ground based inlet vortex entered the inlet always in the downstream half of the inlet area.

A comparison of Table III with Table II, shows that, except for some data scattering, the inlet vortex was formed at the vertical inlet with a lower inlet velocity than at the horizontal inlet. Therefore, the ground based inlet vortex was visible in all tests with the vertical inlet whereas it was not with the horizontal inlet.

The growing and collapsing cycle of the ground vortex in front of the ground based inlet vortex, which was noticed at the single inlet and the double inlets over ground, did not occur at most test conditions and could hardly be seen for h/D = 3.0 and high free stream velocities.

4. IMAGE INLETS.

It is of high interest to find the vorticity source on which the ground based inlet vortex feeds. One potential source is the boundary layer of the ground plane. Therefore, tests were arranged which had a flow plane of symmetry. This plane can be regarded as a ground plane without boundary layer. We will see that the ground based inlet vortices appeared again in spite of the absence of a ground boundary layer. The test arrangement is illustrated by Figure 18 and the dimensions are shown in Figure 1d.

The formation of the vortex system followed the same pattern as before (Fig. 18). However, at low inlet velocities a region of random motion was formed instead of a dead water region. Shape and location of the random motion area between the two inlets are shown in Fig. 18a. The size of this region grew, when the inlet velocity was increased until it reached both inlets. (Fig. 18b) At this speed short-lived trailing inlet vortices appeared. At somewhat higher inlet velocity (Fig. 18c) a vortex spanning from one inlet to the other formed. This is the equivalent to the two ground

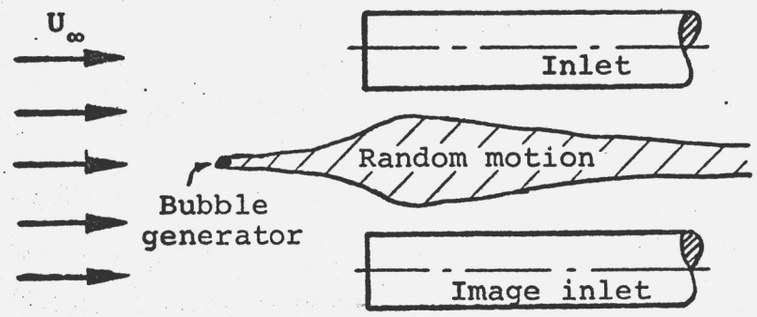

(a) U_{ia}

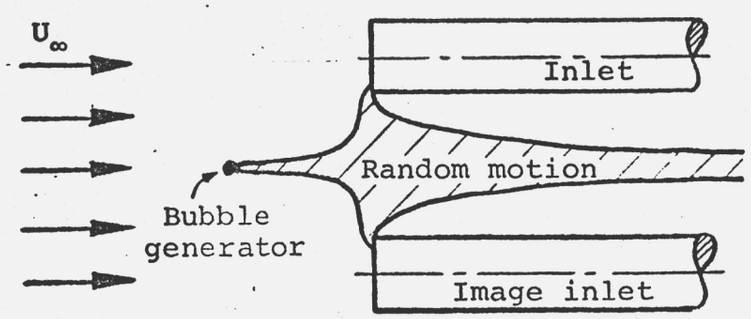

(b) U_{ib}

$U_{ia} < U_{ib} < U_{ic} < U_{id}$; U_∞ = constant

Figure 18. Formation of the vortex system at two image inlets, side views.

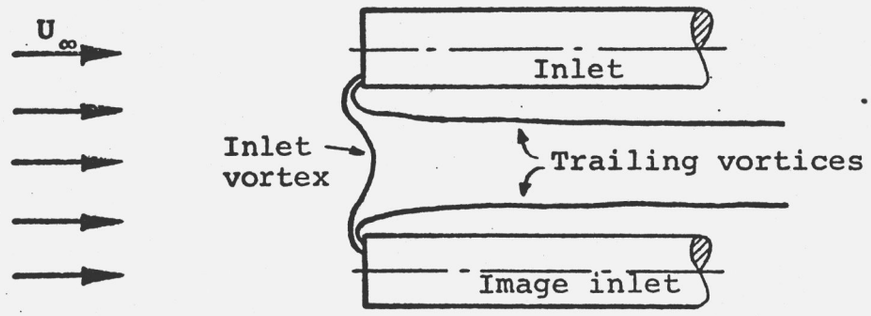

(c) U_{ic}

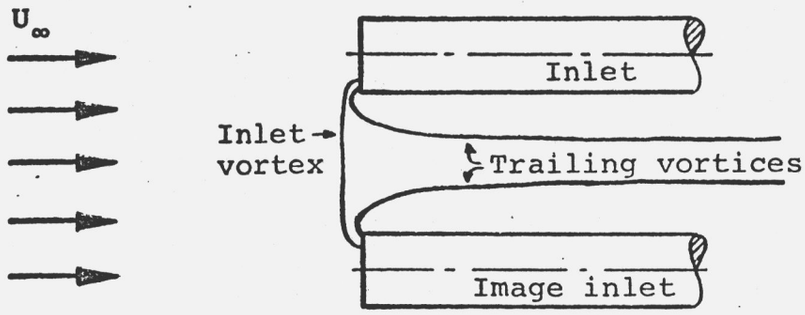

(d) U_{id}

Figure 18. (continued).

based vortices one would have, if there were a material plane between the two inlets. Therefore, we put the adjective "ground based" in quotation marks. An equivalent to the ground vortices did not appear.

Both the "ground based" inlet vortex and the two trailing inlet vortices moved around vigorously. In some tests the vortex system collapsed going through the following steps (Figure 19): The "ground based" inlet vortex and the trailing inlet vortices suddenly increased their rotational speed and size. This higher rotation moved the trailing inlet vortices against the flow, away from the inlet tubing (Figures 19a and 19b). At an angle of about 45 degrees relative to the inlet axis, the farther downstream parts of the trailing inlet vortices broke up and formed several ring vortices (Figure 19c) which drifted downstream. The two parts of the trailing inlet vortices remaining at the inlets linked together. This new "ground based" inlet vortex, spanning from one inlet to the other, increased its strength further, moved in front of the inlets and combined with the original "ground based" inlet vortex (Figures 19c and 19d). Because of their opposite rotation the two vortices extinguished each other. For a moment no vortex was visible but then the vortex system formed again and the growing and collapsing sequence repeated with irregular frequency.

The tests with a single inlet had been performed with inlet flow rates up to the maximum rate obtainable with the available pump. Because the same pump was used for operating both inlets simultaneously the maximum flow rate for one inlet in the image inlet configuration was only about half of the maximum flow rate of the single inlet configuration. This reduced the upper limit of the test range of the inlet velocities. The inlet velocities at which the "ground based" inlet vortex first appeared, are given in Table IV.

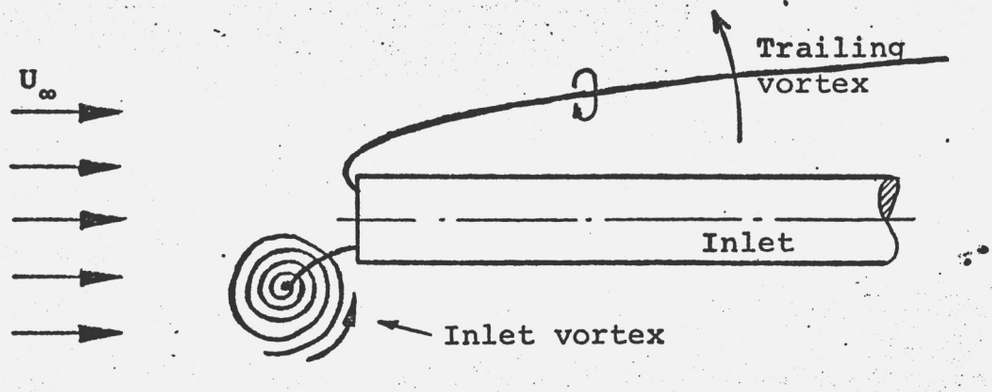

(a) Trailing vortex starts moving outwards

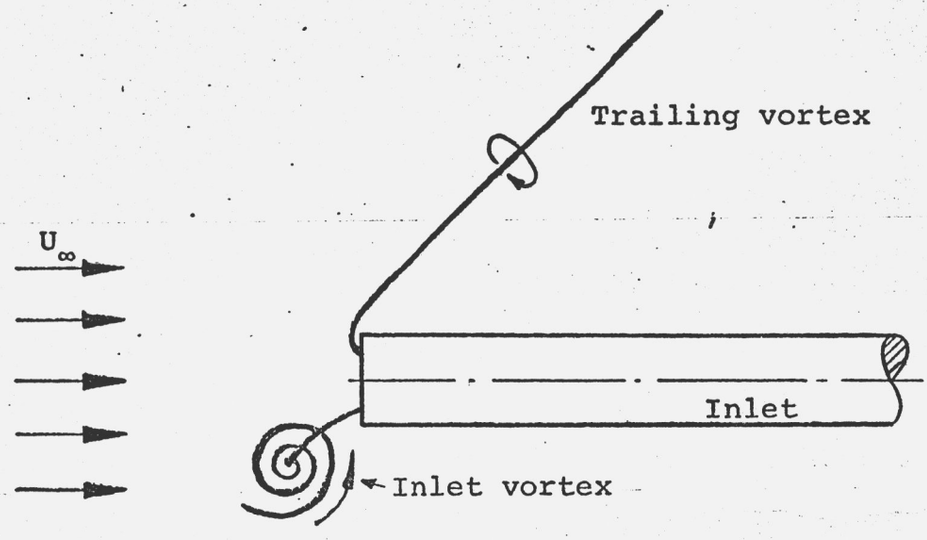

(b) Trailing vortex reaches final position

Figure 19. Collapsing of the vortex system on inlet with image, top views.

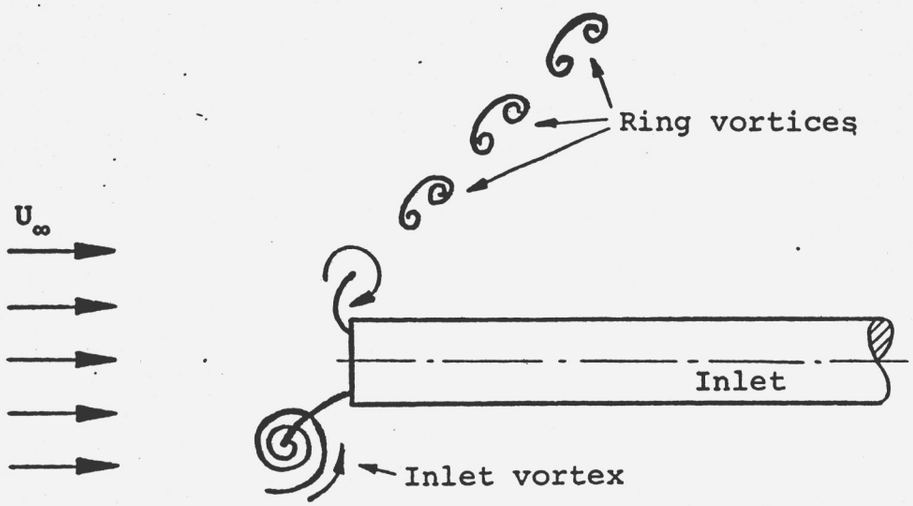

(c) Trailing vortex breaks into ring vortices and additional "inlet vortex"

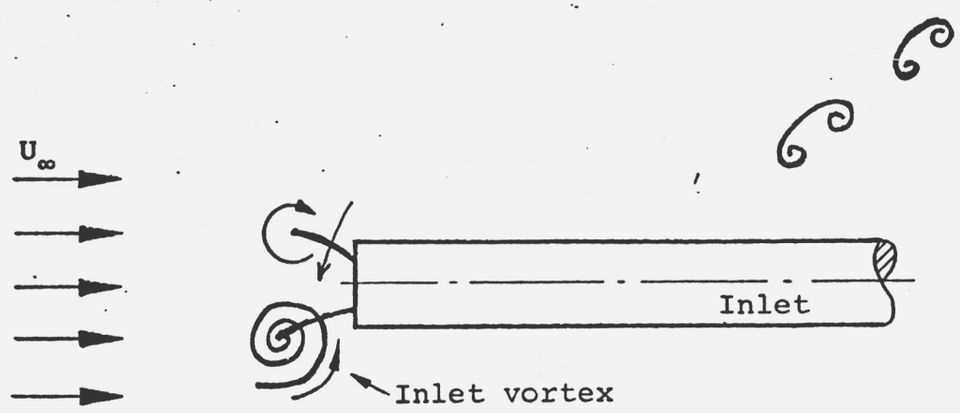

(d) New "inlet vortex" collapses into inlet vortex

Figure 19. (continued).

Figure 20 through 22 show the streaklines in the symmetry plane between the two inlets at different flow conditions. The view is from the top and slightly from the front of the two inlets. For U_i = 60 cm/sec (20 psig) and U_i = 150 cm/sec (15 psig) on Figure 20 the flow is symmetrical, i.e., the vortex system did not yet form. The flow is unsymmetrical for U_i = 215 cm/sec (10 psig) and U_i = 270 cm/sec (5 psig). This is due to the vortices located between the two inlets where they are not visible.

On Figure 21 the trailing inlet vortices disturb the flow on the right side (looking upstream) of the inlets in the first three pictures at U_i = 100 cm/sec (18 psig). The pictures at U_i = 180.0 cm/sec (13 psig) show the breaking-up of the trailing vortex at various stages. In Fig.21 (cont.) in the photograph in the upper left hand corner, one of the trailing vortices can be seen partially as a white conical tube on the side of the inlet tubing. Again on Figure 22 the violent breaking-down of the vortex system is captured. With the help of a bubble line generator the lower trailing inlet vortex is visualized on Figure 23 in a side view.

TABLE IV

INLET SPEED FOR FIRST APPEARANCE OF INLET VORTEX, INLET WITH IMAGE.

h/D	U_∞ (cm/sec)	U_i (cm/sec)	U_i/U_∞
1.5	2.5	80	32
1.5	6.6	150	23
1.5	10.0	240	24
1.5	14.0	270	19
1.5	17.0	-	-
2.0	2.5	115	46
2.0	6.6	260	39
2.0	10.0	-	-
2.0	14.0	-	-
2.0	17.0	-	-
2.5	2.5	270	108
2.5	6.6	-	-
2.5	10.0	-	-
2.5	14.0	-	-
2.5	17.0	-	-

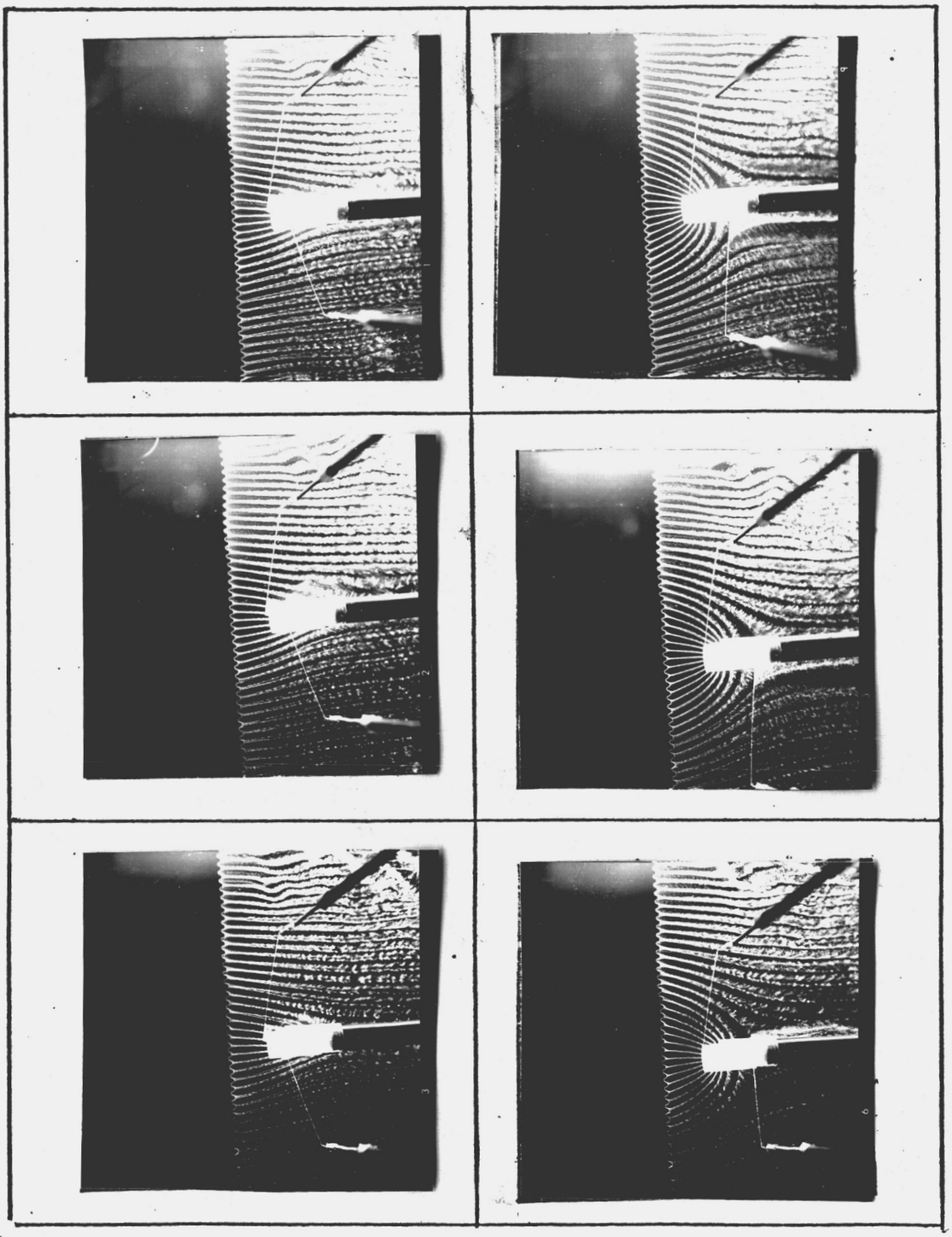

U_i = 60 cm/sec U_i = 150 cm/sec

Figure 20. Image inlets, top view, h/D = 1.5, U_∞ = 2.5 cm/sec.

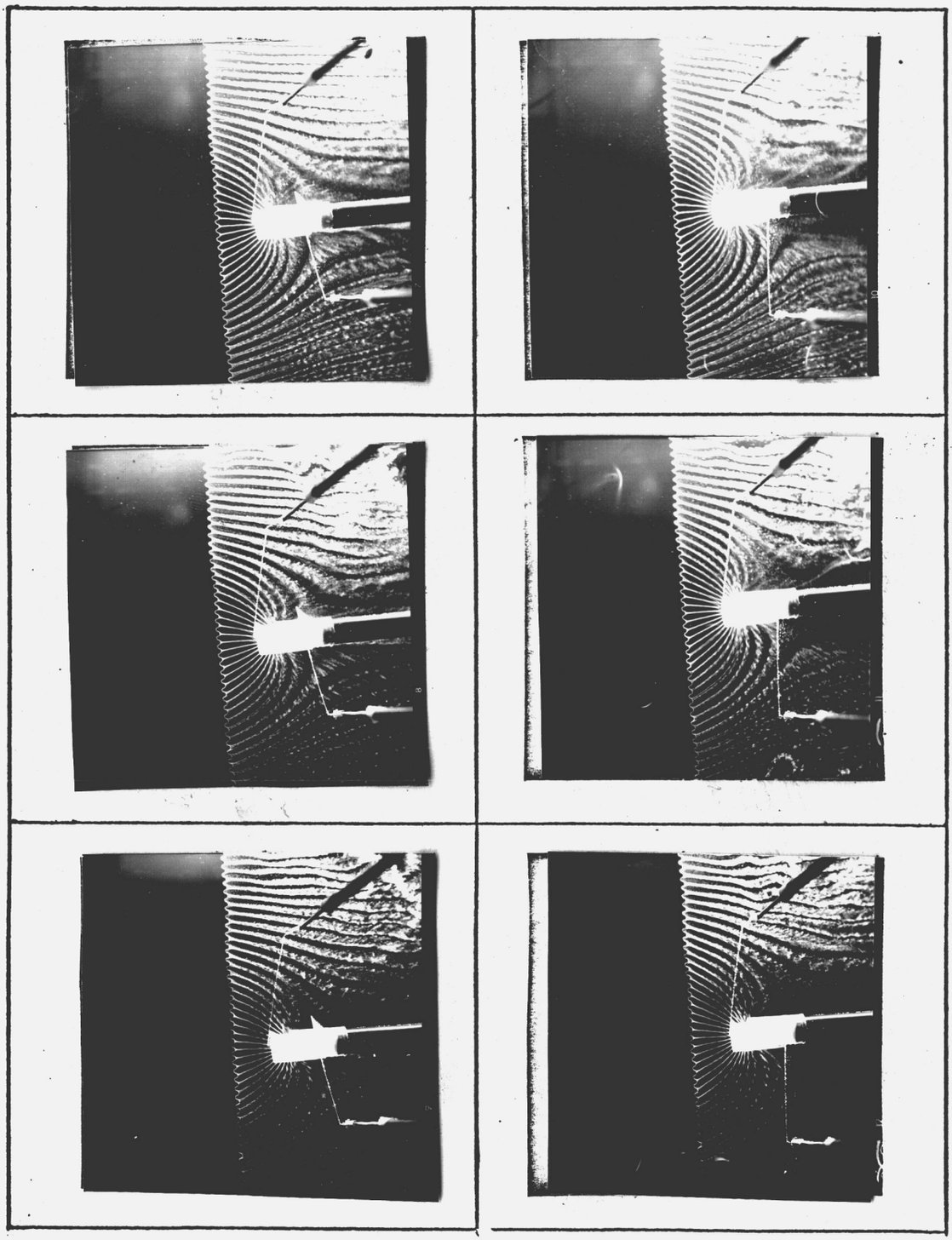

U_i = 215 cm/sec

U_i = 270 cm/sec

Figure 20. (continued).

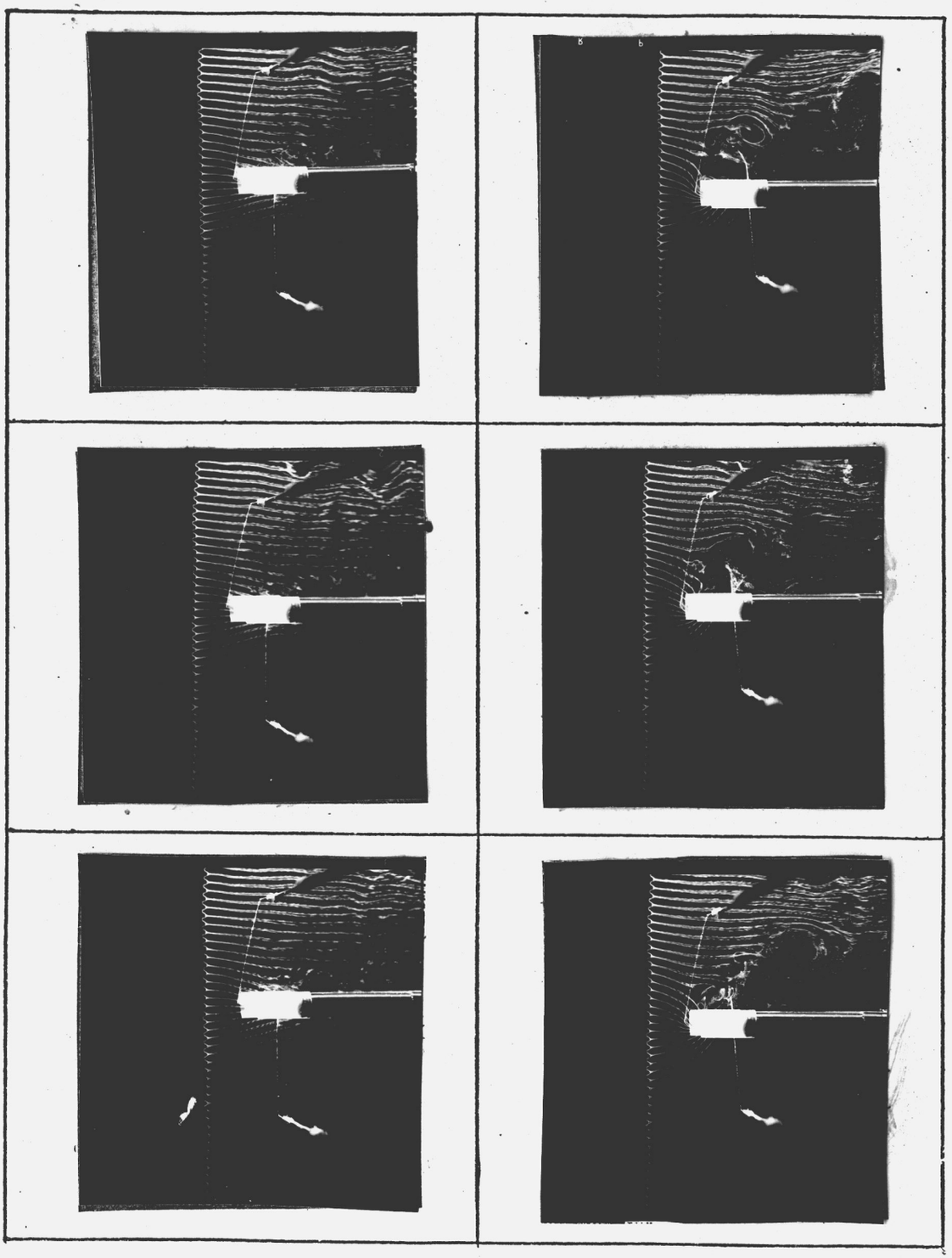

U_i = 100 cm/sec U_i = 180 cm/sec

Figure 21. Image inlets, top view, h/D = 1.5, U_∞ = 6.6 cm/sec.

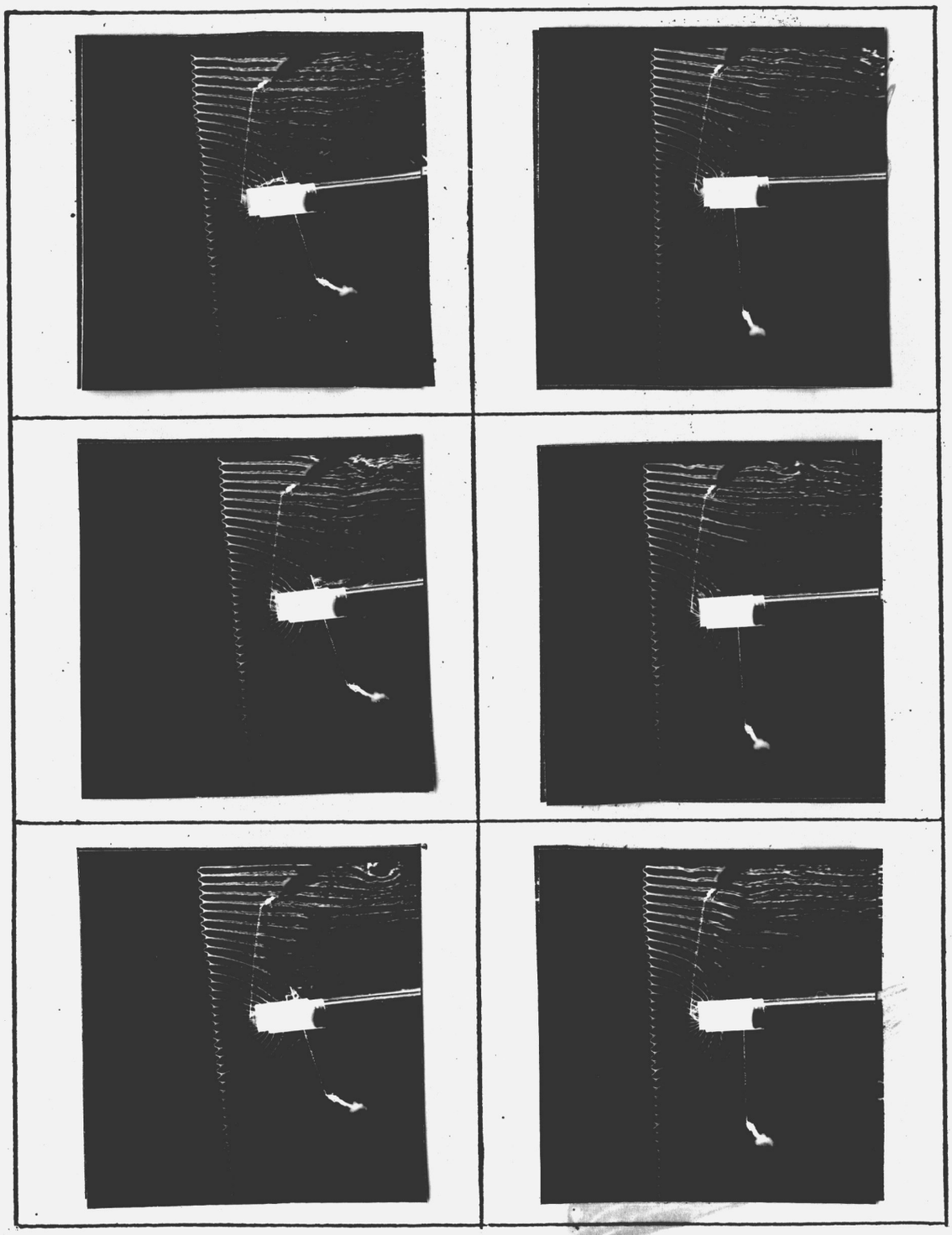

U_i = 230 cm/sec

U_i = 270 cm/sec

Figure 21. (continued).

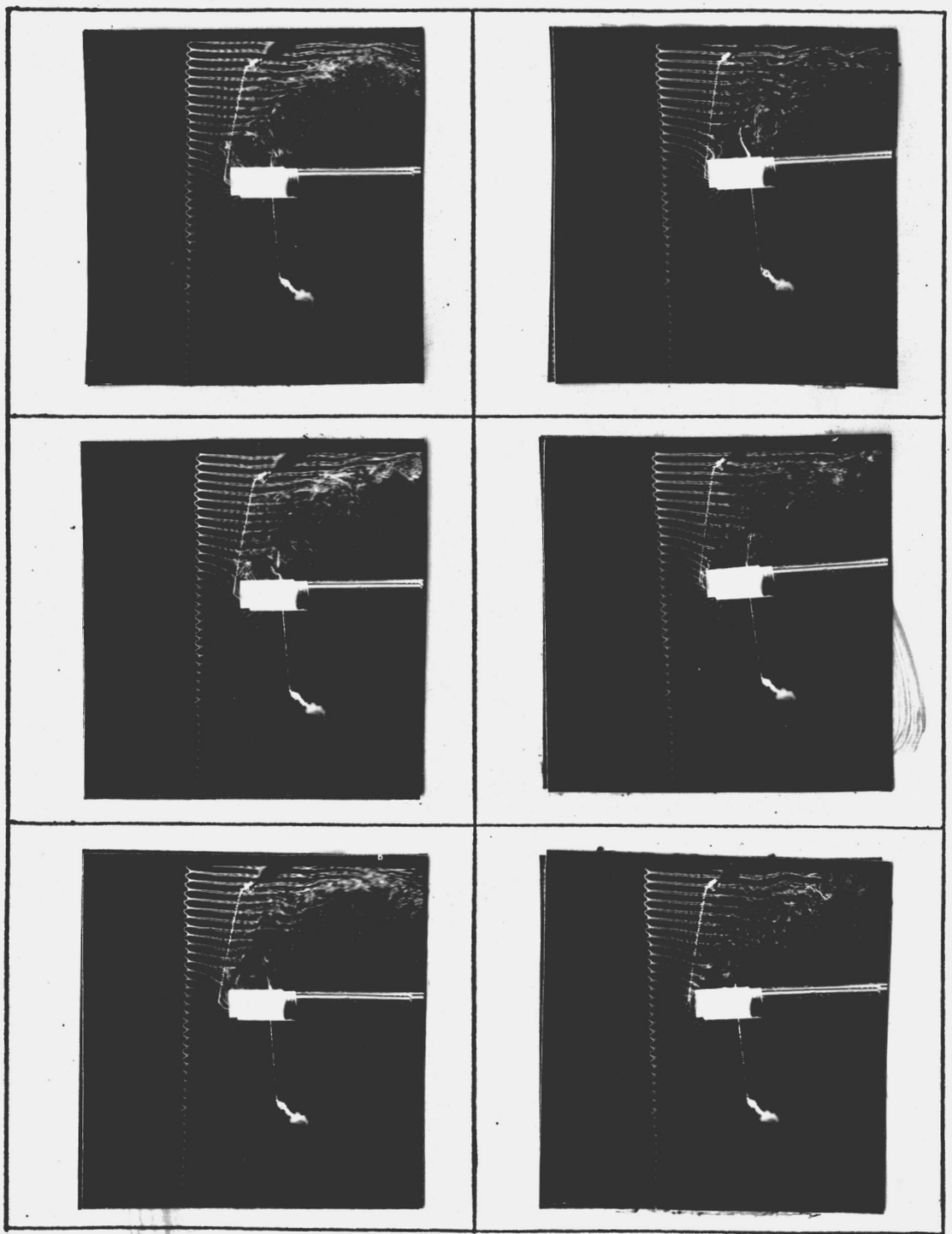

U_i = 200 cm/sec U_i = 230 cm/sec

Figure 22. Image inlets, top view, h/D = 1.5, U_∞ = 10 cm/sec.

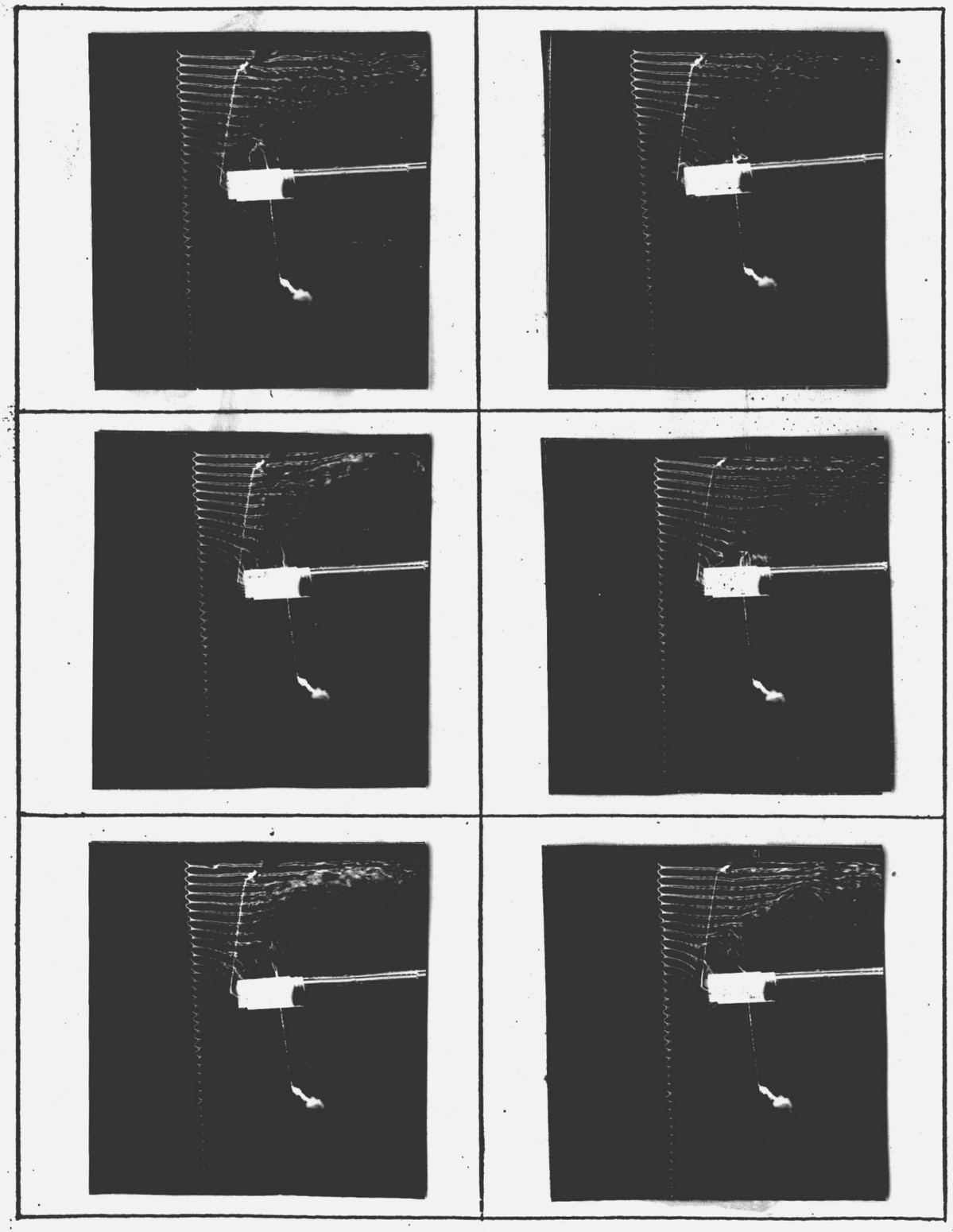

U_i = 250 cm/sec U_i = 270 cm/sec

Figure 22. (continued).

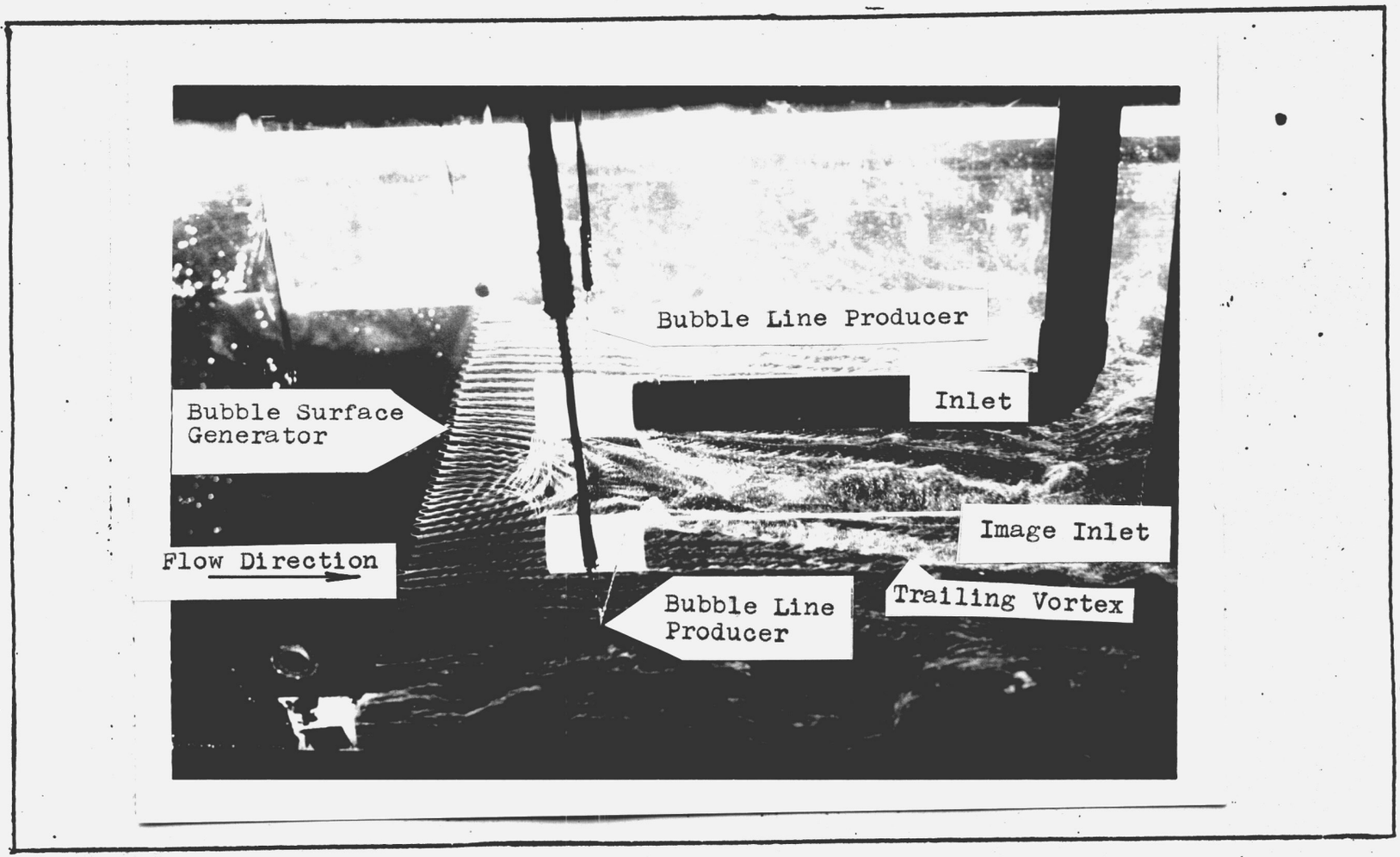

Figure 23. Trailing inlet vortex at image inlet.

A series of exploratory tests was conducted besides the described systematic tests. The influence of the flow uniformity was investigated by using an additional screen (15 mesh, 0.25 mm wire diameter, 73.1 percent open area) spanning the whole test section. The maximum distance of that screen from the inlets was 60 cm, the minimum distance about 15 cm. The closer the screen came to the inlet, the more unstable the inlet vortex system became (the vortices jumped around wildly) and the more the bubble-lines produced by the bubble generator became fuzzy and the quality of the visualization deteriorated.

In other tests a vertical bubble surface generator in the plane of the inlet axes was used. With the flow arranged such that a streakline hit either the stagnation point S_2, below the lower inlet or the stagnation point, S_1, above the upper inlet (See Fig. 24), one could there observe the forming of vortices. The streaklines, which hit these stagnation points, were split into two branches, one going into the inlet the other going downstream with the free stream flow. The downstream branch of the vortices was straight with an angle α to the inlet axis. (See Figure 24.) This angle increased for larger free stream velocities but never exceeded about 10 degrees. The vortices occurred for all free stream velocities except for the very low U_∞ = 4.7 cm/sec (1 mA). They formed and disappeared irregularly. It looked as if they wanted to form but did not succeed and broke down, their rotational speed increasing steadily during this process. A preferred turning direction could not be detected. Tests with a bubble line producer instead of the vertical bubble surface generator showed that now much weaker vortices were formed everywhere around the inlet tubing. The bubble line producer was mounted in the test section under different angles to the free stream flow direction.

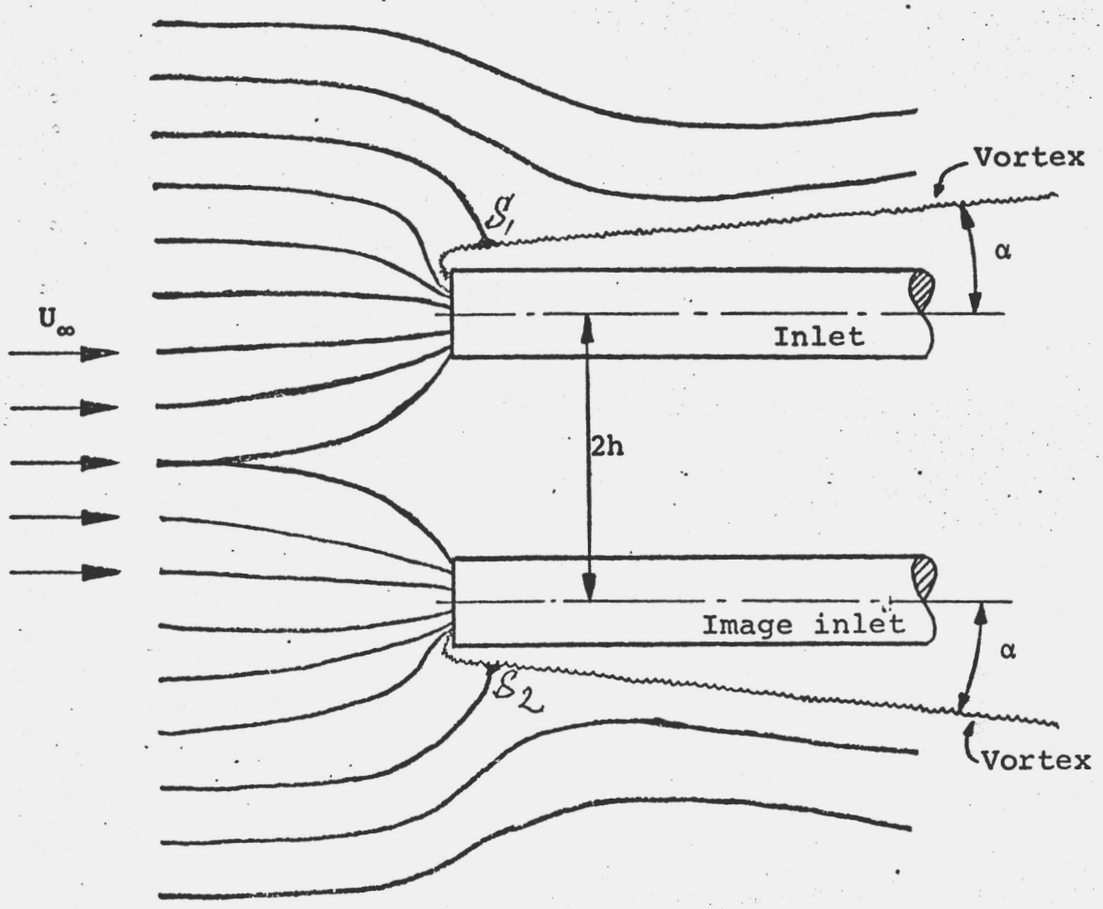

Figure 24. Vortices around inlets, side view.

A test with h/D = 2.5, U_∞ = 2.5 cm/sec (0.0 mA), and U_i = 270 cm/sec (5 psig) showed the influence of the bubble generator wire and its position on the inlet vortex. With the horizontal bubble surface generator about 1 1/2 inches in front of the inlets and in their symmetry plane the inlet vortex spanned from inlet to inlet moving only slightly. This inlet vortex became weaker and weaker until it disappeared when the bubble generator wire was shifted out of the symmetry plane for about half an inch. This diminishing was visualized with the help of two bubble line producers one on each side of the inlet vortex. For smaller h/D values this effect could not be observed.

At the same h/D value several thin secondary vortices in the front part of the two trailing inlet vortices (see Figure 25) could be seen. Sometimes one of them moved forward and joined the inlet vortex which bent and moved around because of this interaction. Most of the secondary vortices formed and disappeared again as if torn apart. Their turning direction as shown in Figure 25 is explained in Chapter IV.

Some other tests showed the dependence of the inlet vortex on the free stream vorticity. On Figure 26 one sees a side view of the image inlets with a strong "ground based" inlet vortex turning clockwise. The thin white line is its core. There is an obstacle consisting of a flat piece of wood (about 2 1/2 cm wide) on the left side in front of the inlets. The inlet vortex has the same turning direction of the vortices which are shed on the side of the obstacle closest to the inlets. Without the obstacle there would be a relatively stable and weak inlet vortex turning counter-clockwise. That means the vorticity of the obstacle wake is strong enough to switch the sense of rotation of the inlet vortex from counter-clockwise into a clockwise turning vortex. So the turning direction and the strength of the inlet vortex are determined by the free stream vorticity.

The watertunnel walls are a natural source of vorticity. As expected, the turning direction of the inlet

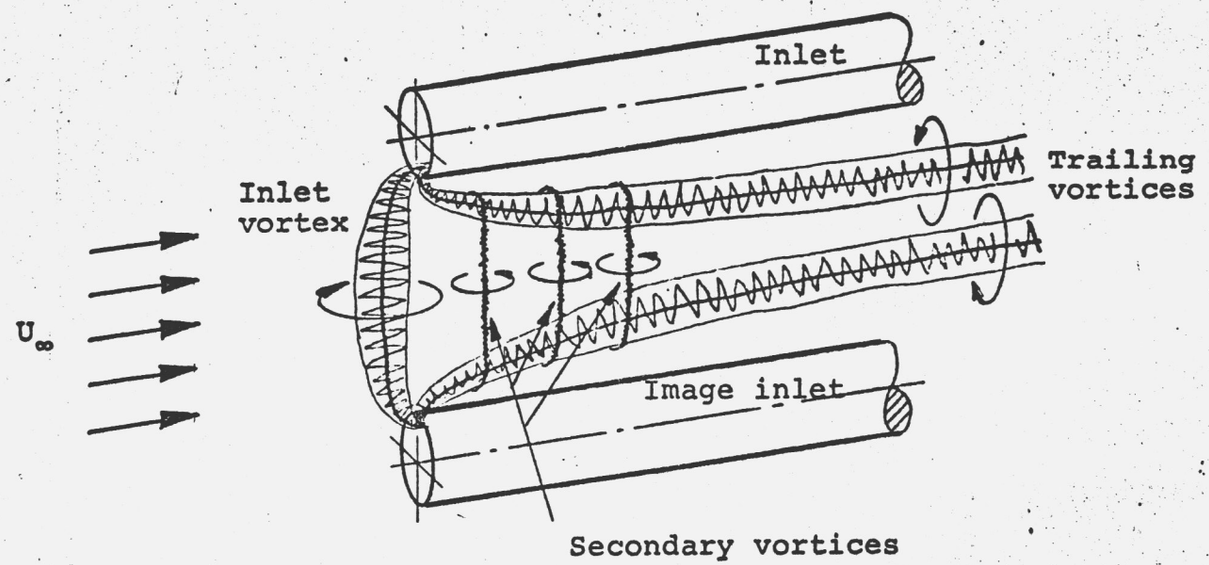

Figure 25. Secondary vortices.

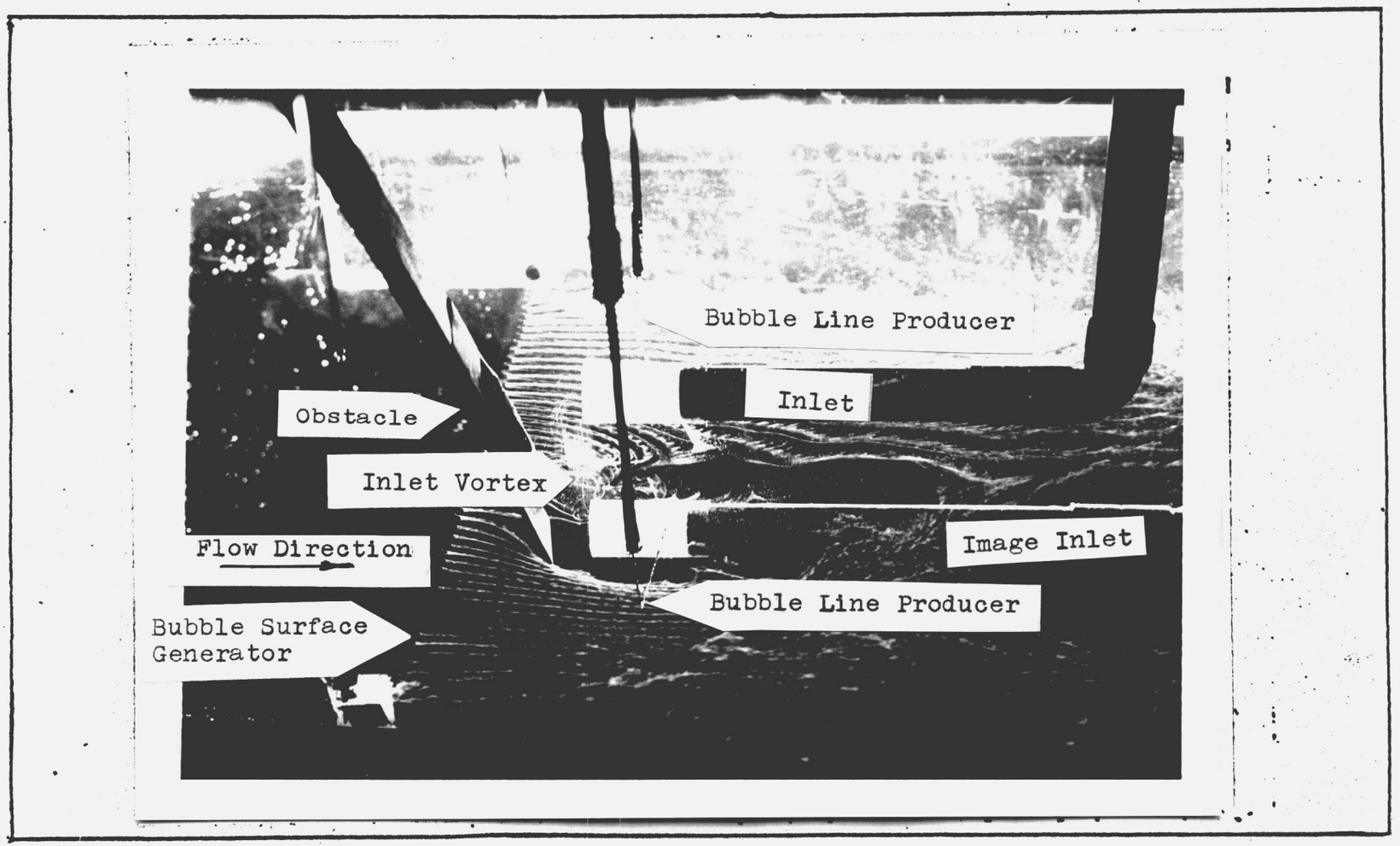

Figure 26. Influence of free stream vorticity on inlet vortex.

vortex could be switched to that of the wall vorticity by moving the inlets out of the tunnel center closer to the walls. The same happened with inlets inclined to the free stream. When they pointed more to one tunnel wall, vorticity from that wall dominated the flow field and the inlet vortex system. This was the reason for not conducting tests with inclined inlets.

5. SUMMARY OF TESTS.

The tests described above verify the following four characteristics of the ground based inlet vortex mentioned in the literature. First: It is unstable. Second: It can form only, when there is a stagnation point on the ground. Third: It draws its vorticity from the ambient flow vorticity which is transported toward that stagnation point. Fourth: The ground boundary layer is not necessary for the appearance of a ground based inlet vortex.

In addition, the tests in the water tunnel show that the ground based inlet vortex is a member of a vortex system which also includes a trailing inlet vortex, ground vortices and secondary vortices. Instability of the ground based inlet vortex can be induced by instability of the trailing inlet vortex.

The form of the inlet plays no significant role in the inlet vortex formation. The inlet vortex also forms underneath an inlet which points vertically down as long as there is a stagnation point on the ground. Because this stagnation point exists for the vertical inlet at higher free stream velocities than in the case of the horizontal inlet, the inlet vortex also exists for higher free stream velocities. This difference is shown by a comparison of Table II, with Table III.

Vortex stretching, an obvious cause for concentration of vorticity could be seen all around the inlet. Too much vortex stretching has been observed to be the reason for the disappearance of the ground vortices and the secondary vortices.

IV. MATHEMATICAL FLOW MODELS.

1. STAGNATION POINTS AND THEIR EFFECT ON THE FORMATION OF THE INLET VORTEX SYSTEM.

The tests have shown that the inlet vortex is part of an unsteady and unstable vortex system. A thorough mathematical model describing this system is considered too complex for treatment with the available means. However, the stagnation points in this flow field play an important role in the behavior of the inlet vortex system. Therefore, the following analysis, which is confined to an investigation of the existence and location of the stagnation points, brings some valuable insight.

A line vortex which does not move with the free stream has to end in a stagnation point. Therefore, it is important to know how many stagnation points exist in the flow field around the inlet. A lower limit for the number of the stagnation points can be obtained by means of potential flow calculations where the inlet in ground effect is replaced by a sink and an image sink in a uniform flow. The stagnation points and the flow field for this sink arrangement are calculated. Changes of this flow field produced by the vortices can be added later.

Consider a potential flow field in a coordinate system as shown in Figure 27. The free stream flows from left to right in the positive x-direction. There is a sink of strength m at $z^* = h$ and an image sink of the same strength at $z^* = -h$.

The physical values of lengths, coordinates, velocities sink-strength etc. have physical dimensions and are marked by an asterisk *. The asterisk is ommitted, when these magnitudes have been made dimensionless.

In the equations nondimensional magnitudes are used. Velocities are made nondimensional by dividing by the undisturbed wind velocity U_∞, lengths are divided by the altitude, h, of the inlet above ground and the mass flux is divided by $U_\infty h^2$.

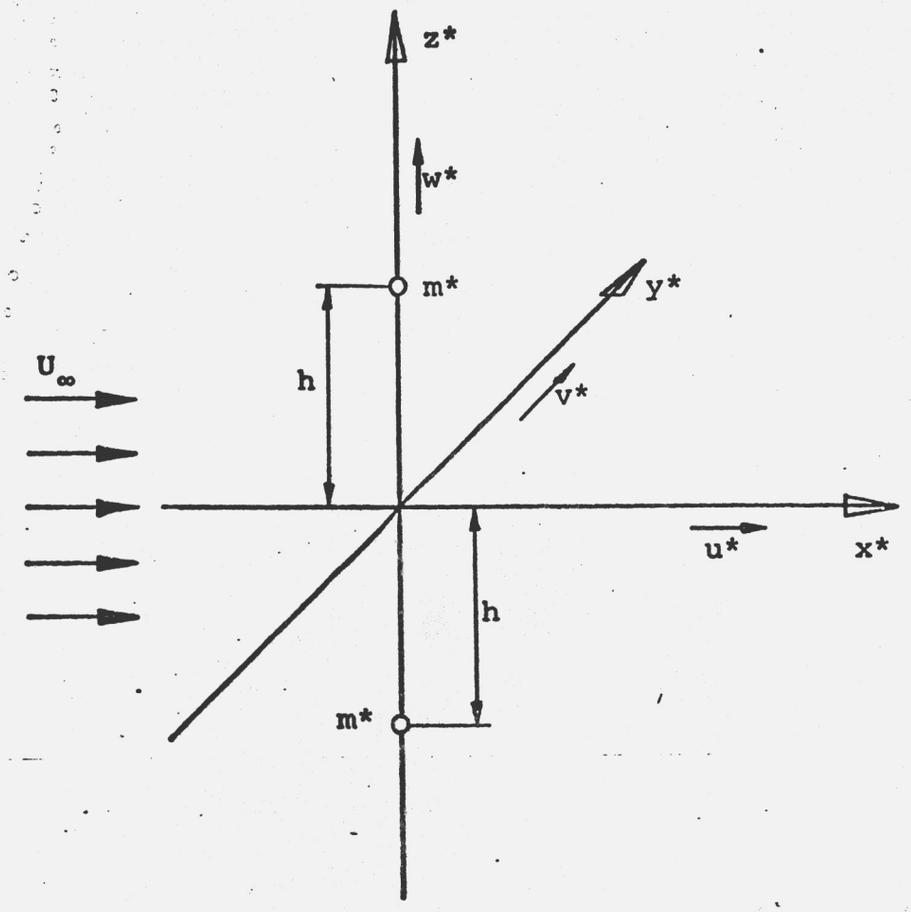

Figure 27. Coordinate system used for potential flow calculations.

The nondimensional velocity potential is

$$\phi = m\left\{\frac{1}{\left[x^2+y^2+(z-1)^2\right]^{\frac{1}{2}}} + \frac{1}{\left[x^2+y^2+(z+1)^2\right]^{\frac{1}{2}}}\right\} + x \qquad (1)$$

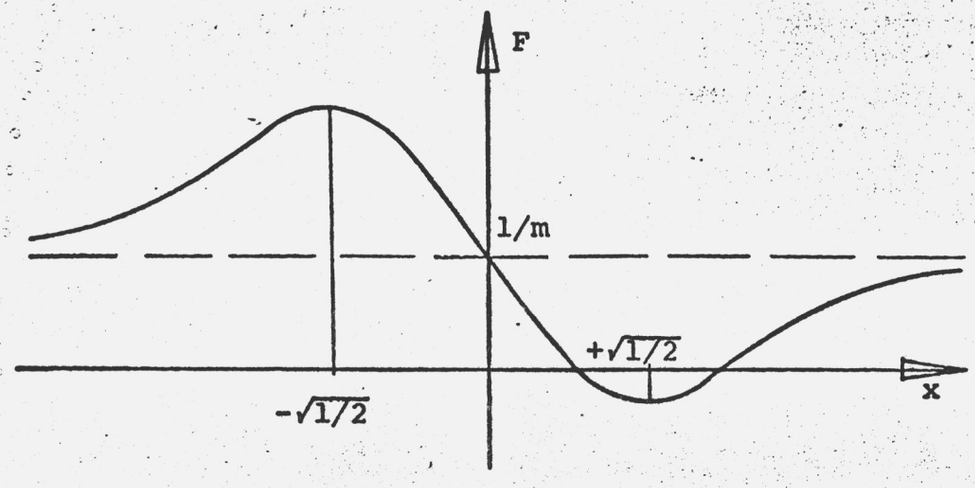

Figure 28. Sketch of function F.

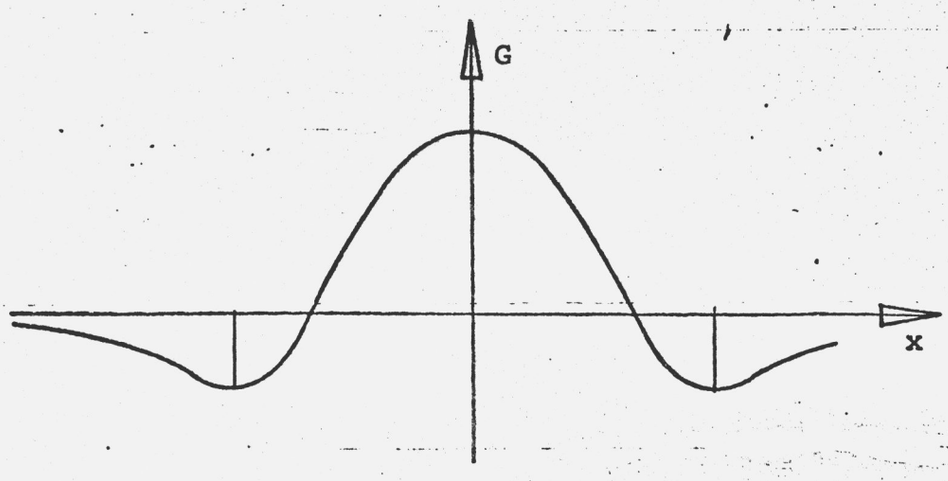

Figure 29. Sketch of function G.

The conditions for a stagnation point are that the velocity is zero, or

$$u = \frac{\partial \phi}{\partial x} = 0 \qquad v = \frac{\partial \phi}{\partial y} = 0 \qquad w = \frac{\partial \phi}{z} = 0 \quad (2)$$

which gives the three equations

$$F = -\frac{x}{[x^2 + (z-1)^2]^{3/2}} - \frac{x}{[x^2 + (z+1)^2]^{3/2}} + \frac{1}{m} = 0 \quad (3)$$

$$y = 0 \quad (4)$$

$$G = -\frac{(z-1)}{[x^2 + (z-1)^2]^{3/2}} - \frac{(z+1)}{[x^2 + (z+1)^2]^{3/2}} = 0 \quad (5)$$

All stagnation points are located in the x-z-plane.

For $z = 0$, F is sketched in Figure 28. One sees that there is either no stagnation point or one stagnation point at $x = \sqrt{1/2}$ or two stagnation points, one of which goes to $x = 0$ and the other to $x = \infty$ for increasing sink strength m. The form of Equation 3 suggest that the plot of F for a value of z different from zero will not much differ from that of Figure 28.

A plot for G is shown in Figure 29. Because for $z \neq 0$, F and G have to be zero simultaneously and G has only one zero, one can expect one or no stagnation point for one given value of z.

The actual positions of the stagnation point on and above the x-axis were found with the help of a computer program. They are plotted for different sink strength m in Figure 30. The streamlines for the different flow conditions are sketched in Figure 31. For a small sink strength there is only one stagnation point A off the x-axis (Fig. 31a). This stagnation point moves downstream and closer to the x-axis for increasing m until at $m_b = 1.299$ a second stagnation point is formed on the x-axis, B/C in Figure 31b. For further

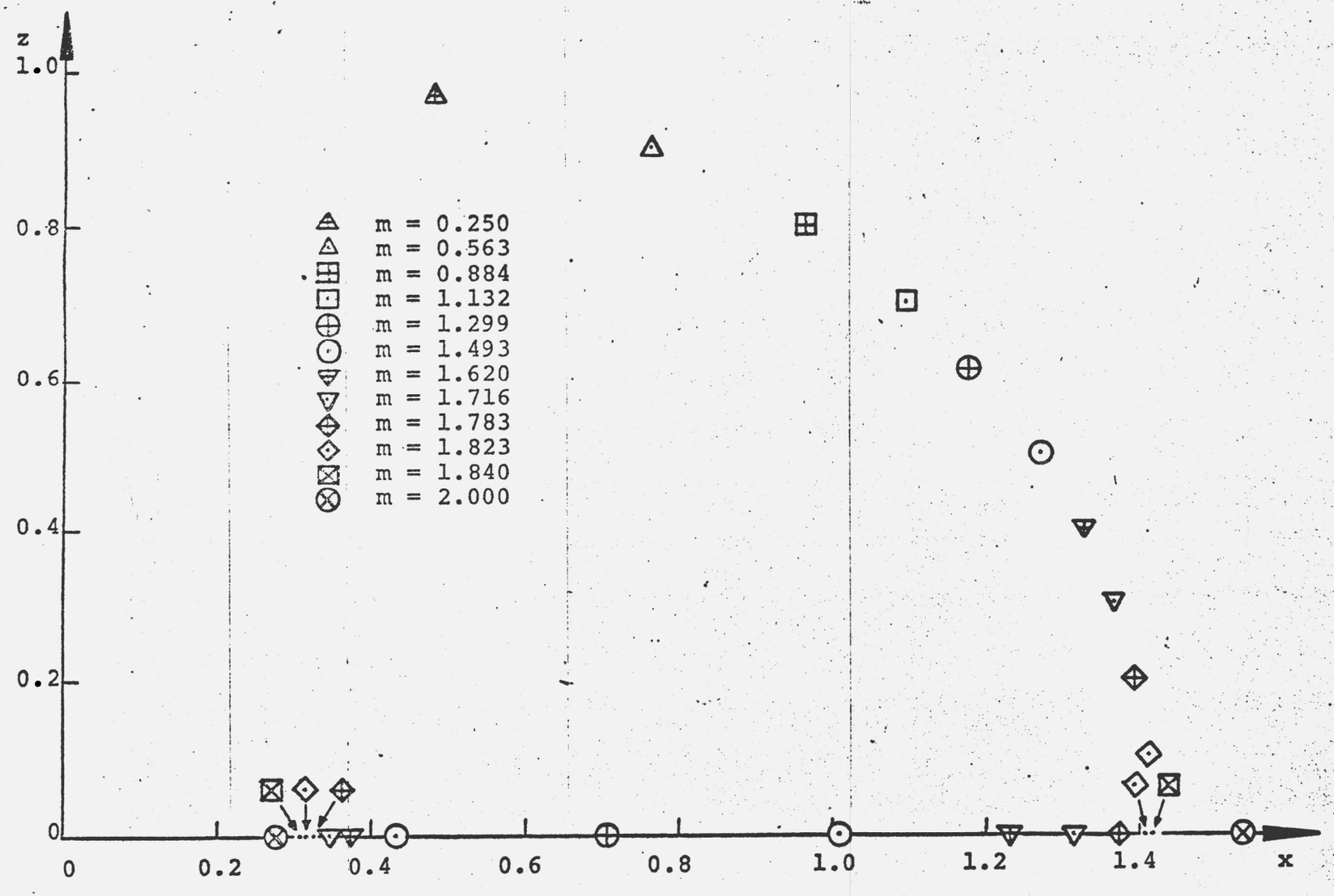

Figure 30. Stagnation points as function of sink strength m.

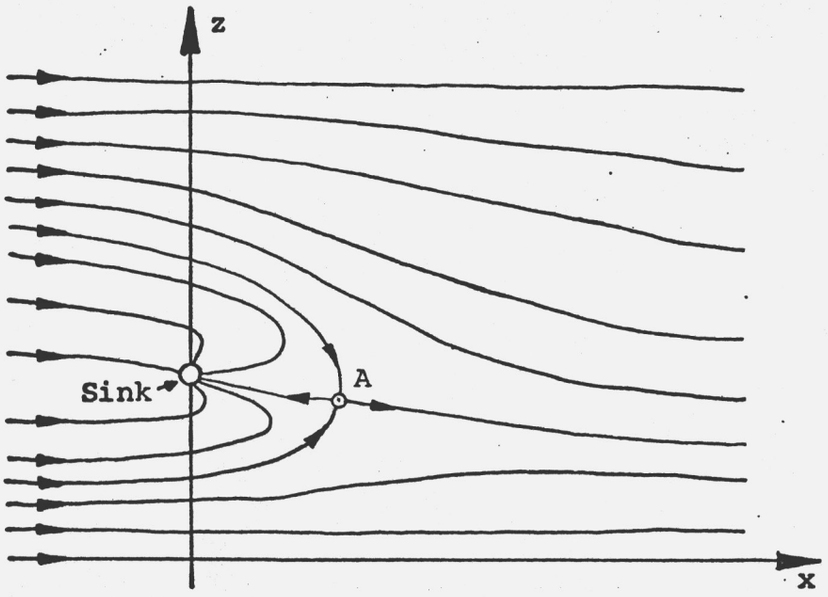

(a) Sink strength m_a

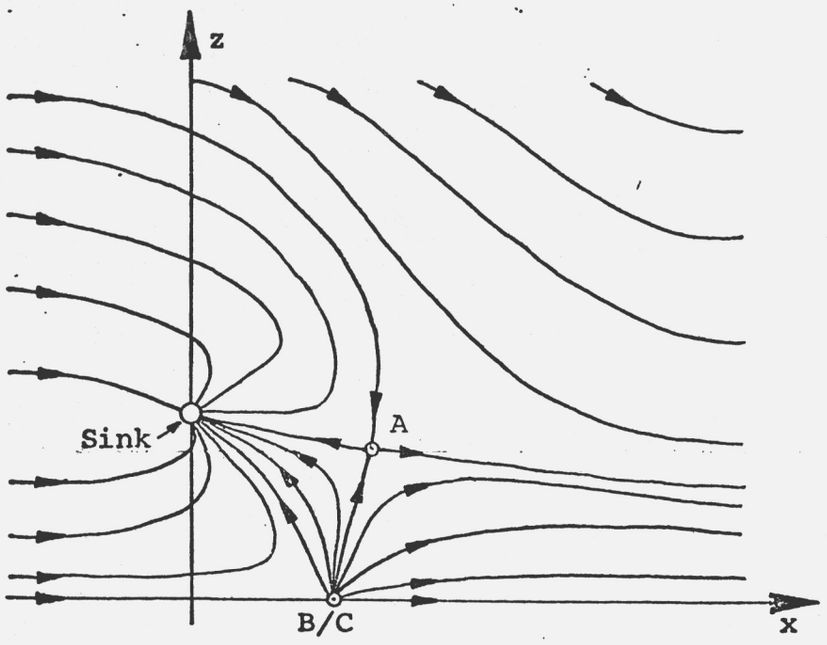

(b) Sink strength m_b

$m_a < m_b < m_c < m_d$; U_∞ = constant

Figure 31. Sketch of streamlines for different sink strengths in x-z-plane.

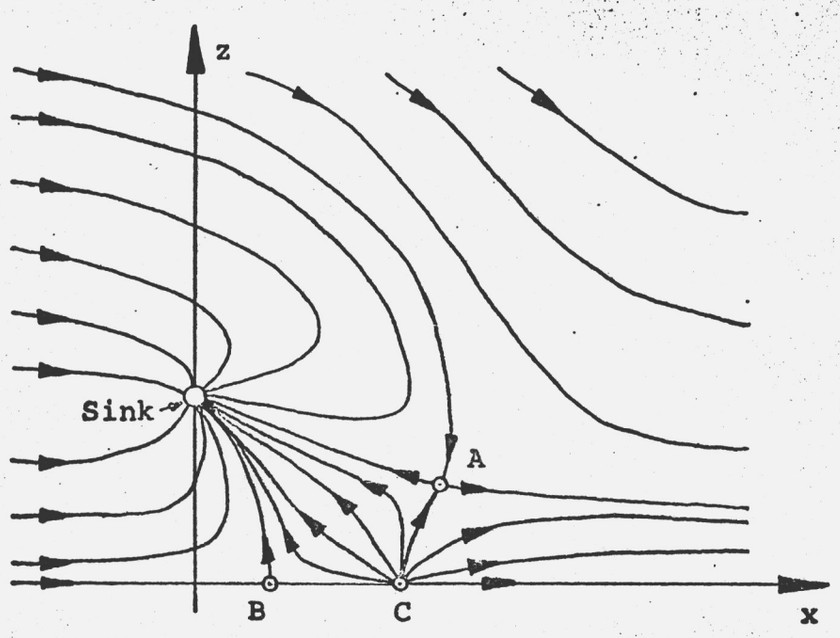

(c) Sink strength m_c

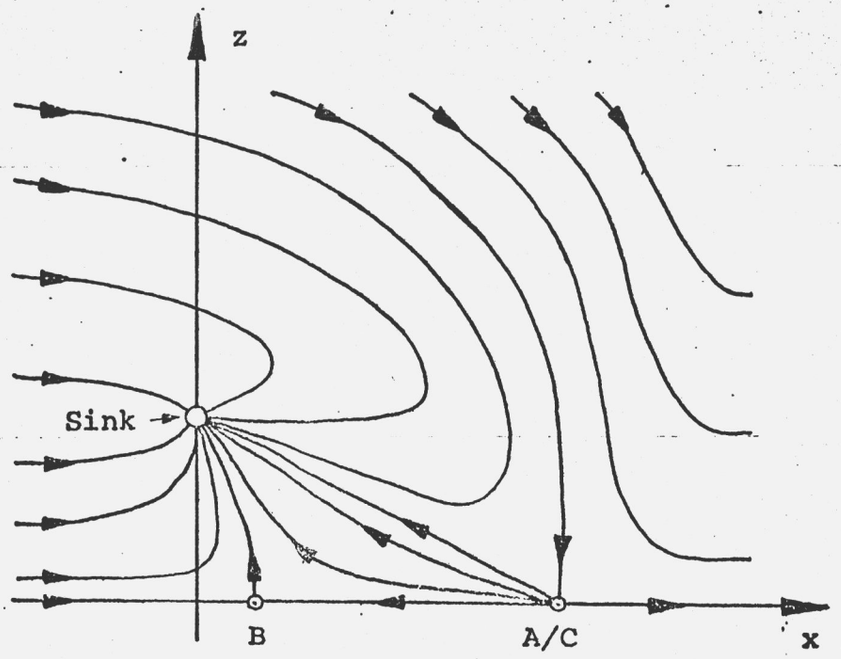

(d) Sink strength m_d

Figure 31. (continued).

increasing m the stagnation point B/C splits up into stagnation points B and C, B moving upstream towards the origin and C downstream (Figure 31c). Stagnation point A comes closer to the x-axis to finally coincide with stagnation point C (Figure 31d).

Figure 32 shows the calculated streamlines in the x-y-plane for the same values of m. For the sink strengths m_c, m_d and higher the flow approaches the stagnation point B nearly radially. At B the streamlines leave the x-y-plane turning sharply in a direction perpendicular to that plane. The same sudden turning happens at stagnation point A. The flow inside the catching surface (Figure 33a) approaches A from all sides to be ejected into two directions, upstream towards the sink and downstream into the free stream. It is this flow field around the stagnation points A and B which is responsible for the formation of the inlet vortex system.

All particles which pass the line $\overline{F^*G^*}$ in Fig. 33a are collected at stagnation point B. If these particles carry vorticity, it is accumulated at B. Because the flow out of B is in z direction, vorticity parallel to the z-axis is stretched. When the accumulation and the stretching are strong enough to overcome the dissipation of vorticity due to viscosity, a ground based inlet vortex will form between the stagnation point B and the sink. Vorticity of particles passing the arc F*H*G* on the catching surface (see Fig. 33a) is collected at the stagnation point A. From A the flow continues on streamlines normal to the catching surface. Therefore, the vorticity component parallel to the normal is stretched and a trailing inlet vortex may be formed.

It is clear that the mathematical model used above considers the action of the potential flow on the vortices but neglects the changes of the potential flow caused by the vortices. Actually as soon as the ground based inlet vortex and the trailing inlet vortex have formed, these two vortices interact and move each other out of the x-z-plane (Figure 2d). The stagnation points B and A are located on opposite sides of the x-z-plane.

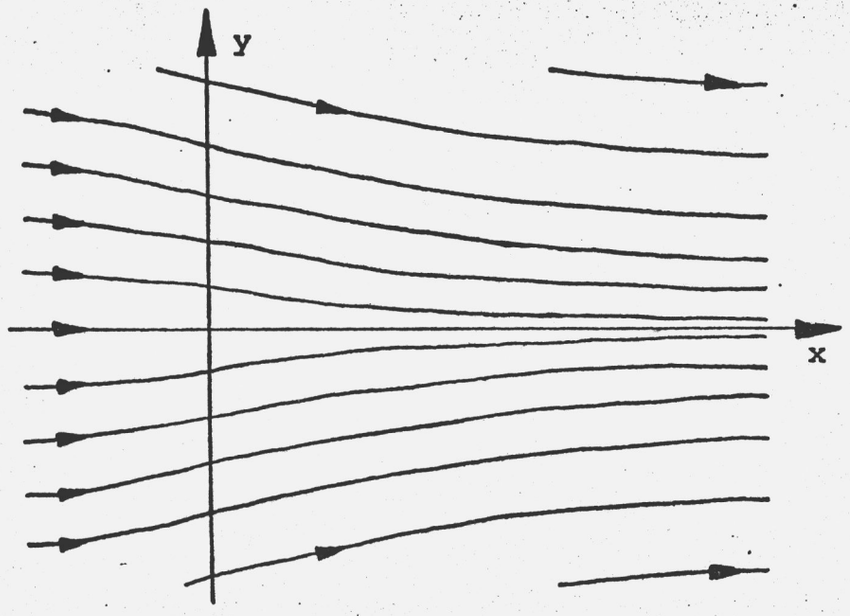

(a) Sink strength m_a

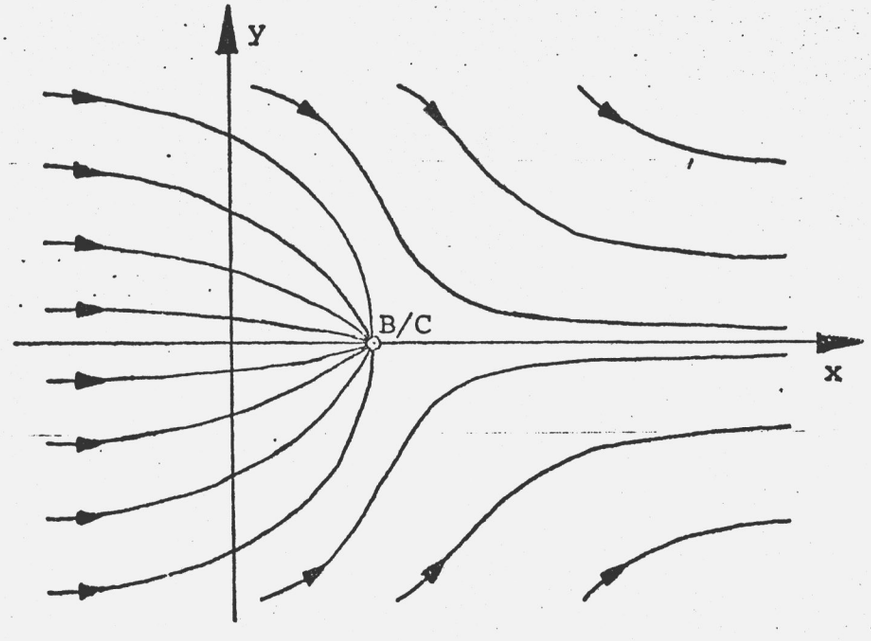

(b) Sink strength m_b

$m_a < m_b < m_c < m_d$; U_∞ = constant

Figure 32. Sketch of streamlines for different sink strengths in x-y-plane.

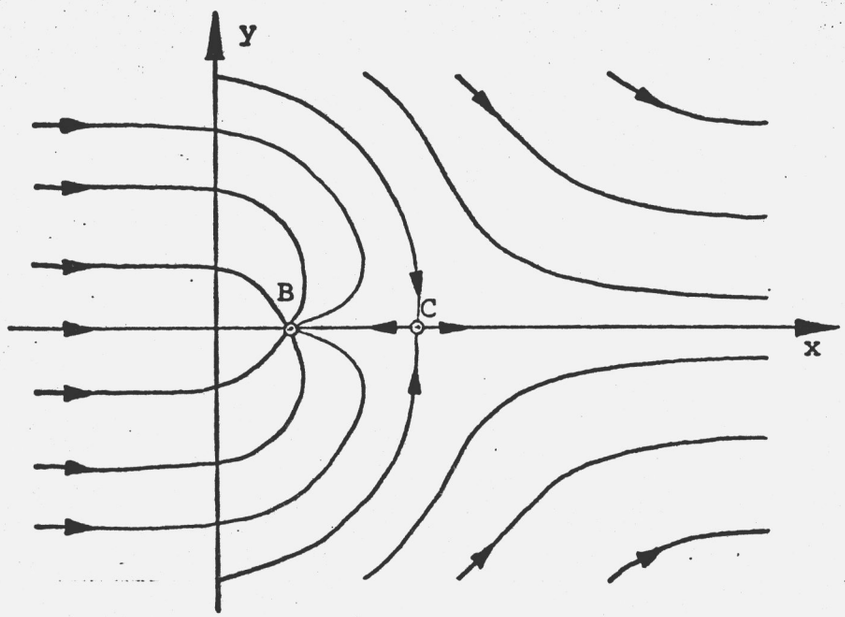

(c) Sink strength m_c

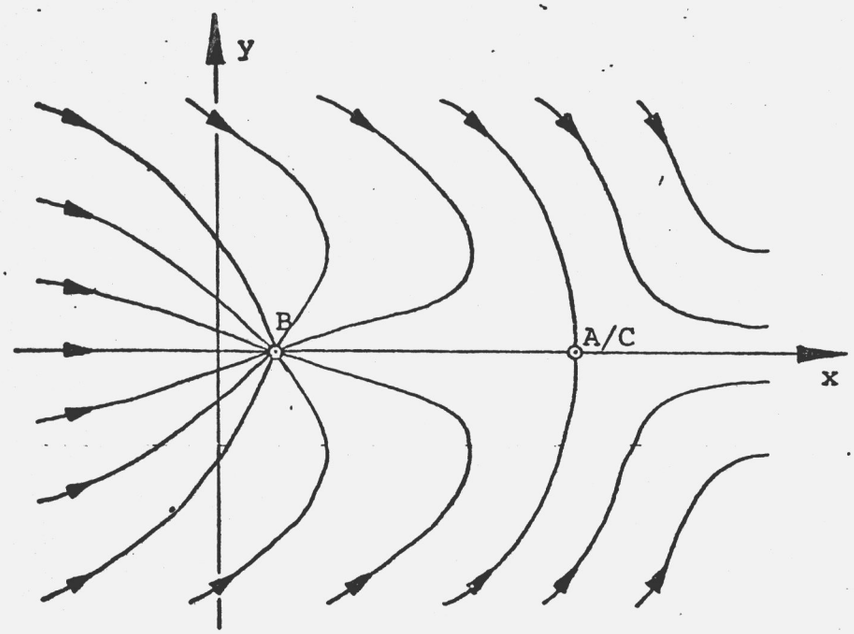

(d) Sink strength m_d

Figure 32. (continued)

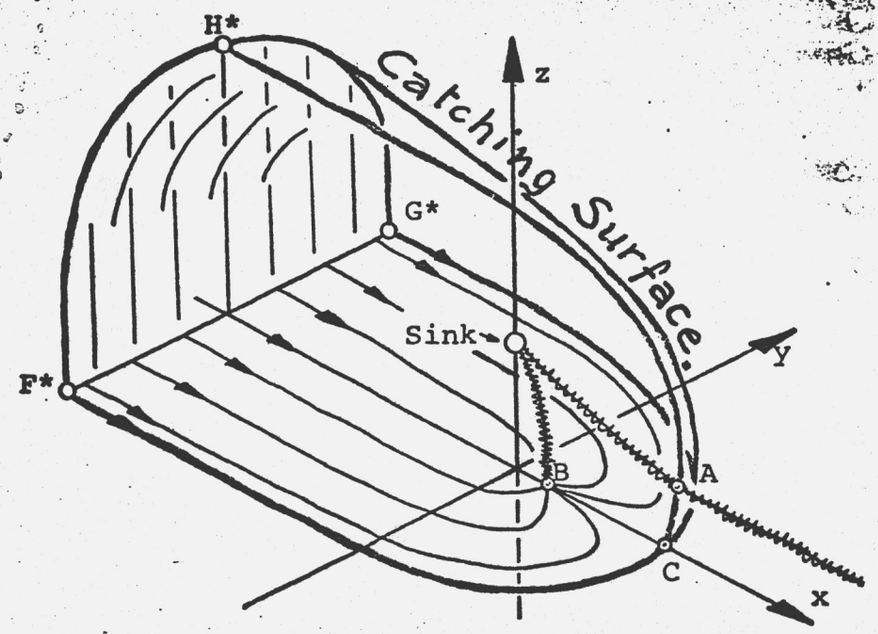

(a) Perspective view of sink-flow for infinitesimal vortax strength.

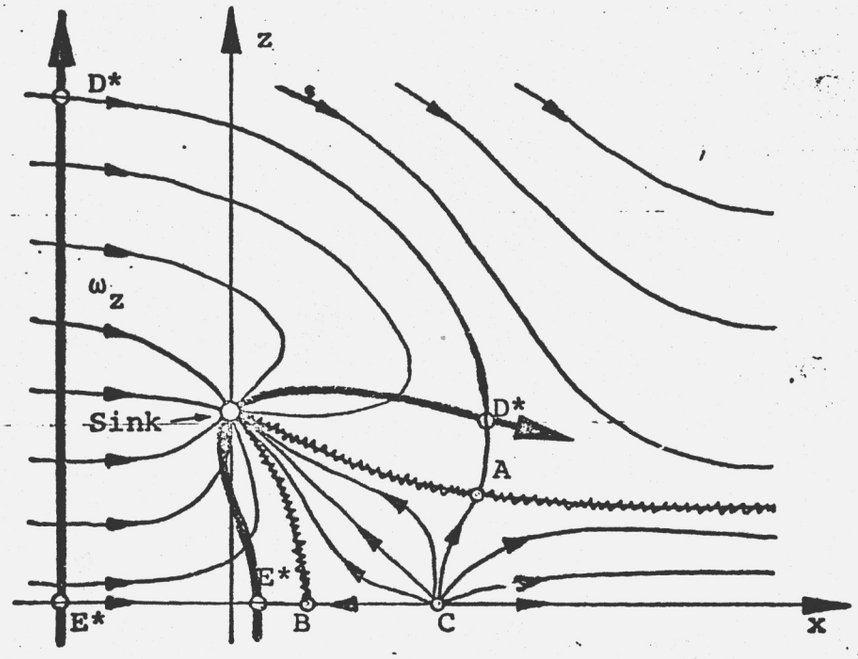

(b) Side view of sink flow

Figure 33. Deformation of free stream vorticity.

To which side B is moving depends on the sense of rotation of the ground based inlet vortex. As can be seen in the Appendix, the vortex at the stagnation point B moves out of the x-z-plane by its own induction.

A cut parallel to the y-z-plane through the stream-surfaces between the stagnation points B and C gives the picture shown in Figure 34a. The trailing vortex increases the velocity in the z-direction in the vicinity of the streamline through C and provides the possibility of vortex stretching in the z-direction. Because there is no stagnation point along this streamline in which this stretched vorticity can be collected, this process leads to weak vortices only wrapped around the trailing vortex and moving along it upstream or downstream depending on whether they are formed inside or outside the catching surface. These vortices are called secondary vortices in Figure 25.

The ground vortices observed in the tests are the same vortices which are known to form in the boundary layer of a flat plate on which a blunt-nosed obstacle is mounted. Here the obstacle is the inlet vortex around which the ground vortices are bent until they are either destroyed by viscosity or they reach their final position parallel to the streamline through C. Figure 34b shows a cut through the trailing vortex and two ground vortices in their final position.

The dead water region observed underneath the inlet, when the inlet flux is just not high enough to form a stagnation point on the ground, can be expected from the streamline picture of the sink flow for this condition. If one would draw Fig. 31a for this case, one would obtain a thin wedge shaped region between the catching surface and the ground. This region would be filled with ground boundary layer and so produce the dead water.

Summarizing one can say that the overall structure of the inlet vortex system can be explained and described by a potential flow model of a sink and its immage in a free stream.

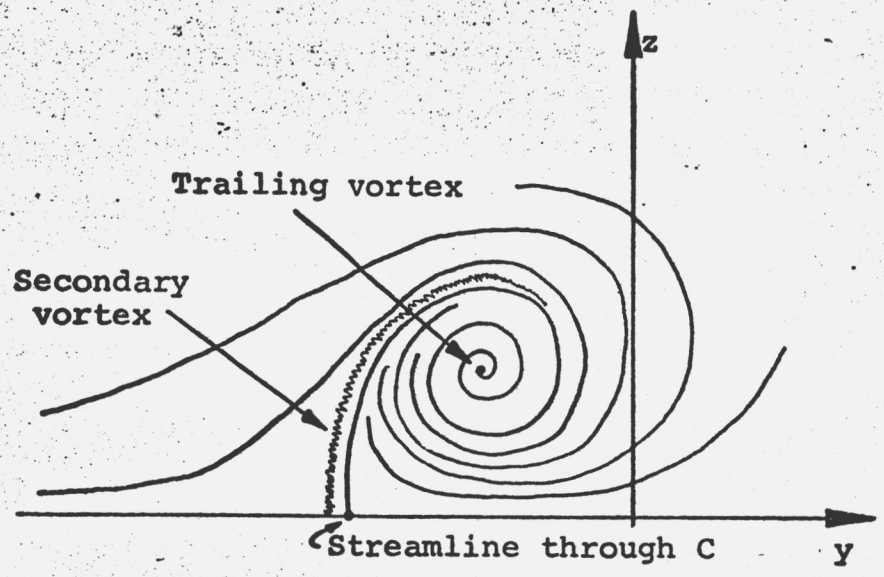

(a) Flow field without ground

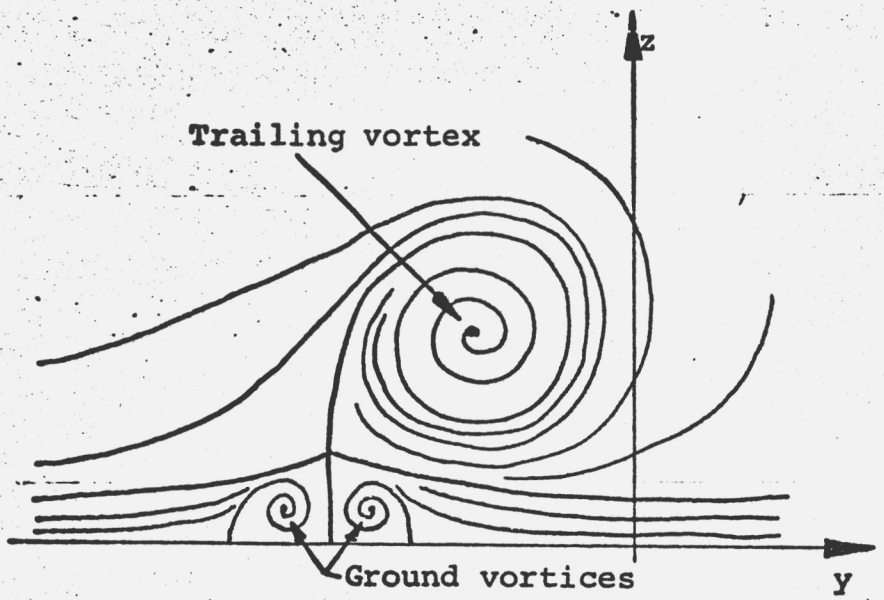

(b) Flow field with ground

Figure 34. Cut through stream surfaces in a plane parallel to y-z-plane.

2. VORTICITY AMPLIFICATION AT A THREE-DIMENSIONAL STAGNATION POINT

It was mentioned before that the flow around a stagnation point with radial inflow and axial outflow increases the vorticity component parallel to the outflow direction. This means that this type of stagnation point flow can produce a vortex, if suitable vorticity is transported into the stagnation point.

This statement is a modification of analytical and experimental findings by Sadeh, Sutra and Maeder [13], [15] and is backed up by the visualization tests performed in the UTSI water tunnel. The analytical derivation for the vortex amplification as it occurs on the ground based inlet vortex was given by Bissinger [20] and is reproduced here in compressed form.

Assume an undisturbed flow field is produced by sinks of strength m*, located in the points

$$x^* = y^* = 0 \; ; \; z^* = h$$

and

$$x^* = y^* = 0 \; ; \; z^* = -h$$

then the flow potential ϕ^* of the sinks written in cylindrical coordinates

$$r^* = \sqrt{x^{*2} + y^{*2}}; \; z^*;$$

is

$$\phi^* = \left\{ \frac{1}{\left[\left(\frac{r^*}{h}\right)^2 + \left(\frac{z^*}{h} - 1\right)^2 \right]^{\frac{1}{2}}} + \frac{1}{\left[\left(\frac{r^*}{h}\right)^2 + \left(\frac{z^*}{h} + 1\right)^2 \right]^{\frac{1}{2}}} \right\} U_\infty h \qquad (6)$$

From it follow the velocity components in cylindrical coordinates by differentiation. If one linearizes them by neglecting terms of the order r^{*2} and z^{*2} and smaller, one gets for the physical velocity components

$$\left.\begin{aligned} v_r^* &= -2 r^* \frac{V_o^*}{h} \\ v_\psi^* &= 0 \\ v_z^* &= 4 z^* \frac{V_o^*}{h} \end{aligned}\right\} \qquad (7)$$

The reference velocity, V^*_{ref}, is defined by

$$V^*_{ref} = \frac{m^*}{h^2} \tag{8}$$

We change now to dimensionless magnitudes by dividing all lengths by the ground distance, h, and dividing all velocities by V^*_{ref} and omitting the asterisk.

The linearized expressions for the sink flow are now

$$v_r = -2r \tag{9}$$

$$v_\varphi = 0 \tag{10}$$

$$v_z = 4z \tag{11}$$

Equations (9), (10), and (11) are considered the components of the undisturbed velocity vector $\bar{V}_o(v_r, v_\varphi, v_z)$. To this undisturbed flow, a perturbation velocity with the absolute value

$$|\bar{v}_1| << |\bar{v}_o| \tag{12}$$

is superimposed. If the vorticity vector of $\bar{V}_1$ is designated by

$$\bar{\omega} = \bar{\nabla} \times \bar{V}_1 \tag{13}$$

then the vorticity transport equations can also be linearized and written in the form

$$(\bar{V}_o \cdot \bar{\nabla})\bar{\omega} = (\bar{\omega} \circ \bar{\nabla})\bar{V}_o + \frac{1}{Re}(\nabla^2 \circ \bar{\omega}) \tag{14}$$

where the Reynolds number has the value

$$Re = \frac{m^*}{h\nu} = \frac{V^*_{ref} h}{\nu} \tag{15}$$

The components of the vorticity transport equation are somewhat lengthy and may be thought as produced by a vorticity distribution of the form

$$\bar{V}_1 = \left[f_r(r,z) \sin(k\varphi);\quad f_\varphi(r,z) \cos(k\varphi);\quad f_z(r,z) \sin(k\varphi) \right] \tag{16}$$

where k is an integer number.

From the continuity equation

$$\frac{\partial v_r}{\partial r} + \frac{1}{r} v_r + \frac{1}{r} \frac{\partial v_\psi}{\partial \psi} + \frac{\partial v_z}{\partial z} = 0 \tag{17}$$

can be derived that f_ψ has the form

$$f_\psi = -\frac{r}{K}\left[\frac{dF(r)}{dr} + \frac{1}{r} F(r) + G(r)\right] \tag{18}$$

where F(r) and G(r) are functions to be determined.

The vorticity components can now be written

$$\omega_r = z\, G(r) \frac{K}{r} \cos K\psi \tag{19}$$

$$\omega_\psi = -z\, G'(r) \sin K\psi \tag{20}$$

$$\omega_z = \frac{3}{Kr}\left(F' - F\right) + \frac{r}{K} F'' + \frac{2}{K} G + \frac{r}{K} G' \tag{21}$$

In addition to the assumption that in the area of interest r^2 and z^2 can be neglected, we assume that the Reynolds number defined by (15) is large enough so that $\frac{1}{r\,Re}$ can also be neglected. Splitting the vorticity transport equation, (14), up into its three components, one can eliminate F(r) and obtains then for G(r) the differential equation

$$G'(r) - \left[\frac{1}{r} + \left(1 - \frac{4}{1-K^2}\right) r\, Re\right] G(r) = 0 \tag{22}$$

It has the solution

$$G(r) = C_1\, r \exp\left[\frac{Re}{2}\left(1 - \frac{4}{1-K^2}\right) r^2\right] \tag{23}$$

Substitution of (23) into (19), (20) and (21) and a limit process for r approaching zero gives

$$\lim_{r \to 0} \quad w_r = C_1 z K \cos K\psi \tag{24}$$

$$\lim_{r \to 0} \quad w_\psi = - C_1 z \sin K\psi \tag{25}$$

$$\lim_{r \to 0} \quad w_z = C_2 \frac{r^{k^2}}{(r^2 Re + 1)^{\frac{k^2}{2}+1}} \cos K\psi \tag{26}$$

If the disturbances have axial symmetry, k has to be zero, for this case is

$$w_r = 0 \tag{27}$$

$$w_\psi = 0 \tag{28}$$

$$w_z = \frac{C_2}{r^2 Re + 1} \tag{29}$$

The last equation shows that the vorticity component perpendicular to the ground plane is amplified, when it approaches the stagnation point. The amplification increases, when Re is increased, i.e. when the vortex strength , m, increases and when the ground distance is reduced.

This amplification effect was also found by Rott [14] who derived an exact solution of the Navier-Stokes equations for the linearized flow of equations (9), (10) and (11).

3. INLET VORTEX STRENGTH AND LOCATION OF VORTEX FOOT.

From the practical point of view the strength of the vortex, which sucks the harmful debris into the engine, is of high interest. Therefore several attempts for measuring the vortex strength with a vortex meter were made. They failed, however, due to the weakness and the nonstationary behavior of the vortices.

Therefore a geometrical measurement of the vortex strength was contemplated. There is a relation between the vortex produced displacement of the stagnation point, in which the inlet vortex meets the ground, and the vortex strength. This displacement could be measured with flow visualization methods. The relation between foot point coordinates and the vortex strength is now derived with the help of a very simplified mathematical vortex model.

Assume the curve of the vortex shape would be given as the vector relation $r = r(\psi)$, where ψ is the angle of inclination of the vortex curve against the vertical (see Fig. 36). Then the vortex induced velocity, w_i, at the foot point would be given by the Biot-Savart law

$$w_i = \frac{\Gamma}{4\pi} \int_{\text{Vortex}} \frac{\bar{r} \times d\bar{s}}{r^3} \tag{30}$$

where $d\bar{s}$ is the vector of the element of the vortex arc length and Γ is the circulation of the vortex. In our case, the integral has to be extended over the physical vortex and its mirror image.

The absolute value of the vector product is

$$| \bar{r} \times d\bar{s} | = r^2 \, d\psi$$

Therefore the induced velocity (30) can be written

$$w_i = \frac{\Gamma}{4\pi} \int_{\text{Vortex}} \frac{d\psi}{r} \tag{31}$$

If a reasonable vortex curve is assumed so that not only the induced velocity is finite but also an explicit evaluation of the integral is possible, then (31) is an explicit relation between the induced velocity, the circulation strength and the coordinates of the foot point.

The vortex curve is assumed as

$$\nu = a\sqrt{\psi^* - \psi} \tag{32}$$

with

$$a = \sqrt{\frac{\xi_0^2 + 1}{\tan^{-1}\xi_0}} \tag{33}$$

ψ^* and ξ_0 are defined by Figure 36.

The shapes of the curves (32) for different values ξ_0 are plotted in Figure 37. Since ξ_0 values above 0.7 are hardly ever expected, the curves look realistic.

The integrations in (31) can now be performed. One obtains

$$w_i = \frac{\Gamma}{2\pi a} \int_{\text{real vortex}} \frac{d\psi}{\sqrt{\psi}} = -\frac{\Gamma}{\pi a}\psi_1 = -\frac{\Gamma}{\pi a}\sqrt{\tan^{-1}\xi_0}$$

or

$$w_i = -\frac{\Gamma}{\pi}\frac{\tan^{-1}\xi_0}{\sqrt{\xi_0^2 + 1}} \tag{34}$$

The velocity w_i is normal to the projection of the vortex on the ground plane. Therefore are the induced velocity components on the ground

$$w_{ix} = w_i \frac{y_0}{\sqrt{x_0^2 + y_0^2}} \tag{35}$$

$$w_{iy} = -w_i \frac{x_0}{\sqrt{x_0^2 + y_0^2}} \tag{36}$$

where (x_0, y_0) designates the coordinates of the vortex foot point.

The stagnation point resulting from sink flow, vortex flow and uniform tunnel flow is given by the conditions

$$-\frac{\partial \phi}{\partial x} + w_{ix} + 1 = 0 \tag{37}$$

$$-\frac{\partial \phi}{\partial y} + w_{iy} = 0 \tag{38}$$

where ϕ is found in equation (2). Substitution of the expressions for ϕ and w_i gives

$$F_1 = -\frac{2x_0 m}{(x_0^2+y_0^2+1)^{3/2}} + \frac{\Gamma}{\pi}\frac{\tan^{-1}\sqrt{x_0^2+y_0^2}}{\sqrt{x_0^2+y_0^2+1}} \cdot \frac{y_0}{\sqrt{x_0^2+y_0^2}} + 1 = 0 \tag{39}$$

$$G_1 = \frac{2y_0 m}{(x_0^2+y_0^2+1)^{3/2}} - \frac{\Gamma}{\pi}\frac{\tan^{-1}\sqrt{x_0^2+y_0^2}}{\sqrt{x_0^2+y_0^2+1}} \cdot \frac{x_0}{\sqrt{x_0^2+y_0^2}} \tag{40}$$

Equations (39) and (40) were solved by finding the points of intersection of the two curves $F_1 = 0$ and $G_1 = 0$ given by these two equations. Figure 38 shows the results. There are two types of intersection points as illustrated for one example in Figure 39. Figure 38a presents the solutions of Type I located close to the origin of the coordinate system. Figure 38b gives the solutions of Type II further away from the origin. The two types of stagnation points show a remarkable difference in so far as the velocities in the points of Type II are directed away from the stagnation point, but towards the stagnation points for Type I. Therefore, the stagnation points of Type I are called statically stable, the stagnation points of Type II statically unstable.

Concerning the use of Figure 38a one should remember that the x_o coordinate is very much different for a sink and a jet intake, while the differences in the y_o coordinate can be expected to be smaller. Therefore, one should use the y_o coordinate only, if one wants to find the circulation by means of Figure 38a. More than order of magnitude accuracy, however, should not be expected from this diagram, even under this precaution. If a higher accuracy is desired, one would have to refine the calculations by using a better mathematical model for the jet flow and by adding the effect of the trailing inlet vortex.

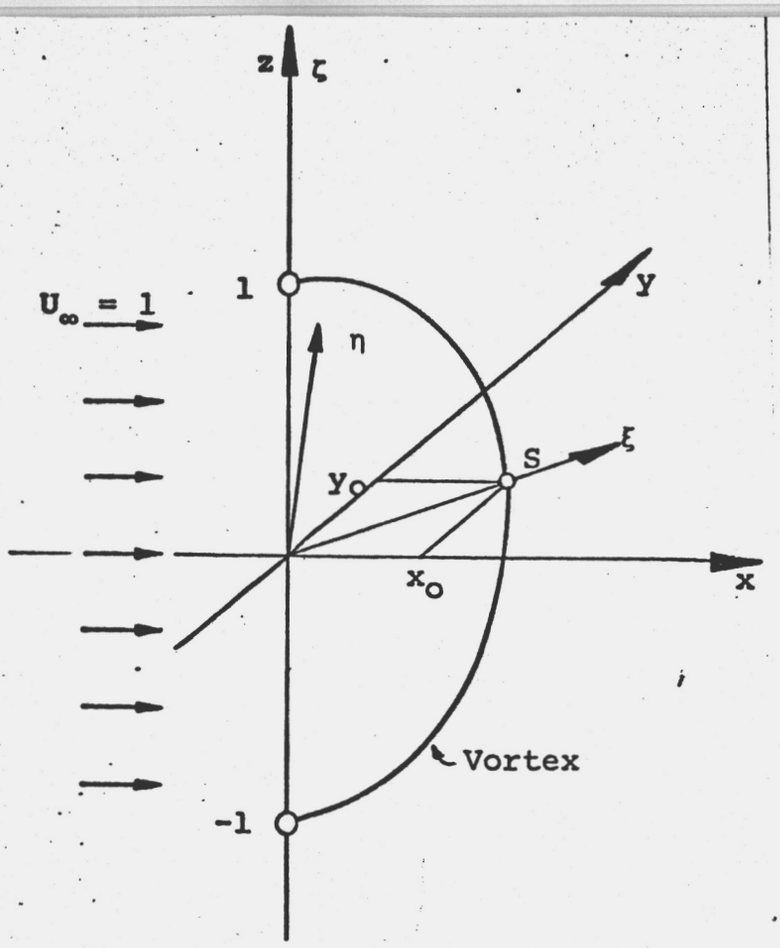

Figure 35. Coordinate system for approximation of inlet vortex.

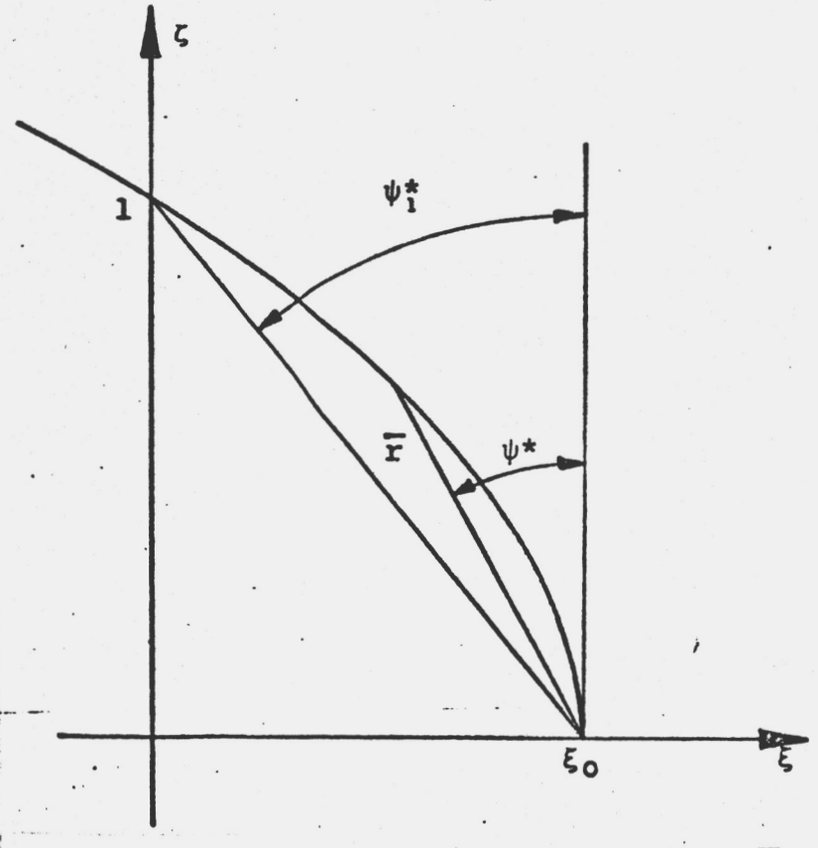

Figure 36. Definition of curve $r = a\sqrt{\psi}$.

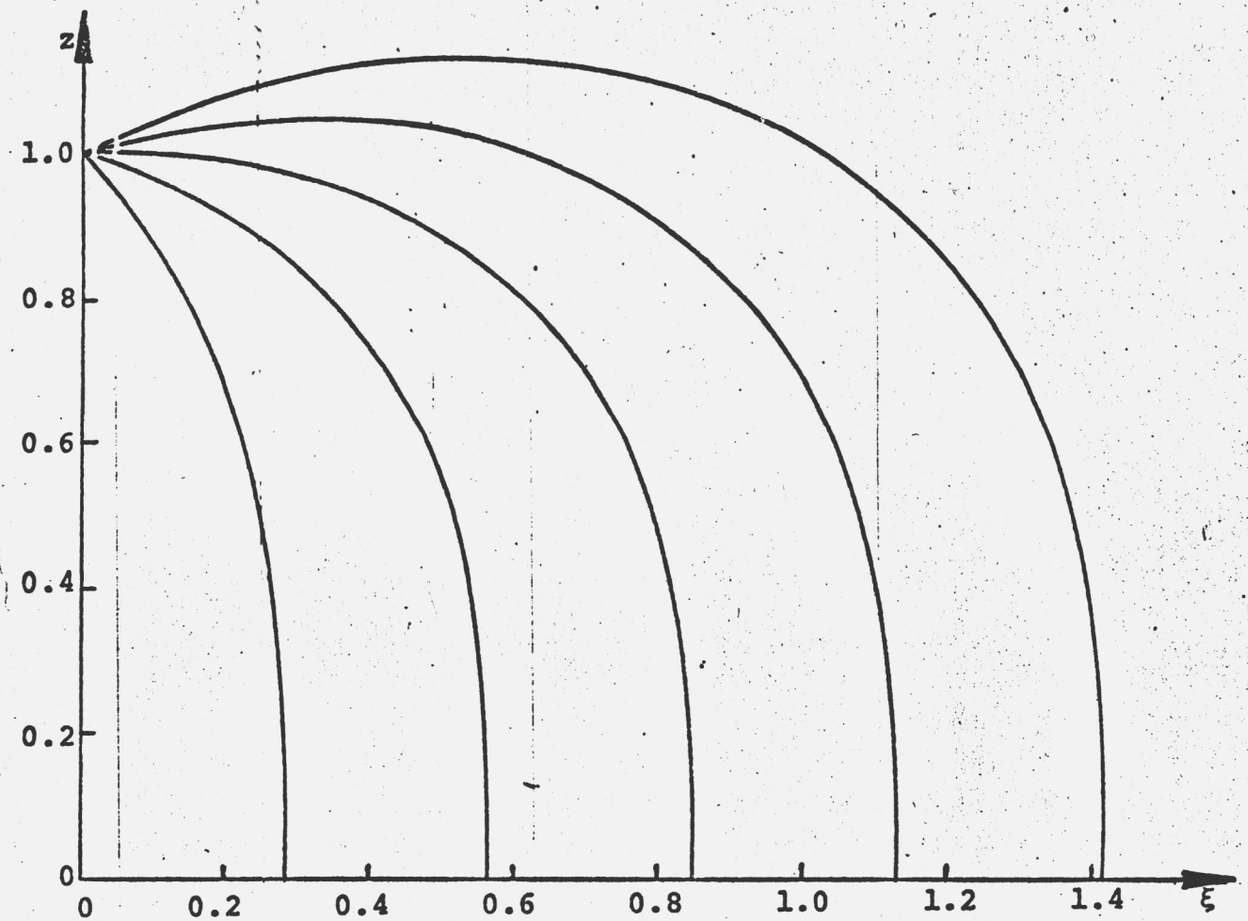

Figure 37. Curve $r = a\sqrt{\psi}$ for different ξ_0.

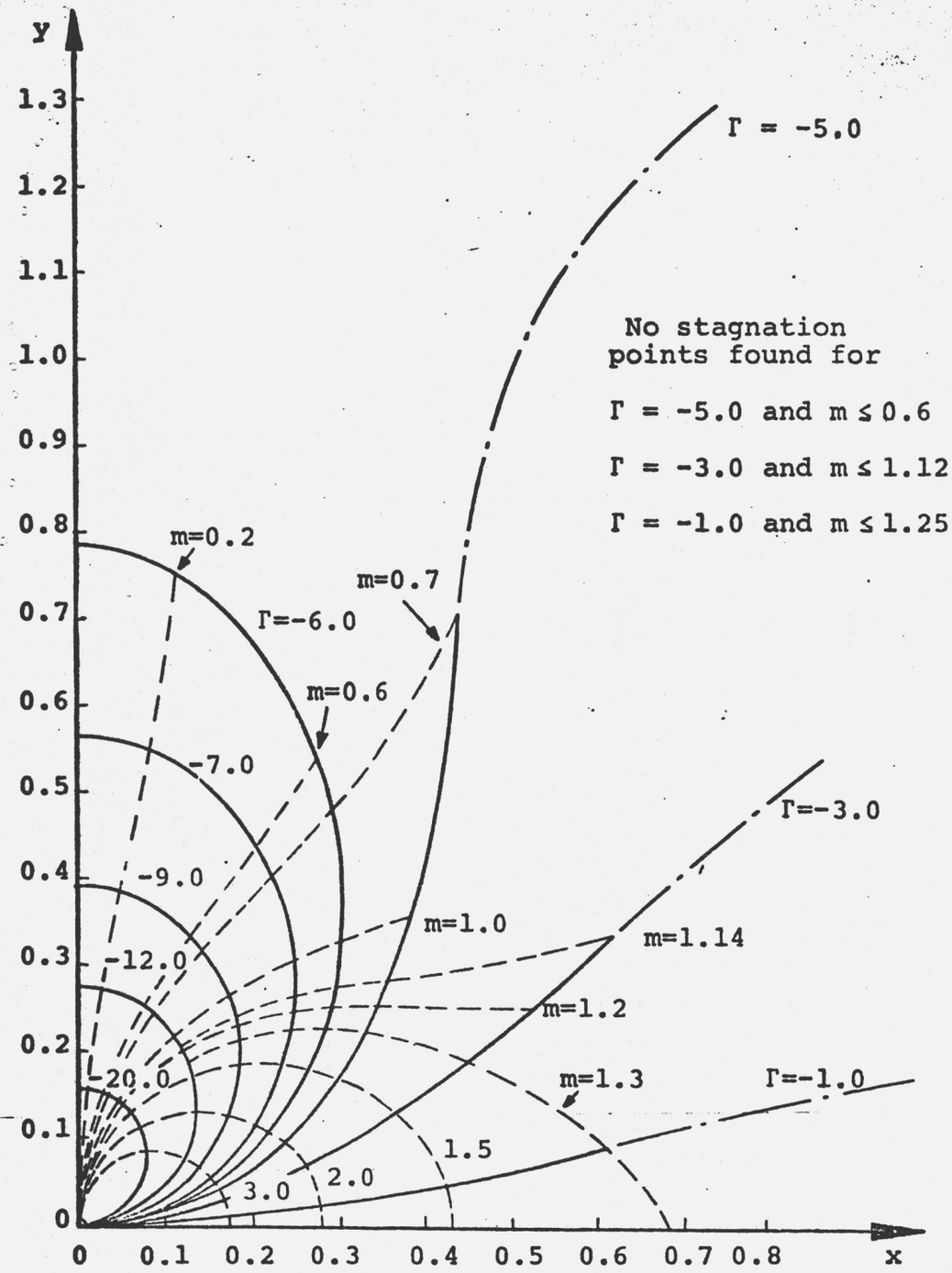

(a) Statically stable positions

Figure 38. Position of stagnation point as function of circulation Γ and sink strength m.

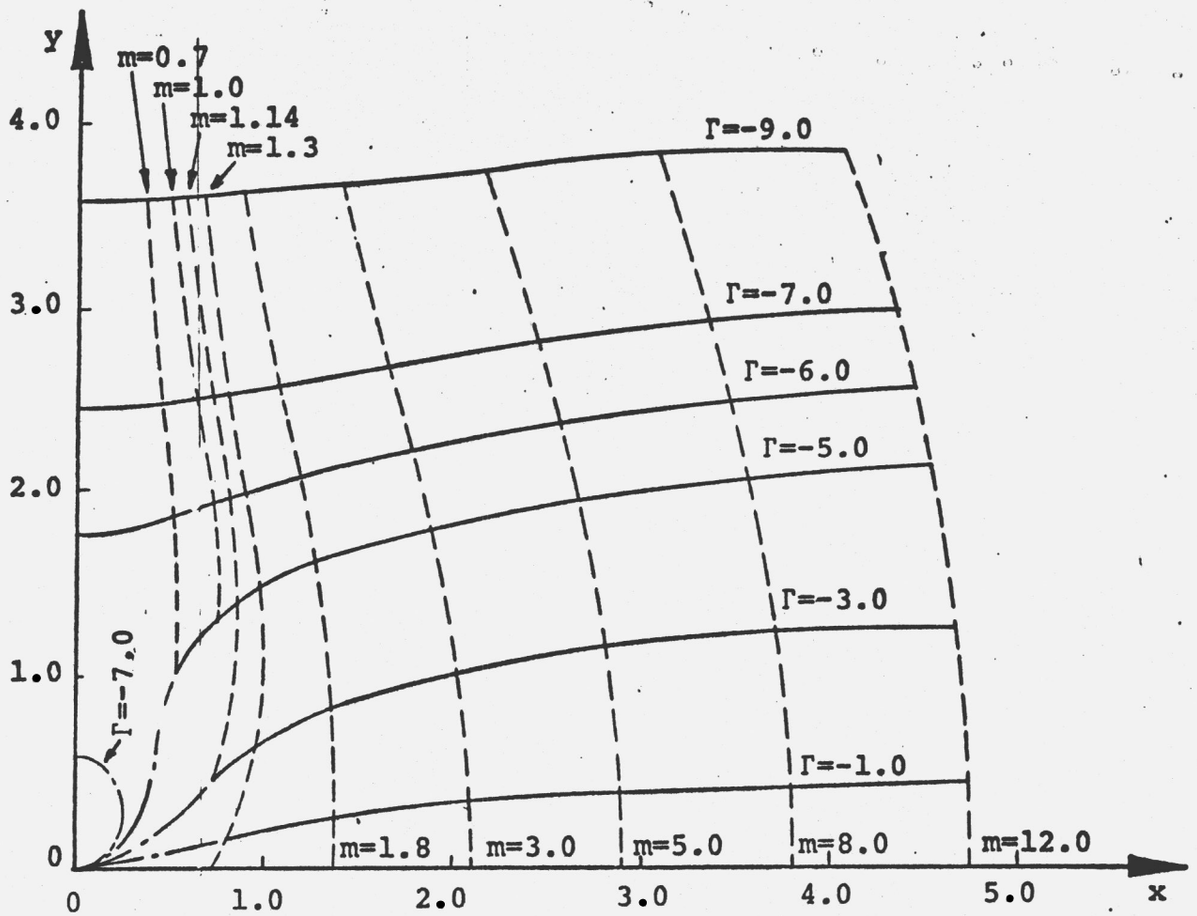

(b) Statically unstable positions

Figure 38. (continued).

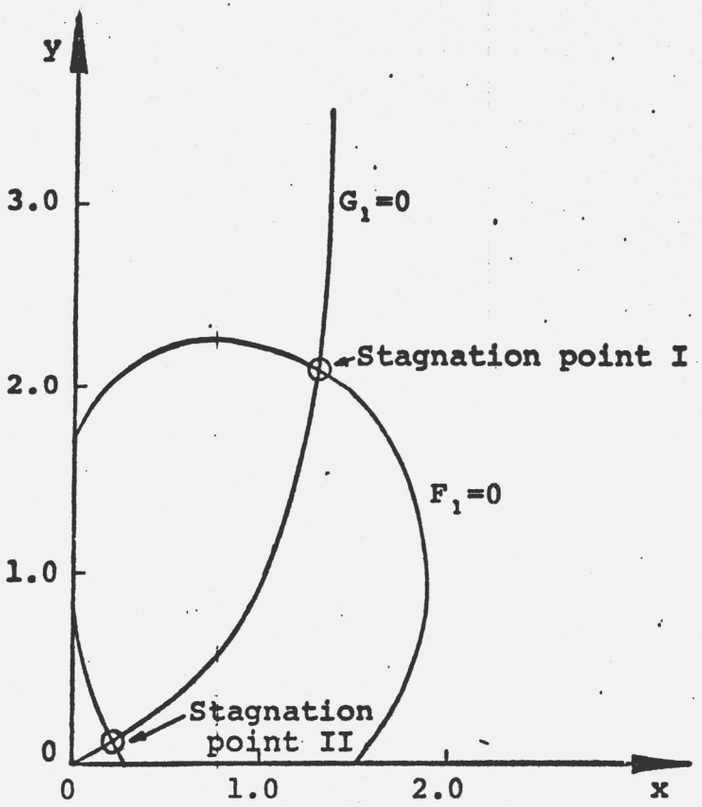

Vortex given by
$r = a\sqrt{\psi}$

Sink strength m = 2.0
Circulation Γ = -6.0

Figure 39. Zeros of velocity components in x- and y-direction.

V. CONCLUDING REMARKS.

The basic difference between the flow visualization tests in the water tunnel and the reports in the literature is, that a whole vortex system was observed in the water tunnel, but a single vortex only in the other tests. The question is, if this difference can be explained by a Reynolds number difference.

TABLE V.

FULL SCALE AND MODEL INLET DATA

JT3C Jet Engine	Inlet Model in Water Tunnel
U_i = 130 m/sec	U_i = 500 cm/sec
D_i = 0.77 m	D_i = 1.6 cm
ν_{air} = 14.9 x 10^{-6} m^2/sec	ν_{water} = 1.0x10^{-2} cm^2/sec
h = 2.32 m	h = 4.8 cm
$Re_i = \frac{U_i D_i}{\nu_{air}}$ = 6.7x10^6	$Re_i = \frac{U_i D_i}{\nu_{water}}$ = 8.0 x 10^4

Table V presents a comparison of the factors contributing to the Reynolds numbers and the values of the Reynolds numbers. The Reynolds number of the full scale configuration is by a factor of almost one hundred larger than the Reynolds number of the water tunnel tests.

In principle, this difference could explain a difference in vortex formation, which, after all, is a viscosity effect. However, the analysis indicated that the production of the inlet vortices is caused by the presence of stagnation points and the vortex stretching occurring in the stagnation point flow. This means independence of Reynolds number. It has also been demonstrated that the ground based inlet vortex does not depend on the presence of boundary layer vorticity. Therefore, the conditions for the production of the trailing inlet vortex are the same as for the ground based vortex. When one exists, the other has also to be there. The trailing vortex must have been overlooked in the full scale tests because

it is less important and less conspicuous, since it is not filled with ground dust.

The ground based vortices are a common phenomenon which can be observed in front of any substantial obstacle. Since the ground based inlet vortex has the characteristics of a flow obstacle, it is safe to assume, that the ground vortices also exist under full scale conditions.

Since the secondary vortices are weak and unimportant, the difference in their observation may be ignored here. Then one can say: The essential elements of the vortex system observed in the water tunnel can also be expected in full scale engine inlet flow.

Finally, an answer should be tried to the question, how to protect a jet engine against debris ingestion. It was shown that the position of the ground based inlet vortex depends upon the strength of the vortex. The vortex strength depends on the vorticity in the free air which is variable in wide limits so that the inlet vortex becomes nonstationary. Therefore, it is not suggested to try to blow down the stagnation point from the ground. Instead the following two countermeasures may be tried, which each by itself may give a satisfactory solution.

a. A retractable screen with its surface parallel to the engine cowling should be located closely below the engine inlet (Figure 40a). In this position the screen would cause only a small reduction of the inlet flow and the screen area could be kept small because there the trajectories of the debris particles would vary very little with vortex intensity and particle weight.

b. The engine axis should be tilted upward as long as the aircraft is close to the ground. This would produce an upward thrust component, which would be of benefit for the take-off maneuver. But the important effect for the engine protection is that the catching surface is tilted upward with the engine and this moves the foot point of the inlet vortex forward (Figure 40b). As a con-

sequence the vortex curve is stretched horizontally and the debris is liable to fall back to the ground before it reaches the intake. There is some danger of overheating the ground. But this danger could be negligible, if, as estimated, an engine inclination of about 10^{o} would be sufficient.

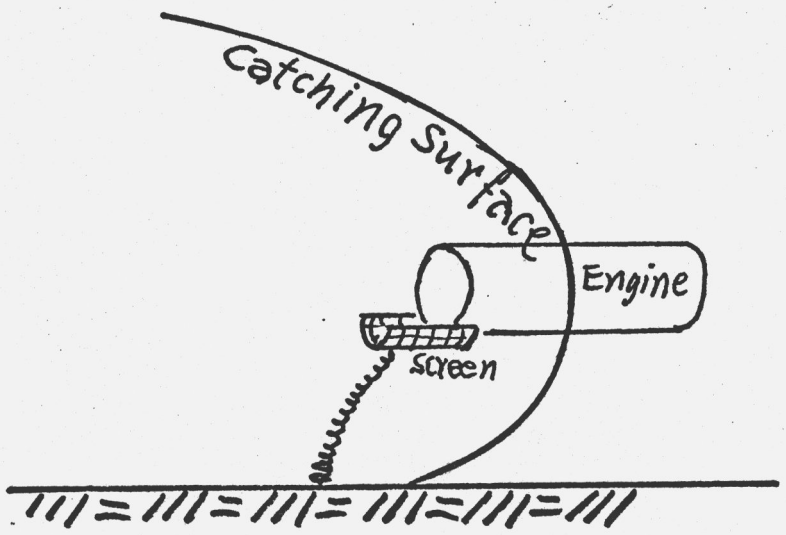

a. Retractable Screen

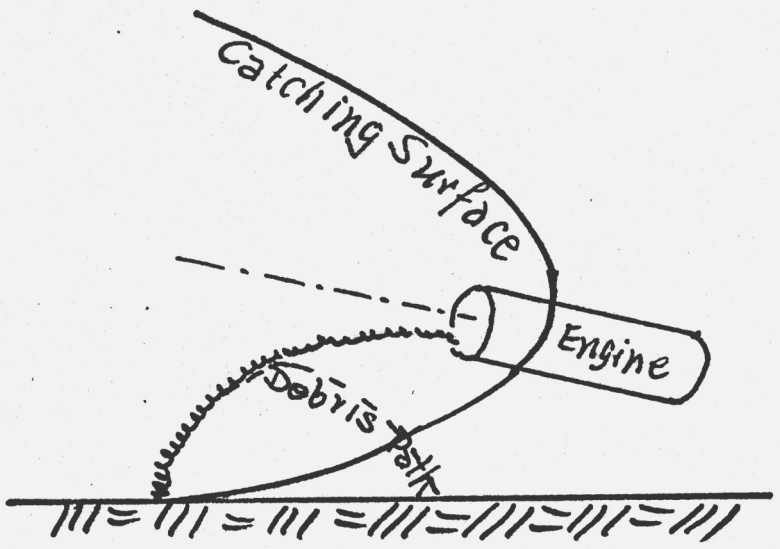

b. Up-Tilt of Engine

Figure 40. Suggested Countermeasures Against Debris Ingestion.

VI. BIBLIOGRAPHY

1. Klein, H. "An Aerodynamic Screen for Jet Engines." Institute of the Aeronautical Sciences, Preprint No. 676, presented at the 25th annual meeting, January 28-31, 1957.

2. Rodert, L. A., and F. B. Garrett. "Ingestion of Foreign Objects into Turbine Engines by Vortices," National Advisory Committee for Aeronautics TN 3330, Washington, D.C., February, 1955.

3. Klein, H. "Small Scale Tests on Jet Engine Pebble Aspiration," Douglas Aircraft Company Report SM-14885, August, 1953.

4. Glenny, D. E. "Ingestion of Debris into Intakes by Vortex Action." Ministry of Technology, Aeronautical Research Council C.P. No. 1114, London, 1970.

5. Miroshnichenko, A. Ya. "The Vortex at the Inlet of an Air Intake," (in Russian), Samoletostroenie I Technika Vozdushnogs Flota, No. 12, 1967, pp. 128-129.

6. Colehour, J. L., and B. W. Farquhar. "Inlet Vortex," Journal of Aircraft, Vol. 8, No. 1, January, 1971, pp. 39-43.

7. Rubbert, P. E., et al. "A General Method for Determining the Aerodynamic Characteristics of Fan-In Wing Configurations," D-6-13476-1, November, 1967, The Boeing Company, Seattle, Washington.

8. Colehour, J. L. "A Study of Foreign Particle Ingestion for a 747 Type Inlet," Document D6-23238, August, 1969, The Boeing Company, Seattle, Washington.

9. Kendall, J. M., Jr. "Experimental Study of a Compressible Viscous Vortex," TR No. 32-290, June, 1962, Jet Propulsion Laboratory, C.I.T., Pasadena, CA.

10. Crawford, R. A. "A Combined Potential and Momentum Roll-Up Model for the Jet in Cross Flow." Ph.D. dissertation, The University of Tennessee, Knoxville, August, 1971.

11. Butkewicz, P. J. "An Investigation of the Vortex Wake and Induced Entrainment for a Jet in Low Reynolds Number Cross Flow." Ph.D. dissertation, The University of Tennessee, Knoxville, August, 1970.

12. Clutter, D. W., A. M. O. Smith, and J. G. Brazier, "Techniques of Flow Visualization Using Water as the Working Medium." Douglas Report ES 29075, El Segundo, California, 1959.

13. Sadeh, W. Z., S. P. Suter , and P. F. Maeder. "Analysis of Vorticity Amplification in the Flow Approaching a Two-Dimensional Stagnation Point." ZAMP, Vol. 21, 1970, pp. 699-716.

14. Rott, N. "On the Viscous Core of a Line Vortex," ZAMP, Vol. IXb, 1958, pp. 543-553.

15. Sadeh, W. Z., S. P. Sutera, and P. F. Maeder. "An Investigation of Vorticity Amplification in Stagnation Flow," ZAMP, Vol. 21, 1970, pp. 717-742.

16. Küchemann, D. "Report on the I.U.T.A.M. Symposium on Concentrated Vortex Motions in Fluids," Journal of Fluid Mechanics, Vol. 21, Part 1, 1965, pp. 1-20.

17. Quick, M. C. "Efficiency of Air-Entraining Vortex Formation at Water Intake," Journal of the Hydraulics Division, Proceedings of the American Society of Civil Engineers, Vol. 96, July, 1970, pp. 1403-1416.

18. Weske, J. R. "On the Origin and Mechanism of Vortex Motion at the Inlet of Intakes Placed Near a Flat Surface," Technical Note BN-152, November, 1958, University of Maryland, College Park, MD.

19. Motycka, D. L., W. A. Walter, and G. L. Muller. "An Analytical and Experimental Study of Inlet Ground Vortices." American Institute of Aeronautics and Astronautics Paper No. 73-1313, AIAA/SAE 9th Propulsion Conference, Las Vegas, Nevada, November 5-7, 1973.

20. Bissinger, Norbert C. "On the Inlet Vortex System," Ph.D. dissertation, The University of Tennessee, Knoxville, Tennessee, March, 1974.